UNIVERSITY OF KWAZULU-NATAL

COLLEGE OF AGRICULTURE, ENGINEERING AND SCIENCE.

Contributions to Optical Coherence Tomography Fingerprint Images

Presented by:
Sboniso Sifiso Mgaga
218087996

Supervisor:
Prof. Jules-Raymond Tapamo

Co-Supervisor:
Nontokozo Portia Khanyile

In fulfilment of the academic requirements of the degree of Master of Science in Engineering, School of Engineering, University of KwaZulu-Natal.

January 25, 2021

Preface

The research discussed in this dissertation was conducted at the University of KwaZulu-Natal under the supervision of Prof. Jules-Raymond Tapamo and Ms. Nontokozo Portia Khanyile. I hereby declare that all materials incorporated in this dissertation are my own original work except where acknowledgement is made by name or in the form of reference. The work contained herein has not been submitted in part or whole for a degree at any other university.

Sboniso Sifiso Mgaga
January 25, 2021

Declaration 1 - Supervisor

As the candidate's Supervisor, I agree to the submission of this dissertation.

_____

Prof. Jules-Raymond Tapamo

Declaration 2 - Co-Supervisor

As the candidate's Co-Supervisor, I agree to the submission of this dissertation.

_____

Ms. Nontokozo Portia Khanyile

Declaration 3 - Plagiarism

I, Sboniso Sifiso Mgaga, declare that

1. The research reported in this dissertation, except where otherwise indicated, is my original research.
2. This dissertation has not been submitted for any degree or examination at any other university.
3. This dissertation does not contain other person's data, pictures, graphs or other information, unless specifically acknowledged as being sourced from other persons.
4. This dissertation does not contain another person's writing, unless specifically acknowledged as being sourced from other researchers. Where other written sources have been quoted, then:
   a) Their words have been rewritten but the general information attributed to them has been referenced.
   b) Where their exact words have been used, their writing has been placed in italics and inside quotation marks, and referenced.
5. This dissertation does not contain text, graphics or tables copied and pasted from the Internet, unless specifically acknowledged, and the source being detailed in the dissertation and in the References section.

Sboniso Sifiso Mgaga

Declaration 4 - Publications

I, Sboniso Sifiso Mgaga, declare that the following publications came out of this dissertation.

1. Mgaga, S.S., Khanyile, N.P. and Tapamo, J-R., 2019, October. "A Review of Wavelet Transform based Techniques for Denoising Latent Fingerprint Images". In 2019 Open Innovations (OI) (pp. 57-62). IEEE.
2. Mgaga, S.S., Tapamo, J-R. and Khanyile, N.P. "Optical Coherence Tomography Latent Fingerprint Image Deniosing". Lecture Notes in Computer Science, Springer-Verlag December 2020. (To appear)
3. Mgaga, S.S., Tapamo, J-R. and Khanyile, N.P. "Latent Fingerprint Acquisition using Optical Coherence Tomography". 7th IEEE CSDE. (Under Review)
4. Mgaga, S.S., Khanyile, N.P. and Tapamo, J-R. "Ridge Structure Enhancement of Optical Coherence Tomography Latent Fingerprint Images". 7th IEEE CSDE. (Under Review)

Acknowledgements

I would like to thank my supervisors Prof. J.-R. Tapamo and Ms N.P. Khanyile for their support, patience and endless insight. They made a valuable impact on my work. I would also like to acknowledge the Identity Authentication Research Group of the CSIR Defence and Security. Lastly I want to thank my loving family and friends who provided me with emotional support and endless motivation to keep going and give it my best.

Sboniso Sifiso Mgaga
January 25, 2021

Abstract

Latent fingerprints serve as crucial evidence for law enforcement agencies to capture perpetrators. They are found at almost every crime scene. Conventionally, latent fingerprints are obtained by using destructive methods such as chemicals, dyes, and tape to lift the fingerprint sample. These conventional methods are destructive and contaminate the sample, leaving no room for further processing such as touch DNA. Furthermore, some surfaces render it difficult or impossible to lift the fingerprints by using such methods, e.g., a fingerprint deposited on a thin sheet of plastic or sandwiched between tapes. In recent years, the forensic community has been moving towards using contactless techniques to acquire latent fingerprints in efforts to overcome the limitations of contact-based latent fingerprint acquisition.

Optical coherence tomography (OCT) is one of the new technologies currently being investigated for latent fingerprint acquisition. The OCT technology uses light to capture a high-resolution 3D representation of an object. This technology presents advantages such as high-resolution images, contactless acquisition, and the ability to penetrate a few millimetres into the surface of the object being imaged. This research proposes OCT as an alternative nondestructive solution to acquire latent fingerprints.

OCT has been used successfully to acquire latent fingerprints from glass, plastic, mirror, stainless steel knife, brass door handle, and bullet case, therefore OCT is a viable technology for latent fingerprint acquisition. However, OCT technology is known to present some challenges when it comes to its imaging capabilities. The images produced by the OCT system are often immersed in speckle-noise; therefore, this research proposes an effective enhancement technique. Two models to enhance latent fingerprint images are proposed.

The first part proposes a wavelet transform-based speckle noise denoising technique. This technique uses a stationary wavelet transform to transform an image into the wave domain. It uses the mean instead of the conventional median estimator to estimate noise on the diagonal subband details, and the optimal threshold is computed by using the product of adaptive threshold and a constant. This constant depends on the length of the subband details and the level of decomposition. In this work, we propose a denoising technique which is robust at removing speckle noise and returns the highest peak to-signal-noise-ratio (PSNR) while minimizing the root mean square error (RMSE) compared to VisuShrink, BayesShrink, SUREShrink, NormalShrink and adaptive threshold.

A ridge structure enhancement technique is also proposed. Latent fingerprint ridges require enhancement to improve the contrast between ridges and valleys and improve the texture and connectivity of ridges. Normalization, orientation field estimation, Gabor filtering, and other methods fall under ridge structure enhancement. Ridge structure enhancement is often performed after denoising and helps to define the structure of ridges and valleys, to improve the accuracy of minutiae extraction. The proposed wavelet denoising and ridge structure enhancement are combined to improve the performance of the orientation certainty level (OCL) of the OCT latent fingerprint images.

Contents

List of Figures **xii**

List of Tables **xv**

1 Introduction **1**

1.1 Overview 1

1.2 Background 3

1.3 Motivation 4

1.4 Research Problem Statement 6

1.5 Main Aim and Specific Objectives 7

1.6 Delineations and Limitations 7

1.7 Contributions 8

1.8 Dissertation Outline 8

2 Literature Review **9**

2.1 Destructive Methods 9

2.2 Nondestructive Methods 11

2.2.1 Alternative light source 11

2.2.2 Infrared imaging 12

2.2.3 Ultraviolet imaging 13

2.2.4 Lasers 13

2.2.5 Other sensors 14

2.3 Noise Commonly Found on Images . . . 15
2.3.1 Speckle noise . . . 15
2.3.2 Gaussian noise . . . 16
2.3.3 Photon noise . . . 16
2.3.4 Impulse noise . . . 16
2.3.5 Fractal noise . . . 17
2.3.6 Gamma noise . . . 17
2.4 Latent Fingerprint Denoising . . . 18
2.4.1 Spatial domain filters . . . 18
2.4.2 Frequency domain filters . . . 19
2.4.3 Wave domain techniques . . . 20
2.5 Fingerprint Ridge Structure Enhancement . . . 21
2.5.1 Orientation field estimation . . . 21
2.5.2 Ridge filtering . . . 22
2.5.3 Segmentation . . . 23
2.5.4 Binarization . . . 24
2.6 Quality Estimation . . . 25
2.6.1 Quality estimation based on local features . . . 25
2.6.2 Quality estimation based on global features . . . 26
2.6.3 Quality measure based on classifier . . . 27
2.7 Summary . . . 27

3 Fingerprint Image Denoising **28**

3.1 Introduction . . . 28
3.2 Background to the Proposed Method . . . 28
3.2.1 Wavelet transform . . . 29
3.2.2 Wavelets . . . 32

3.2.3 Shrinkage schemes . . . 33
3.2.4 Shrinkage rules . . . 35
3.3 Proposed Improved Denoising Technique . . . 39
3.4 Segmentation . . . 40
3.4.1 Morphological operations . . . 41
3.4.2 Latent fingerprint segmentation . . . 42
3.4.3 Contour smoothing . . . 42
3.5 Summary . . . 42

4 Ridge Structure Enhancement 44

4.1 Introduction . . . 44
4.2 Normalization . . . 45
4.3 Ridge Orientation Field . . . 45
4.4 Ridge Frequency Estimation . . . 47
4.5 Ridge Filtering . . . 49
4.6 Binarization . . . 51
4.7 Summary . . . 51

5 Quality Estimation 52

5.1 Introduction . . . 52
5.2 Orientation Certainty Level . . . 52
5.3 Quality Assessment Metrics . . . 54
5.4 Summary . . . 55

6 Experimental Results and Discussion 56

6.1 Data Acquisition . . . 56
6.1.1 Optical coherence tomography . . . 56

6.1.2 Acquisition process 57

6.2 OCT Compared to Traditional Fingerprints 59

6.2.1 Robon powder blue 59

6.2.2 Unfired Bullet Cartridge 63

6.2.3 Section summary 64

6.3 Denoising Results 65

6.3.1 Wavelet filter based analysis 75

6.3.2 Technique-based analysis 76

6.3.3 OCL values after segmentation 76

6.3.4 Section summary 80

6.4 Ridge Structure Enhancement 81

6.4.1 Orientation estimation results 82

6.5 Recommended Enhancement 85

6.6 Summary 85

7 Conclusions **86**

7.1 Conclusions 86

7.2 Application 87

7.3 Future Work 87

List of Figures

1.1 Fingerprint image before and after erosion operation 3

1.2 OCT latent fingerprint image and its corresponding plain fingerprint. 5

2.1 Fingerprint dusting and tape lifting. 10

2.2 Latent fingerprint detection by using (a) natural and (b) ALS (near blue light). . 12

2.3 Gradient based orientation estimation steps. 22

2.4 Ridges and valleys of a fingerprint. 23

2.5 Quadrants of the original LOQ measure (taken from [27]). 26

3.1 Proposed OCT latent fingerprint image enhancement 29

3.2 Proposed OCT latent fingerprint image denoising 29

3.3 Discrete wavelet transform decomposition where $g(n)$ is the low-pass filter, $h(n)$ represents the high-pass filter. LLs represent the approximation and (LH, HL and HH) represents the detail coefficients (taken from [102]). 31

3.4 Stationary wavelet transform where $h(n)$ is the high-pass filter and $g(n)$ is the low-pass filter. 32

3.5 (a) Image wavelet decomposition. (b) Actual fingerprint image decomposed up to level 2. The fingerprint image was obtained from the NIST online database [79]. 32

3.6 Different wavelets families. (a) Daubechies (b) Symlets (c) Coilets and (d) Biorthogonal. 34

3.7 The basic structure of the proposed wavelet transform-based OCT latent fingerprint image denoising technique. 40

3.8 Fingerprint image before and after erosion operation (taken from [116]). 41

3.9 shows the fingerprint images segmentation from input to output. (taken from [114]) 43

4.1 Ridge structure enhancement flow diagram. 44

4.2 Orientation field of a ridge at pixel (i, j). 46

5.1 Non-overlapping 32×32 pixels blocks that. 53

5.2 Fingerprint blocks. 54

6.1 Schematic diagram of the SD-OCT (adapted from [125]). 58

6.2 Conversion of 3D to 2D latent fingerprint images, (a) 3D-image and (b) 2D-image with z the vertical axis and x the horizontal axis 58

6.3 Latent fingerprint images captured by OCT, (a) Brass, (b) Glass, (c) Mirror, (d) Plastic (e) Stainless steel (f) Bullet cartridge. 59

6.4 Latent fingerprint image taken from glass. 60

6.5 latent fingerprint image taken from door knob 61

6.6 Latent fingerprint image taken from plastic. 61

6.7 Latent fingerprint from a mirror. 62

6.8 Latent fingerprint obtained from stainless steel. 62

6.9 Latent fingerprint from a bullet case. 63

6.10 Some latent fingerprint images denoised by VisuShrink, (a) Brass, (b) Glass, (c) Mirror, (d) Plastic (e) Stainless steel (f) Bullet cartridge. 69

6.11 Some latent fingerprint images denoised by BayesShrink, (a) Brass, (b) Glass, (c) Mirror, (d) Plastic (e) Stainless steel (f) Bullet cartridge. 70

6.12 Latent fingerprint images denoised by SUREShrink, (a) Brass, (b) Glass, (c) Mirror, (d) Plastic (e) Stainless steel (f) Bullet cartridge. 71

6.13 Latent fingerprint images denoised by NormalShrink, (a) Brass, (b) Glass, (c) Mirror, (d) Plastic (e) Stainless steel (f) Bullet cartridge. 72

6.14 Latent fingerprint images denoised by adapt. threshold, (a) Brass, (b) Glass, (c) Mirror, (d) Plastic (e) Stainless steel (f) Bullet cartridge. 73

6.15 Latent fingerprint images denoised by the proposed method, (a) Brass, (b) Glass, (c) Mirror, (d) Plastic (e) Stainless steel (f) Bullet cartridge. 74

6.16 OCL values of *haar* and *db2* wavelet filters after successfully denoising, segmenting and applying ridge structure enhancement: (a) *haar* wavelet filter, (b) *db2* wavelet filter. 78

6.17 OCL values of *sym4* and *bior2.6* wavelet filters after successfully denoising, segmenting and applying ridge structure enhancement: (a) *sym4* wavelet filter, (b) *bior2.6* wavelet filter. 79

6.18 Latent fingerprint images denoised by the proposed technique, (a) Brass, (b) Glass, (c) Mirror, (d) Plastic (e) Stainless steel (f) Bullet cartridge. 81

6.19 OCL values of *haar* and *db2* wavelet filter after successfully denoising, segmenting and applied ridge structure enhancement: (a) *haar* wavelet filter, (b) *db2* wavelet filter. 83

6.20 OCL values of *sym4* and *bior2.6* wavelet filter after successfully denoising, segmenting and applied ridge structure enhancement: (a) *sym4* wavelet filter, (b) *bior2.6* wavelet filter 84

6.21 Recommended OCT enhancement procedure. 85

List of Tables

5.1 Classification levels of the orientation certainty value [28]. 54

6.1 Specifications of the customized latent fingerprint OCT acquisition device. 57

6.2 PSNR, SNR and RMSE and SSIM values for each technique with *haar* as a wavelet filter at decomposition levels 1 to 4. 65

6.3 PSNR, SNR and RMSE and SSIM values for each technique with *db2* as a wavelet filter at decomposition levels 1 to 4. 66

6.4 PSNR, SNR and RMSE value for each technique with *sym4* as a wavelet filter at decomposition levels 1 to 4. 67

6.5 PSNR, SNR and RMSE value for each technique with *haar* as a wavelet filter at decomposition levels 1 to 4. 68

6.6 OCL measure of each fingerprint image denoised by different denoising techniques with different filters at different levels of decomposition. 75

6.7 OCL values of fingerprint images after successful denoising and segmentation of the fingerprint images. 77

6.8 OCL values of fingerprint images after successfully applying denoising, segmentation and ridge structure enhancement. 82

List of Acronyms

OCT	Optical Coherence Tomography
DNA	Deoxyribonucleic Acid
OCL	Orientation Certainty Level
ALS	Alternative Light Sources
CWL	Chromatic White Light
UV	Ultraviolet
IR	Infrared Light
SD-OCT	Spectral Domain Optical Coherence Tomography
EVISCAN	Evidence scanner
DWT	Discrete Wavelet Transform
SWT	Stationary Wavelet Transform
DFT	Discrete Fourier Transform
FFT	Fast Fourier Transform
db2	Daubechies 2 Wavelet
db3	Daubechies 3 Wavelet
db4	Daubechies 4 Wavelet
coif2	Coiflets 2 Wavelet
boir2.6	Biorthogonal 2.6 wavelet
NIST	National Institute of Standards and Technology
SNR	Signal-to-noise ratio
PSNR	Peak-signal-to-noise ratio

Chapter 1

Introduction

1.1 Overview

Biometrics refers to the measurement and statistical analysis of people's unique physical or behavioural characteristics. Biometric traits include ears, voice, gait, face and fingerprints. Fingerprints are the most used trait because of their uniqueness, performance and universality [1]. Fingerprint images are divided into three types; rolled, plain and latent fingerprints. The rolled fingerprints are acquired by rolling a finger from nail to nail in order to capture all the ridge information [2]. Plain fingerprints are obtained by pressing a finger flat on to a scanner. Plain and rolled fingerprints are usually of good quality since they are obtained intentionally, whereas latent fingerprints are obtained from objects that have been unintentionally touched or handled.

Latent fingerprint recognition is the process of distinguishing and affirming the identity of an individual by comparing their latent fingerprints, collected from a crime scene, to rolled or plain fingerprints that are stored in a certain database. Lifting latent fingerprints at a crime scene is not an easy task. There are various current methods for lifting latent fingerprints [3–11]. The methods of lifting latent fingerprints can be classified into two groups: destructive contact-based methods and non-destructive contactless methods.

Destructive methods use chemicals to develop the latent fingerprint. This is often followed by a destructive method to lift the fingerprint, such as using tape to lift the sample. These methods suffer from the fact that if anything goes wrong during the acquisition process, the print is destroyed since the acquisition process cannot be reversed. Furthermore, the use of chemicals contaminates the sample. Because of this, it is not possible to perform any further analysis of the sample, such as for touch DNA [12–14] and drug analysis [15, 16].

Nondestructive methods do not involve the use of chemicals. They consist of some

form of sensor which is used to acquire a fingerprint without needing tape to lift it first, as well as some form of a light source to help localize the fingerprints prior to acquiring. These sensors are often quick and take either 2 or 3-dimensional images of the fingerprint. However, these sensors do present some challenges. The images acquired by using contactless sensors or cameras can suffer from various types of noise.

Latent fingerprint images may be corrupted by noise during acquisition and/or transmission. Noise degrades the quality of images by interfering with the original image signal, which results in the variation of pixels. The noise signal may appear as additive or multiplicative on an image [5, 17]. Additive noise signal includes impulse noise, salt & pepper noise and Gaussian white noise, whereas the multiplicative noise signal includes speckle noise. The effects of noise may be suppressed by a process referred to as denoising.

Denoising is the process of reconstructing a noise free signal from a noisy signal. A signal can be any action, gesture or sound that is used to convey information. In image processing, a signal is an image which is defined as a matrix of pixels arranged in columns and rows. Denoising fingerprint images is essential for better performance of any authentication system. Removal of noise on fingerprint images reveals important details such as minutiae points and minimizes the processing time of subsequent operations. Various techniques for image denoising have been developed [18–21]. Denoising fingerprint images is not sufficient for automatic fingerprint recognition system. It is also essential to improve the texture, as well as the contrast between the ridges and valleys, so that the distinguishing features are more visible and easier to reliably extract. The process of improving the texture and contrast of fingerprints is referred to ridge structure enhancement in this work.

Ridge structure enhancement uses an orientation field to enhance the ridge flow of fingerprint images. Orientation field estimation is a technique used to enhance the global features of fingerprint images. It describes the local orientation of the ridge-valley structure at each point of a fingerprint image [22]. The orientation field can be used in singular point detection, segmentation, fingerprint image enhancement and classification [23–25].

Quality of fingerprint images may be defined as the number of features contributing to matching [26] or the degree of clarity of ridges and valleys. A few measures of the quality of fingerprint structure have been proposed. These include orientation certainty level (OCL), local orientation quality (LOQ) and consistency measure (CM) [27–29]. Since we are working with images taken by the optical scanner, OCL will be used to assess the quality.

Latent fingerprints are formed when sweat, blood, dust and other materials on a finger are deposited on a surface. The Optical Coherence Tomography (OCT) technology penetrates a few millimetres into these deposits to produce a 3D-representation of the fingerprint. Images produced by OCT contain speckle noise.

1.2 Background

At crime scenes, fingerprint identification plays a crucial role in identifying the culprits. Fingerprints are the tiny ridges, whorls and valley patterns on the tip of each finger. They can be acquired by using different techniques such as powders, ink, fingerprint scanners, digital cameras, etc. Fingerprint images may be classified into three classes, namely, plain, rolled, and latent. Figure 1.1 shows these three types of fingerprint image. Plain fingerprints are acquired by pressing the finger down on a flat surface. Rolled fingerprints are acquired by pressing and rolling a finger from nail-to-nail in order to capture all the ridge details. Plain and rolled fingerprint images are acquired either by using a live-scan or by scanning the inked impression on paper. Plain and rolled fingerprint images are often of a good quality since they are acquired in an attended mode [30]. Fingerprints acquired at crime scenes are called latent images, *i.e.* fingerprints left unintentionally on surfaces. They may be lifted through a variety of means ranging from simply photographing the print to a more complex procedure such as dusting or chemical processing. These latent fingerprint images are often of poor quality, as the person leaving the prints does not do so carefully. The ridge details of latent fingerprints often have low ridge-valley contrast [31] and are immersed in noise, making the automatic processing of latent fingerprints a challenging process.

(a) Rolled fingerprint (b) Plain fingerprint (c) Latent fingerprint

Figure 1.1: Fingerprint image before and after erosion operation

The traditional techniques of lifting latent fingerprints are destructive and contaminate the sample. It has become more common practice for investigators to use alternative light sources (ALS) to localize and examine latent fingerprints left on the surface. This is followed by a non-destructive sensors such as specialized digital cameras to acquire the fingerprints [5, 32]. Surfaces such as duct tape, heavily grained wood, printed glossy magazines and thin plastic bags present challenges for dusting and tape lifting. ALS are nondestructive, but the prints still need to be lifted following successful localization. This is where contactless sensors come in. These sensors include chromatic white light (CWL) sensors, infrared cameras, specialized digital cameras, thermal imaging devices

and lasers. It is important however to note that not all contactless technologies are able to preserve DNA evidence. For example, ultra-violet light is known to be detrimental to DNA.

OCT is a truly nondestructive, contactless sensor that is able to preserve DNA evidence. It is a non-invasive cross-sectional imaging technique that is mainly used in the medical field. It works by penetrating a few millimetres into a surface. Scanning and producing the internal structure (tomography) of the surface. Latent fingerprints are formed when sweat, sebum, blood, dust and other materials on the finger are deposited on a surface. The OCT technology penetrates a few millimetres into these deposits and produce a 3D-representation of the fingerprint.

OCT has been proposed in [4, 33] for contactless acquisition of fingerprints. The 3D-images produced by OCT always need to be converted to 2D-images in order to be able to use them to match with existing databases such as the law enforcement AFIS databases [21]. Even though OCT takes high resolution images, the images may nevertheless contain noise that affects the image quality and makes it difficult to extract features [21]. Image enhancement techniques such as wavelet transformation, segmentation and filtering can be applied to the noise and enhance fingerprint images.

1.3 Motivation

Developing latent fingerprints by using traditional methods such as dusting, fuming and sophisticated chemicals is tedious and time consuming. Often these traditional methods are followed by an adhesive tape to lift the fingerprint. Latent fingerprints are fragile so that if anything goes wrong while lifting, the evidence is destroyed, since the process can not be reversed. Moreover, further processing of the same sample is not possible.

In the past, forensic science relied heavily on destructive methods of acquiring fingerprints. Recently, however, there has been a move towards non-destructive methods such as the use alternative light sources, specialized digital cameras, infrared cameras for acquiring fingerprints in an effort to preserve crime scenes.

OCT is a technology that is often used in the medical field to image the skin and retina. It works by penetrating a few millimetres into a surface and producing that surface's tomography in a 3D-image representation. Assume that you want to lift a fingerprint that is a sandwiched in tape, in this case separating or pealing off the tapes will certainly destroy the fingerprint, while chemicals are unlikely to reach the fingerprint between tapes if the tapes are not separated. The study in [33] showed that OCT technology could be applied successfully in such cases, since it penetrates the surfaces. Some unresolved criminal cases that involve latent fingerprints may possibly be solved by using this technology.

The use of contactless methods can benefit the law enforcement tremendously. It opens up the opportunity of performing further analysis on fingerprint samples at a crime scene where forensic experts are often forced to choose between preserving the DNA evidence or recovering the fingerprint evidence. Such analysis may include touch DNA and drug analysis [34]. Touch DNA consists of skin cells left behind when an individual comes into contact with an item [35], hence latent fingerprints have the potential of containing touch DNA, for forensic analysis. The process of extracting touch DNA involves swabbing, taping, or scraping trace amounts of epithelial cell tissue from surfaces such as doorknobs, windows – and even clothing and food [36]. Nondestructive lifting methods give investigators the choice of performing DNA analysis and drug analysis thus gathering more information from one sample of evidence. Destructive methods completely take away this opportunity, latent fingerprints can contain trace amounts of drugs if that individual has recently consumed drugs, thus providing proof of drug use [37, 38]. Contactless latent technology also makes it possible to capture the same fingerprint sample multiple times if it was not captured correctly the first time. This is not possible with the nonreversible destructive techniques.

Research has shown that it is not easy to obtain latent fingerprints from fired or unfired gun cartridges. Spears *et al.* [39] investigated how easy it is to lift latent fingerprints from gun cartridges. The study revealed that it is very difficult to lift prints from fired or unfired cartridges. Only 25% of bloody fingerprints were successfully lifted from unfired cartridges while 0% were lifted from sweat prints and 25% were lifted from oily prints. Only 12.5% of bloody fingerprints were successfully lifted from fired cartridges while 0% were lifted from sweat prints and 0% were lifted from oily prints. OCT has the potential of helping in this regard. This will be investigated by attempting to acquire a fingerprints deposited on an unfired bullet cartridge.

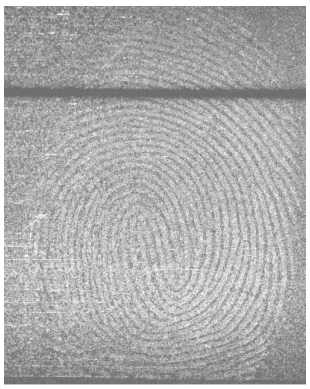

(a) OCT latent print with speckle noise

(b) Corresponding plain fingerprint

Figure 1.2: OCT latent fingerprint image and its corresponding plain fingerprint.

While the OCT technology has the capability to produce high resolution images in less than ideal surface environments, images taken by OCT are often affected by speckle noise as shown in Figure 1.2. Speckle noise is seen in images captured by using coherence imaging systems such as medical ultrasound, active radar, OCT etc. It is produced during image acquisition due to the effects of environmental conditions on the imaging sensor [17]. Images that contain speckle noise often suffer from low contrast which makes it difficult to perform image-processing operations such as segmentation and feature extraction [17, 40].

Extraction of reliable minutiae points relies on the quality of images. Good-quality images enhance the extraction of reliable minutiae points; therefore, it is essential to remove speckle noise from OCT images.

1.4 Research Problem Statement

Forensic scientists have for centuries utilised fingerprints in criminal investigations as a method of identification. Fingerprint identification is amongst the most critical criminal examination instruments. They are reliable because of their permanence and uniqueness. No two individuals share the same fingerprints [41].

Latent fingerprints are the kind of fingerprints that are encountered at crime scenes. They are left behind inadvertently when an individual makes contact with a surface. Conventional techniques of acquiring latent fingerprints focus heavily on contact-based methods which use different chemicals, dyes, powders and lifting instruments [42]. These methods are destructive. This means they can completely alter the sample. Chemicals and dyes that are used introduce contaminants which hinder any possible additional analysis of the sample such as touch DNA [36] and drug analysis [21]. Moreover, lifting a fingerprint from a surface by using tape is an irreversible, unrepeatable and a time-consuming procedure.

The forensic community has been making efforts to move towards nondestructive, non-contaminative techniques of acquiring latent fingerprints in an effort to preserve evidence. Such techniques include specialized high resolution digital cameras, ultraviolet (UV) cameras, infrared cameras and infrared spectroscope [9, 10], thermal imaging, alternative light sources and lasers [43]. All these techniques are contactless in nature and do not make physical contact with the sample.

The technologies mentioned have their strengths and weaknesses. For example, while UV cameras are cheap and fast, their accuracy is low. Furthermore, UV light is known to be damaging to DNA. Infrared spectroscopy devices take a long time to capture the fingerprints and are immobile [43] thus the crime scene has to be brought to the device. Alternative light sources can successfully image limited surfaces.

OCT is one of the promising imaging technologies that can be used to lift latent fingerprints without contact and nondestructively [4]. OCT penetrates a few millimetres into a substrate or material such as glass and produce the tomography of the surface. Because human fingerprints leave residue (residues consist of secretions of sweat and sebum), these residues form a layer on top of the surface on which they have been deposited. By producing the tomography of the surface, fingerprint details can be visualised in 3D by the OCT technology [44].

This research proposes using OCT as a supplementary technology to acquire latent

fingerprints in a nondestructive way which preserves the crime scene. We will conduct research to find out from which types of surface OCT can reliably acquire fingerprints. Additionally, OCT images suffer from speckle noise which reduces the contrast of the ridges and valleys, which makes it difficult to extract reliable minutiae points [42, 45–47]. Therefore an efficient method that will denoise speckle noise and enhance the structure or texture of the OCT latent fingerprint images is needed.

1.5 Main Aim and Specific Objectives

The main goal of this work is to propose a method to enhance the quality of latent fingerprints. To achieve this goal the following specific objectives will be pursued:

1. To investigate which surfaces are feasible for OCT to acquire latent fingerprints from and lift fingerprints from various forensically relevant surfaces using OCT.
2. To review literature on latent fingerprint acquisition and latent fingerprint image enhancement; and investigate and implement different methods of reducing speckle noise from the fingerprint images acquired by using OCT, and recommend or modify the most efficient method.
3. To implement and modify, where possible five techniques of removing or reducing speckle noise from fingerprint images, and once implemented, to test their performance and recommend the most efficient and/or accurate technique.
4. To implement and modify, where possible a technique to estimate orientation field for poor-quality fingerprint images.
5. To estimate the quality of the enhanced fingerprint images.
6. To recommend a way to acquire fingerprints by using OCT reliably and to successfully enhance the image.

1.6 Delineations and Limitations

The main focus of this research is on proving whether OCT is a viable solution for latent fingerprinting. This will be achieved by first investigating the types of substrate from which OCT can successfully acquire usable latent fingerprints and secondly by improving the quality of the captured fingerprint images.

NOTE: while all the steps for ridge structure enhancement of fingerprints will be implemented, the research will only focus on investigating methods to reduce speckle

noise and on investigating methods to estimate orientation, as well as quality estimation, which in turn will improve the subsequent steps of ridge structure enhancement such as Gabor filtering.

1.7 Contributions

This work contributes to the existing knowledge domain in the following ways:

- It presents a list of forensically relevant substrates from which OCT can successfully acquire latent fingerprints.
- It presents a database of latent fingerprint images acquired by using OCT.
- It proposes a novel speckle noise removal technique. The technique may be applied to latent fingerprint images, as well as medical OCT images.
- It proposes an adapted structural enhancement method to improve the ridge clarity and texture of latent fingerprint images.
- It contributes towards the progress in enabling the extraction of DNA from fingerprints by offering a reliable nondestructive technique to acquire fingerprint images from crime scenes.

1.8 Dissertation Outline

This dissertation is structured as follows: Chapter 1 presents the introduction, background and motivation. In Chapter 2, a literature review on existing fingerprint acquisition methods, denoising and structural enhancement is presented. In Chapter 3, different wavelet based denoising techniques are discussed and the proposed technique for computing an optimal threshold is presented. The structural enhancement used in this work is discussed in Chapter 4. Quality estimation techniques used in this work are presented in Chapter 5. Chapter 6 presents latent fingerprint acquisition, experimental results and discussion of the results achieved. Conclusion and future work are presented in Chapter 7.

Chapter 2

Literature Review

This chapter presents a review of literature on existing fingerprint acquisition methods. Section 2.1 investigates some destructive fingerprint acquisition methods, and presents possible applications and their limitations. Section 2.2 discusses nondestructive fingerprint acquisition techniques, and strengths and weaknesses of each method are identified. Section 2.3 presents some of the noise commonly found on fingerprint images. Section 2.4 investigates some of the frequently used fingerprint image enhancement techniques. Section 2.5 presents some ridge structure enhancement techniques. Quality estimation techniques are discussed in Section 2.6. The summary of findings is presented in Section 2.7.

2.1 Destructive Methods

Traditionally latent fingerprints have been collected through destructive methods which include the use of instrumental methods, dyes and chemicals such as iodine, Ninhydrin, siver nitrate etc. Figure 2.1 shows two traditional print-lifting methods ((a) tape lifting and (b) dusting). Methods that use destructive chemicals, dyes and instruments are discussed below.

Powders are used to dust the fingerprints, rendering them visible to the human eye. They are generally useful on newer prints only. They are only used on dry, relatively smooth surfaces. The powder should be a different colour from that of the background. Powders can be used along with chemicals such as ninhydrin and cyanoacrylate [32]. The fluorescent powder is a special type of powder used for confused background but a forensic light source is required to see the fingerprint. The developed fingerprints may be lifted by photography or by tape.

(a) Dusting [48]

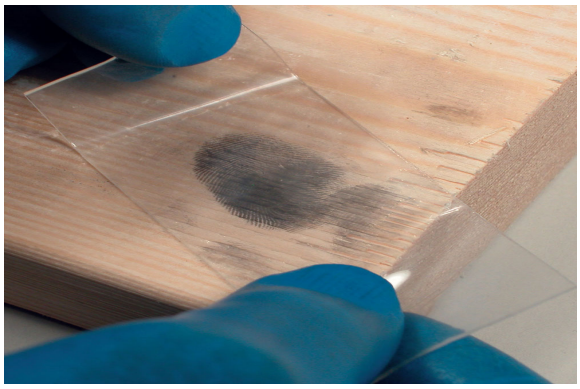

(b) Tape lifting [49]

Figure 2.1: Fingerprint dusting and tape lifting.

Iodine [32] may be used to develop fresh fingerprints on porous, nonporous and nonmetallic surfaces. Developed prints must be photographed quickly since the reaction will rapidly fade away [32]. Iodine may be used before ninhydrin and silver nitrate. Another chemical that needs to be photographed immediately because the reaction time is short is silver nitrate. Silver nitrate reacts with chlorides in the skin secretions to form silver chlorine. Silver nitrate may be used after ninhydrin and iodine. Silver nitrate is not useful on items exposed to water [32].

Ninhydrin is another chemical used to develop latent fingerprints. Ninhydrin produces a purple reaction when reacting with amino acid. This chemical is useful on porous surfaces such as paper. The disadvantage of Ninhydrin is that it takes 10 days to develop the print, but that problem may be solved by applying heat and humidity. Ninhydrin maybe used after ioden and before silver nitrate [32].

Rohatgi *et al.* [6] used a basic fuchsin-based particle reagent formulation to develop latent fingerprints on moist and wet nonporous surfaces. The fingerprints that were developed were clear, sharp and detailed even after 45 days of deposition. The authors state that small particle reagent is cheap and nonhazardous. Experiments were conducted with two formulations i.e. formulation A and formulation B. In formulation A, the suspension of 5 gram of basic zinc carbonate in 75 *ml* distilled water, 100 *mg* basic fuchsin dye and 0.3 *ml* commercial liquid detergent was added. Formulation B is similar to formulation A with the difference that 100 *mg* of crystal violet was added in formulation B. The authors tested the formulations on 3 different nonporous surfaces namely, Metallic spoon, Aluminium foil and glass slide.

After experimenting the authors found that: on all three surfaces, B yielded good results for up to 20 days while composition A managed to develop clear and identifiable fingerprints on all three surfaces for 30 days. Aluminium foil was found to be the most productive surface to develop fingerprints under these conditions while glass was found to be a least productive surface under these conditions. It can be concluded that formulation A is good for developing fingerprints on moist and wet nonporous surfaces 30 days after the deposition.

Robin powder blue is a non-toxic, non-hazardous and environmental friendly product commonly used in post wash as whitening agent. Badiye *et al.* [3] used Robin powder blue to develop latent fingerprints on 20 different surfaces. The powder blue was sprinkled over the surface, covering the latent fingerprints. Excess powder was removed by delicately tapping and by gradually using the brush keeping in mind the end goal of obtaining clear prints. The results observed by the authors were as follows: on black and dark surfaces clear visible ridges were observed. Good results were obtained on multicoloured surfaces, meaning that ridges were clear. The prints were collected by photographing them since they had a very good contrast.

Destructive methods have been used for a very long time, and they work very well in some cases. Their main disadvantage is that different chemicals, dyes or instruments are used to develop fingerprints which contaminates the surface, hindering additional analysis such as touch DNA, drug analysis, etc. Moreover, some surfaces prove very challenging for dusting and tape lifting. Such surfaces include duct tape, heavily grained wood, printed glossy magazines and thin plastic bags [3, 6, 32]. Some chemicals that are used may be toxic and can harm the environment or the person using it and lastly latent fingerprints are fragile, hence when dusting extra caution is required.

2.2 Nondestructive Methods

Forensic science has been moving towards the use of nondestructive techniques to process crime scenes. These methods involve using alternative light source (ALS) to localize the fingerprints from different surfaces. This is then followed by the acquisition of the fingerprint by using a contact-less sensor such as a high resolution digital camera, laser, chromatic white light and reflected ultra violet imaging systems [50]. This section will discuss some of these scanning methods.

2.2.1 Alternative light source

Forensic experts use ALS to localize invisible latent fingerprints. Light has a broad spectrum and light at different wavelengths is able to detect human body secretions such as urine, saliva blood and sebum. Fingerprints are mostly composed of sweat secretions and sebum. These two components contain inorganic ions, proteins, amino acids, water and lipids that react with specific light wavelengths such as UV light, blue light, etc. This is how alternative light sources can be used to locate latent fingerprints.. On Figure 2.2 shows why ALS is used instead of natural light.

Dakshinamurthy *et al.* [52] investigated to find out how long ALS could be used as an effective method for detecting latent prints which have been deposited on the surface over time, by evaluating the quality of the latent fingerprints and identifying the best

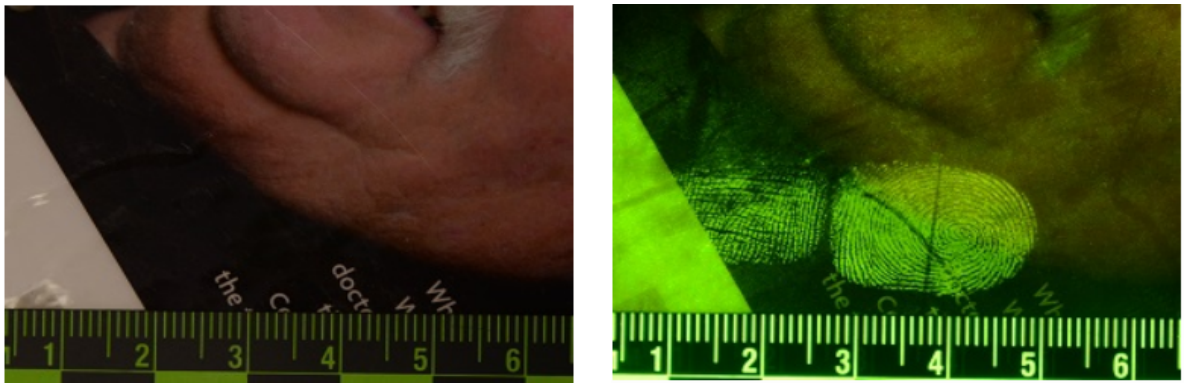

(a) Dusting [51] (b) Tape lifting [51]

Figure 2.2: Latent fingerprint detection by using (a) natural and (b) ALS (near blue light).

light source. The best illumination methods for detecting and photographing the latent fingerprints were identified. To achieve this latent fingerprints were deposited on different materials (including an aluminium utensil, ceramic tile, glass, paper, foam, painted and unpainted wood) and captured immediately. Light sources such as ultraviolet (UV), white light, infrared light (IR) and transmitted light were used. White light, UV and IR were used to detect latent fingerprints at different angles (top angle, oblique angle) while transmitted light was used for surface glass only. Light sources were used to observe and rate the quality of the prints daily for 18 days.

The experimentation results showed that:

- The latent prints were not detectable on the paper, foam, painted wood and unpainted wood surfaces with light sources right from the first day.
- On ceramic tiles, white light was the best light source at the top angle, and white light is better at the oblique angle.
- On a metal surface such as aluminium, white light source and infrared light source were the best, but the infrared light source was better at an oblique angle.
- On the glass surface, at the top angle illumination and transmitted light, the white light source and the infrared light source were the best, but the infrared light source was better at the oblique angle.

2.2.2 Infrared imaging

Infrared cameras are heat sensors that can detect tiny differences in temperature [43]. Lin *et al.* [9] used infrared cameras to visualize different types of forensic evidence. They found that infrared (IR) cameras might be a simple but effective way of searching for latent traces on items at both the scene and in the laboratory. Infrared cameras are not

applicable when the evidence and the background of the evidence (substrate) absorb the IR light.

Crane *et al.* [10] demonstrated the ability of the IR spectroscopy in imaging unprocessed latent fingerprints. IR spectroscopy formed images by analysing the infrared light interacting with a fingerprint. Latent fingerprints were deposited on various porous and nonporous surfaces. The prints were successfully detected by using the IR spectroscope imaging technique. However, the method suffered from slow capturing and immobility.

2.2.3 Ultraviolet imaging

Ultraviolet cameras use light from the ultraviolet (UV) spectrum only [43]. Images taken by this device may reveal structures that are not visible to the human eye. They are cheap, have high capturing speed and have excellent mobility, however the UV light is detrimental to DNA [43].

Saitoh *et al.* [11] investigated fluorescence imaging of fingerprints on a high-grade white paper in the deep UV region with a nanosecond-pulsed Nd-YAG laser system that consisted of a tunable laser and a cooled CCD camera. They found that fluorescence from 255 to 425 nm yielded the best images in an excitation range of 230-280 nm.

2.2.4 Lasers

Dubey *et al.* [4] reported an application of full-filled swept-source OCT for fingerprint identification. The authors modified the conventional OCT by coating the side of the beam with aluminium oxide. This gave the OCT the advantage of having low coherent interferometer. They tested the sensor on a glass substrate by using white fluid and the fingerprint sandwiched between a glass substrate and a cover slip. The first sample was placed at the interferometer arm and the authors observed the interference fringes. The OCT technology was able to acquire the latent fingerprints, proving the concept that OCT can be applied to forensic science.

In cases such as rape, kidnapping and murder criminals may use adhesive tape to tie up victims. Fingerprints may be left on the sticky side of the tape and this can further be complicated when it is a sandwich of tape. Conventional methods would require the tape to be pulled-off and then apply physical or chemical methods to develop and acquire the fingerprints. These methods are complicated and require much time to execute, and it is very likely for whole fingerprint to be destroyed during the attempt to peel-off the tape. OCT is a good candidate to solving this problem. Zhang *et al.* [33] used a custom built time-domain OCT (SD-OCT) system to detect fingerprints underneath different types of tape, namely scotch, electrical and box sealing tape. OCT captured the information

by measuring the back scattered light. The authors demonstrated that OCT eliminated the need to peel-off the tape in order to acquire the fingerprint and it worked fast while preserving the truthfulness of the evidence.

From studies conducted in [4, 33] it is clear that OCT has ability to lift latent fingerprints underneath surfaces or dust. Methods that use chemicals to develop the fingerprint fail in such complex cases.

2.2.5 Other sensors

Evidence scanner (EVISCAN) is a non-invasive automatic latent fingerprint detector system. It combines the latest detector technology with the latest advanced software for digital image processing [53]. Latent fingerprints are scanned, enhanced and preserved in this system. For complex objects the intensity and detector settings can be controlled manually to optimize or achieve the desired results. High quality digital images with resolution of up to 1000 ppi in variety of different formates are produced. It saves reports with case information, overview and output images, logs and even raw data, in secure project file. However, EVISCAN, is a laboratory workstation that is bulky and immobile.

Leich *et al.* [5] investigated the feasibility of using an off-the-shelf chromatic white light (CWL) sensor to acquire latent fingerprints in a nondestructive, contactless manner. They experimented on six forensically relevant surfaces, namely, HDD platter, brushed metal, painted car body, blued metal and veneered plywood. Experiments were conducted to assess the quality of the latent fingerprints acquired from different surfaces. The degradation of the fingerprints was also observed.

The experimentation results showed that:

- On blued metal, latent fingerprints faded within minutes. The authors failed to acquire fingerprints, concluding that latent fingerprints deposited on blued metal surfaces posed a challenge for the CWL sensor.
- On HDD platter, the latent fingerprint was clearly visible after two hours with no significant degradation. The authors concluded that a CWL sensor could acquire high-quality latent fingerprints from HDD platters.
- Latent fingerprints deposited on brushed metal were clearly visible and of good quality with no significant degradation. The authors concluded that a CWL sensor could acquire good quality prints from brushed metal.
- On car bodies, results were highly dependent on the type of paint finish. Prints acquired from non-metallic finish were clearly visible while those acquired from a metallic finishes were barely visible. Authors concluded that the CWL sensor could acquire fingerprints deposited on nonmetallic-finish car bodies.

It can be clearly seen that a CWL sensor serves as a viable latent fingerprint sensor but only works for cases where a fingerprint is visible to the human eye. CWL has not been proven to work on stainless steel, or chrome which are forensically relevant surfaces as most weapons are made of these materials.

2.3 Noise Commonly Found on Images

Any unnecessary alteration of an original image or signal is called noise. It may originate from the hardware of the scanner or the surrounding environment [17]. Noise degrades the quality of an image by interfering with the original signal, which results in variation of pixel values [54]. Different types of noise are known: impulse noise, speckle noise, Gaussian noise etc. Different researchers have developed different techniques to remove these types of noise.

Additive noise occurs when a noise signal is added to the original signal whereas, multiplicative noise occurs when the original signal is multiplied by the noise signal. The additive noise model is much simpler than the multiplicative noise model; therefore the noise may be removed by using different linear filters [54]. Linear filters are, however, not effective at maintaining the edges as the image is blurred [18]. Multiplicative noise is much more complicated than additive noise; therefore the multiplicative noise model is converted to an additive noise model first, before being processed.

2.3.1 Speckle noise

Speckle noise is caused by coherence imaging systems such as OCT, medical ultrasound, active radar etc. It is produced during image acquisition due to the effect of environmental conditions on the imaging sensor, the presence of background noise on the substrate and material refractive index. Speckle noise is signal-dependent, multiplicative in nature and non-Gaussian [54, 55]. Images that contain speckle noise often suffer from low contrast; which hinders further analysis of the image [17]. Multiplicative noise may be modelled as:

$$G(x, y) = F(x, y)n(x, y) \tag{2.1}$$

where the speckle image $G(x, y)$ is the product of the original image $F(x, y)$, and the non-Gaussian noise $n(x, y)$. The indices x, y represent the spatial position over the image.

2.3.2 Gaussian noise

This is an additive noise that has a probability density function of the standard Gaussian distribution. The model of this noise is additive, independent on the signal intensity and independent at each pixel [18, 56]. It is caused by natural sources such as thermal vibration of atoms and the discrete nature of radiation of warm objects [57]. The Gaussian noise is characterized by its probability density function (PDF) with respect to gray values and is defined as:

$$p(g) = \frac{1}{2\sqrt{2\pi}} \exp^{-\frac{(g-\mu)^2}{2\sigma^2}} \tag{2.2}$$

where g, σ and μ represent gray values, standard deviation and mean respectively.

2.3.3 Photon noise

This type of noise is caused by the variation of photons collected by an instrument. These photons are emitted from the incoherent source, and they are distributed according to Poisson distribution [58, 59]. This is true as long as the average intensity is constant over the bandwidth of the instrument [59]. The noise is also called Poisson noise because it obeys Poisson distribution [57]. This noise is presented as:

$$P(k) = \frac{\lambda^k e^{-\lambda}}{k!} \tag{2.3}$$

where λ is the average number of events per interval, e is the Euler's number and $k = 1$, 2, 3, ...

2.3.4 Impulse noise

This type of noise is caused by analogue-to-digital converter errors or bit errors in transmission [60]. The image that contains this type of noise has dark pixels in bright regions and bright pixels in dark regions. For that reason, it is also known as salt and pepper noise. Impulse noise can be eliminated by median filtering and morphological filtering [61, 62]. The intensity value of salt noise is close to 255, and for pepper noise, it is close to 0, and we have:

$$I(i,j) = \begin{cases} 0, & \text{Pepper noise} \\ 255, & \text{Salt noise} \end{cases} \tag{2.4}$$

where $I(i,j)$ represent an image.

2.3.5 Fractal noise

Fractal noise is characterized by its power spectrum that is proportional to the reciprocal of the square of frequency. This means 6dB is dropped per octave. This noise is also called Brownian noise because it resembles Brownian motion and is caused by this motion. Brownian motion is the movement of particles suspended in a fluid. This type of noise can also be generated by integrating white noise [60].

2.3.6 Gamma noise

This type of noise is commonly seen in laser based images. It is called Gamma noise because it resembles Gamma distribution. The noise is characterised by its PDF with respect to gray values; and it is defined as [63]:

$$f = uv \tag{2.5}$$

The noise v follows Gamma distribution

$$p_\eta(v,\theta,k) = \frac{1}{\theta^k \Gamma(k)} v^{(k-1)} e^{(-\frac{v}{y})} \text{ for } v \geq 0$$

where Γ is the usual Gamma-function, θ and k denote the scale and shape parameters in the Gamma distribution, respectively. The mean of η is $k\theta^2$. Now, set a random variable $Y = \frac{1}{\sqrt{\eta}}$, whose probability density function is

$$p_Y(y) = \frac{2}{\theta^k \Gamma(k)} y^{(-2k-1)} e^{(-\frac{1}{\theta y^2})} \text{ for } y \geq 0$$

2.4 Latent Fingerprint Denoising

Denoising or noise reduction is the process of reducing noise from the signal. A signal can be any gesture, action or sound that is used to convey information. Image denoising is necessary for any authentication system to work better. Noise removal on fingerprint images unmasks important details such as minutiae points, and minimizes the processing time for subsequent operations. Various techniques for fingerprint image denoising have been developed [18–21, 64–71]. The denoising techniques are mainly divided into three different groups; spacial-domain, frequency domain and wave-domain filters. Spatial domain filters may be applied direct to the image pixels while in the frequency and wave domains the image is transformed to the frequency domain and wave domain respectively.

The following sections discuss some of the spatial domain, frequency domain and wave-domain denoising techniques used to reduce noise from fingerprint images reported in the literature.

2.4.1 Spatial domain filters

The mean filter, also known as the average filter, is used to reduce the amount of intensity variation between neighbouring pixels. This filter replaces the image pixels by the average of neighbouring pixels [66]. The major drawback of the mean filter is he fact that a single pixel with atypical intensity value can seriously affect the average value of all neighbeighring pixels, therefore the mean filter is not suitable for applications that require sharp edges since it blurs them.
The median filter is a nonlinear edge-preserving filter used in the processing of image denoising and smoothing. It replaces the image pixels with the median value of the neighbouring pixels [66]. The median is calculated by sorting all the neighbouring pixel values in ascending order and then replacing the pixels being considered with the median pixel value.
A Laplacian filter is a two-dimensional isotropic, linear high-pass filter used to enhance the edges of blurred images [67, 68].The Laplacian of an image highlights regions of rapid intensity change and is therefore often used for edge detection. This filter enhances the images by calculating the second derivative of an image. Arif *et al.* [67] used the Laplacian filter to enhance the ridges of fingerprint images. The disadvantage of this Laplacian filter is the fact that it amplifies noise in the darker region while enhancing the edges.

Researchers [69–71] often filter first and then sharpen the image to get better results. Image sharpening is a process of highlighting and extracting fine details from an image and adding this information to the blurred image. There are two sharpening domains: spatial domain image sharpening and frequency domain sharping. The spatial domain includes gray-level transform, histogram, basic spatial filters and unsharp masking. Unsharp masking is a simple process of blurring an image, subtracting the blurred image from

the original and adding the difference to the original image. In the frequency domain, there are many sharpening techniques. These include frequency domain filters such as smoothing filtering and homomorphic filtering [72].

Spatial domain filtering also includes intensity transform techniques such as normalization, contrast stretching and histogram equalization. These types of filter are mainly used as pre-processing for other filters or denoising methods.

2.4.2 Frequency domain filters

Discrete Fourier transform (DFT) is a sampled Fourier transform used to describe the frequency domain of an image. The technique does not contain all frequencies forming an image but only the set of samples which is sufficient to describe the spatial domain fully. This class of technique is mostly used in removing periodic noise [65]. The well-known frequency-domain filter is the Wiener filter. A Weiner filter reduces the noise signal by comparing the received signal with the estimation of the desired noiseless signal.

The Wiener filter needs to know the desired output. For different applications, desired noise removal or image deblurring is achieved by changing different parameters. The problem with the Wiener filter is the fact that the power spectrum of noise and the spectrum of the image have to be estimated. When the blurring filter is singular, the Wiener filtering actually amplifies the noise. Patidar *et al.* [60] investigated how the mean, median and Weiner filter performed with different types of noise (Gaussian, spike, speckle and Poisson noise). The image was subjected to four different noises with a standard deviation of 0.025. After filtering, the authors found that the Wiener filter outperformed the mean and median for all speckle, Poisson and Gaussian noise.

To improve the detection of object contours and region boundaries in natural scenes for gradient-based edge detectors, Qu *et al.* [73] proposed a computational step, frequency domain filtering of gradient image. This computational step was added to the Canny edge detector, thus the concept and effect of the proposed technique were demonstrated. The resulting operator could preserve object contours selectively, and in the meantime, could significantly minimize nonmeaning elements arising from a context texture. Their results showed that the technique was effective and could be implemented as an additional processing stage not only in a Canny operator but in any other gradient based edge detector as well.

Neethu *et al.* [74] presented a Fourier transform based enhancement method. The authors partitioned the fingerprint images into non-overlapping blocks of size (4×4), then each block, S, was transformed to frequency domain by using the fast Fourier transform (FFT). The transformed block S became block F in the frequency domain. In the frequency domain, the noise on block F was filtered by multiplying block F by block $F^{2.2}$. The method produced promising results but there was no evidence that it was better than the existing techniques.

2.4.3 Wave domain techniques

Wave domain techniques transform images from the spatial domain to the wave domain by using wavelet transform. The image is split into four components; approximation and details coefficients. The techniques that make use of wavelet transform for image denoising are discussed.

Yinping *et al.* [75] initiated a wavelet transform adaptive threshold of fingerprint denoising. Their approach used wavelet decomposition based on the Bayesian framework. The image was decomposed up to level three, and it was noted that further decomposition might lead to image distortion. The Daubechies (db4) wavelets of moderate length were used along with soft threshold function to make the noise signal smoother. The authors simulated an experiment to test their technique. In the experiment, fingerprint images of size 256× 256 were subjected to Gaussian noise with standard deviations of (σ = 10, 15, 20). They found that the adaptive threshold enhanced the contrast of ridges, valleys and sweat glands. They also found that the adaptive threshold was better than the soft threshold and the hard threshold in terms of noise removal.

A Gaussian noise reduction technique using stationary wavelet transformation and VisuShrink adjustment was proposed by Sasirekha Sasirekha *et al.* [76]. Their proposed method modified the VisuShrink threshold method (also known as a universal threshold) and median estimator. They replaced the value 2 with the golden ratio value (1.618). They used Daubechies (db2), Symlets (sym4) and db4 wavelet filters. This technique was tested on an FVC2002 [77] fingerprint database. The results showed that the modified universal threshold method, combined with sym4 and db4 for soft and hard thresholding respectively, outperformed the median filter, M3 filter and the traditional universal threshold method.

By using four different wavelet filters, including Haar, db4, Coiflets (coif2) and Biorthogonal (bior3), Iqbal [78] studied stationary wavelet transformation to denoise fingerprint images. For each wavelet, the optimal threshold value was computed by using BayesShrink, VisuShink, NormalShrink and NeighShrink. The techniques were tested on an NIST fingerprint image database [79]. The findings showed that BayesShrink successfully eliminated Gaussian and speckle noise at level 2 when combined with a Haar wavelet filter. Salt-and-pepper noise was removed successfully by NeighShrink combined with a Haar wavelet filter at level 1.

Zaki *et al.* [80] proposed a noise adaptive threshold wavelet transform (NAWT) algorithm for speckle noise removal from fingerprint images which utilised the noise contrast at different wavelet subbands. Their proposed method included image acquisition, wavelet transform, threshold value computation for all subbands, soft thresholding and inverse wavelet transform. The authors used a structureless sample with homogeneous optical properties to estimate the noise signal, and this was done because the speckle noise in OCT images depended on the imaging systems rather than the sample. The method was tested with three different samples, of which two were are not fingerprint images. The

results for the fingerprint sample of the proposed technique outperformed the Gaussian filter (GF) and traditional wavelet transform (WT) by having an SNR value of 20.59 while GF and WT had 18.99 and 17.99 respectively. The traditional WT outperformed NAWT in terms of the parameter (β) which is a correlation coefficient and it quantifies how well the denoised image preserves morphological features of the original image. The value of $\beta = 0.94$ was achieved for WT, which outclassed NAWT and GF by 1% and 4% respectively.

2.5 Fingerprint Ridge Structure Enhancement

This class of enhancement improves texture and contrast of ridges and valleys in the fingerprint image. Normalization, orientation field estimation, Gabor filtering, segmentation, binarization and other methods fall under this category. Ridge structure enhancement is performed after denoising. It helps to define the structure of ridges and valleys, to aid the process of minutiae extraction. This section discusses some of the well-known ridge structure enhancement techniques reported in the literature.

2.5.1 Orientation field estimation

Orientation field estimation is the technique used to enhance global features of a fingerprint image. It describes the local orientation of the ridge-valley structure at each point of the fingerprint image [22]. The orientation field can be used in singular point detection, fingerprint image enhancement and classification [23–25]. Some of the work done on gradient based and pixel-based orientation estimation techniques is reported below.

Wieclaw [81] proposed a technique to estimate the filtering-based orientation field. This technique combined an accurate gradient based method with a resistant to noise pixel based method. The method comprised three steps: normalization, ridge pattern enhancement, and orientation field estimation. Normalization was performed to remove the effect of sensor noise or inconsistency in ridge pattern contrast. Anisotropic Gaussian filter was then used to perform ridge pattern enhancement. Finally the least square method [81–83] was used to the estimated orientation field. The method was tested by using images from the NIST Special Database [79], FVC database samples [84] and a live scanner. The authors found that the method had a 12% lower error level in comparison to the method presented by Hong *et al.* [85]. However, the method was limited to fixed number of 8 discrete reference orientation values and the computational complexity increased proportional to number of references [82].

Kocevar *et al.* [83] presented a two stage fingerprint enhancement technique. In the first stage, anisotropic diffusion was used while oriented local ridge compensation was

applied in the second stage. The first stage was divided into three steps: In step one, the orientation field was computed using a gradient-based method. After computing the orientation field, the image was filtered with an oriented linear anisotropic diffusion which connected disconnected ridges. Lastly, the fingerprint image contrast was improved by using block local normalization. In the second-step enhancement, the fingerprint image was enhanced with an oriented local ridge compensation filter which depended on ridge orientation determined from the image enhanced in the first stage.

Dyre *et al.* [82] proposed a gradient based method for obtaining a reliable fingerprint orientation field. The processing stages are shown in Figure 2.3.

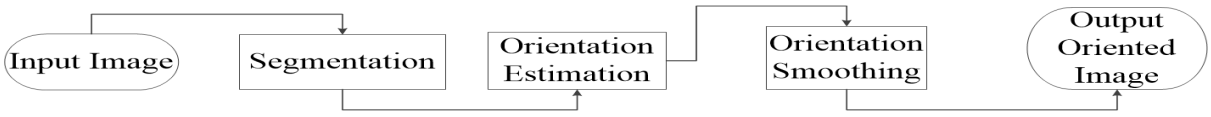

Figure 2.3: Gradient based orientation estimation steps.

In the segmentation step the authors used the mean (M) and variance (VAR) based method for image segmentation [86]. A block size of 8× 8 was used. The variance, $VAR(I)$, and mean, $M(I)$, of the block $w \times w$ in the fingerprint image $I(x, y)$ is given by:

$$M(I) = \frac{1}{w^2} \sum_{x=0}^{w-1} \sum_{y=0}^{w-1} I(x, y) \tag{2.6}$$

$$VAR(I) = \frac{1}{w^2} \sum_{x=0}^{w-1} \sum_{y=0}^{w-1} \Big(I(x, y) - M(I) \Big) \tag{2.7}$$

An 8×8 block size was used to estimate block orientation. The gradient components G_x and G_y were computed by using Sobel convolution mask. The orientation field was then estimated using least square method. For orientation smoothing, the method in [87] based on measure of coherence, was used. Sheba *et al.* [82] found that this method was robust to noise and showed a visibly better orientation field, compared to previous adaptive and nonadaptive gradient based techniques.

2.5.2 Ridge filtering

Ridge filtering is the process of removing unwanted objects from ridges. The major prerequisites for filtering a fingerprint image are ridge orientation and frequency estimations. Ridge orientation estimation is done to obtain the orientation of a fingerprint

image while ridge frequency estimation is done to find the number of ridges within a unit length. This number is then used by Gabor filters to filter the fingerprint image [88].

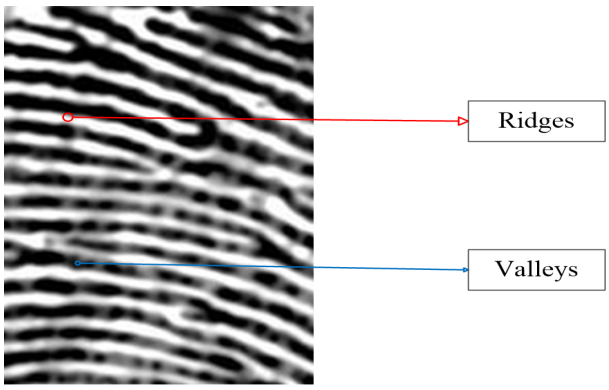

Figure 2.4: Ridges and valleys of a fingerprint.

Ridge frequency
The interdistance measure from the centre of one ridge to the centre of the next ridge in both directions is referred to as ridge frequency distance. The ridge distance, D, is shown in Figure 2.4. The ridge distance is very useful in ridge-filtering techniques such as Gabor [85, 88, 89], but it is very difficult to estimate it due to factors such as noise, fingerprint of the same finger but acquired with different equipment with different resolution, and within the same fingerprint image, different regions may have different ridge distances [88].

Gabor filtering
Ridges and valleys are sinusoidal-shaped waves and change very slowly in a constant local orientation. To remove noise effectively from ridges and valleys, a bandpass filter that is tuned to the corresponding frequency and orientation is required. Hong *et al.* [85] used two-dimensional even-symmetric Gabor filters to remove noise from ridges and valleys of a fingerprint image. However, the technique does not take into account the variations that may occur in the values of the ridge frequency since the standard deviations are fixed to (σ_x and σ_y) a value of 4. To overcome this problem, Thai *et al.* [89] chose the values of the standard deviation to be a function of the ridge parameter. This allowed the technique to specify standard deviation values according to the local ridge frequency.

2.5.3 Segmentation

Image segmentation is the process of segregating a digital image into multiple fragments of group pixels [90]. The aim of segmenting the image is to change the presentation of an image into something that is easier to analyse. Researchers have developed many segmentation algorithms, but it is very difficult to find a segmentation algorithm that works for all cases [91].

Direction total variation
Nimkar *et al.* [1] investigated and compared segmentation algorithms in terms of their measuring parameters, computational complexities, limitations, application and their advantages. The authors found that the algorithms could not handle and process latent fingerprints better, except for the directional total variation model. Krishna *et al.* [92] investigated segmentation algorithm in terms of execution time, accuracy and other important features. They also found that direction total variation performed better for latent fingerprints than other methods.

Thresholding
Threshold segmentation is the basic method of image segmentation. The gray scale information is directly divided based on the value of different targets [91]. The advantage of using this method is the fact that the calculation is elementary and the speed of segmenting is faster, it works very well when the contrast between the target and background is high. The drawback of threshold method is the fact that it is very difficult to get results if the contrast between the target and background is very low. The method is often combined with other methods since it is very sensitive to noise.

The Otsu segmentation method is an example of a global thresholding method. It seeks out the threshold value whenever the sum of foreground and background is at its minimum [93]. The image is segmented into two, light and dark regions [94]. Otsu's thresholding strategy checks all the conceivable thresholding values and calculates the least value of the threshold by using the statistical information of the image [94]. For a chosen value of threshold, T, the variance of clusters, either 0 or 1, is calculated by minimizing the weighted sum of groups of variances [93, 94].

Region-growing segmentation
In a region-growing segmentation, pixels with the same or similar properties are grouped together to form a region [95]. Initial seed points are selected and segmentation identifies neighbouring pixels of initial seeds and checks whether the pixel neighbours should be added to the region. The choice of pixel is very crucial in this method since the region is formed by the pixels that are similar to the pixel of choice. Region-growing segmentation separates the connected regions with same characteristics and provides some good boundary information and segmentation results.

2.5.4 Binarization

Binarization is the process of converting image pixel values to binary values. A threshold pixel value is used to binarize the image into light and dark pixels of 1's and 0's (0 and 255 for display) respectively. Images can be binarized locally or globally. In global binarization a single threshold value is used to binarize the image whilst in local binarization, a threshold value is calculated locally region by region [93]. An example of a global thresholding method is the fixed thresholding method. In the fixed-thresholding

method, the threshold value, T, is used to assign 0's and 1's to all pixels in a given image, f [93]. The resulting binary image, G, is then defined as:

$$G(x,y) = \begin{cases} 1, & \text{if f(x,y)} \geq T \\ 0, & \text{if f(x,y)}<T \end{cases}, \tag{2.8}$$

where, $f(x,y)$ is the value of a pixel in grayscale image. The output of fixed thresholding method depends heavily on the value of the threshold, T, chosen. Different images have different optimal threshold values; hence this is a shortfall of the method since it is very difficult to decide on the optimal threshold value for all the images [93]. Local binarization methods perform better than global binarization with images that are blurry, have low resolution, bad shading and non-uniform illumination. An example of a local binarization method is adaptive binarization, which use a window of $N \times N$ slides over the entire image [93]. A local threshold is computed for each local region under the window using the Niblack, Sauvola, Bernsen method [93].

2.6 Quality Estimation

Fingerprint image quality score may be defined as an expression of the usefulness or predicted performance of the biometric system. A good quality fingerprint image has sufficient minutiae points which are useful in the matching process [96]. This section discusses some of the techniques used to predict the quality of fingerprint images.

2.6.1 Quality estimation based on local features

In this class of quality estimation, the image is divided into non-overlapping square blocks and features are extracted from each block. Blocks near the centroid are usually of good quality, and therefore some methods assign different weights to each block. Local features such as local orientation quality (LOQ), ridge frequency and texture which can indicate fingerprint quality are discussed below [27].

Local orientation quality
Clear local orientations indicate good-quality image. LOQ may be computed in just three steps [27–29]:

Step 1: Sub-block partitioning.
Each subblock is divided into four quadrants as shown in Figure 2.5. After dividing, the absolute orientation difference of these four quadrants is calculated in a clockwise direction. Since the orientation flow in a block is gradually changed, the absolute orientation is slightly greater than zero.

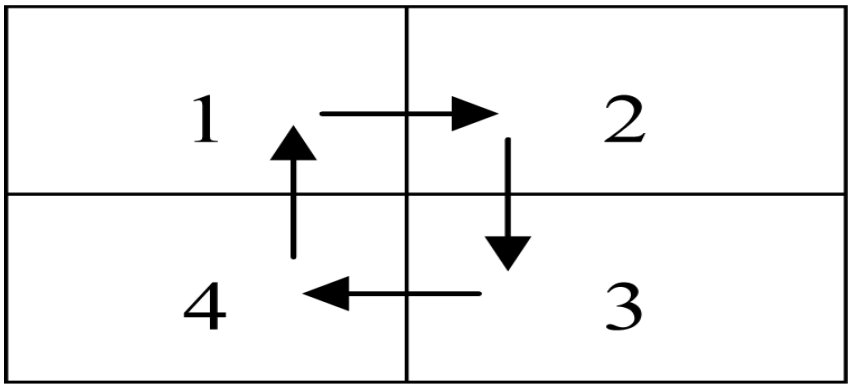

Figure 2.5: Quadrants of the original LOQ measure (taken from [27]).

Step 2: Compute the local orientation quality.
The absolute orientation change of a block should not be greater than 8 degrees otherwise the block is believed to be an invalid curvature change. The local orientation quality is then obtained by summing the four quadrants. In other words, the local orientation quality at the position (i, j), $loq_1(i, j)$ is obtained as follows:

$$loq_1(i, j) = O_{12} + O_{23} + O_{34} + O_{41} \tag{2.9}$$

where,

$$O_{mn} = \begin{cases} 1, & |ori(m) - ori(n)| \leq 8^\circ \\ 0, & |ori(m) - ori(n)| > 8^\circ \end{cases} \tag{2.10}$$

Step 3: Preliminary local orientation computation.
Image LOQ value is then calculated as a change of blocks with $M \times N$ blocks:

$$LOQ_1 = \sum_{i=1}^{M} \sum_{j=1}^{N} loq_1(i, j) \tag{2.11}$$

where $ori(m)$ is the orientation value at quadrant m.

2.6.2 Quality estimation based on global features

Global-feature based techniques examine the whole image and calculate the global quality based on features extracted [27, 29].

Consistency measure
Sudden direction changes between blocks are gathered and mapped into a global direction

score. For high-quality image, ridge directions change smoothly across the whole image. The orientation changes that disobey the smooth trend are gathered by examining the orientation change along each horizontal row and the vertical column of the image block. Changes that disobey the smooth curve are mapped into a global orientation score [27, 29]. The highest score of the global orientation is 1, and the lowest is 0.

2.6.3 Quality measure based on classifier

Classifier-based techniques define the quality measure as the difference between a match and non-match percentage of a given fingerprint image. It predicts the matcher performance before a matcher algorithm is applied [27, 29].

2.7 Summary

Destructive methods have been used for a long time, and they work very well in some cases. Their main disadvantage is the fact that different chemicals, dyes or instruments are used to develop fingerprints which contaminates the sample and hinder possible secondary analysis such as touch DNA, drug analysis, etc. Furthermore, some surfaces prove very challenging for dusting and tape lifting. Such surfaces include duct tape, heavily grained wood, printed glossy magazines and thin plastic bags. Some chemicals that are used may be toxic and can harm the environment or the person using them, and lastly, latent fingerprints are fragile, hence when dusting, extra caution is required.

Nondestructive methods of acquiring fingerprints are advantageous compared to destructive methods. In non–destructive methods fingerprints can be acquired without making any physical contact with the substrate. This allows the sample to be further analysed for touch DNA (provided the type of sensor used is not detrimental to DNA), drug use or any other analysis. The devices that acquire fingerprints contactless have both advantages and disadvantages. The OCT machine is one of the contactless device. It produces high resolution 3D images and it also has the ability to penetrate deeper into the substrate. The drawback of this method is the fact that the images produced are noisy and require advanced enhancement techniques to remove the noise.

Latent fingerprints image often suffer from poor ridge quality due to their very nature when they are left inadvertently on surfaces with which a hand comes into contact. As a result, the crucial information from an image may not be seen. For both destructive and non–destructive methods of lifting latent fingerprints, enhancement is the pre–processing stage. Researchers have proposed ways to enhancing the images of latent fingerprints [75, 85, 91, 97]. There is still a huge debate about methods that can enhance all types of image, as revealed by current literature.

Chapter 3

Fingerprint Image Denoising

3.1 Introduction

This chapter presents the proposed wavelet transform based denoising technique. Section 3.2 presents the background to the proposed method. In Section 3.2.1, we discuss continuous wavelet transform, discrete wavelet transform and stationary wavelet transform. The existing shrinkage schemes and shrinkage rules are discussed in Sections 3.2.3 and 3.2.4 respectively. In Section 3.3, the proposed denoising technique for OCT images of latent fingerprints is discussed, Section 3.4 presents the segmentation technique adopted in this work and Section 3.5 concludes the chapter.

3.2 Background to the Proposed Method

Latent fingerprints are fingerprint impressions left on the surfaces with which a finger comes into contact. This type of fingerprint is formed by the natural secretion of sweat from eccrine glands that are present in the friction ridges. They can also be made by artificial means such as touching ink, dye or any other substances transferred from ridges on the finger to a surface. They are often acquired by using different techniques [3, 6, 9–11, 32, 53]. In this work, OCT technology is used to acquire latent fingerprint images from various surfaces. However, the images acquired by using OCT often suffer from speckle noise. The speckle noise may be removed by denoising the images. The wavelet-based techniques offer a promising solution for speckle noise removal according to literature [75, 76, 78, 80]. The proposed denoising procedure of this work is illustrated in Figure 3.2 and is the subset of the whole enhancement technique. The full enhancement process is shown in Figure 3.1; this chapter will address the denoising process shown in Figure 3.2.

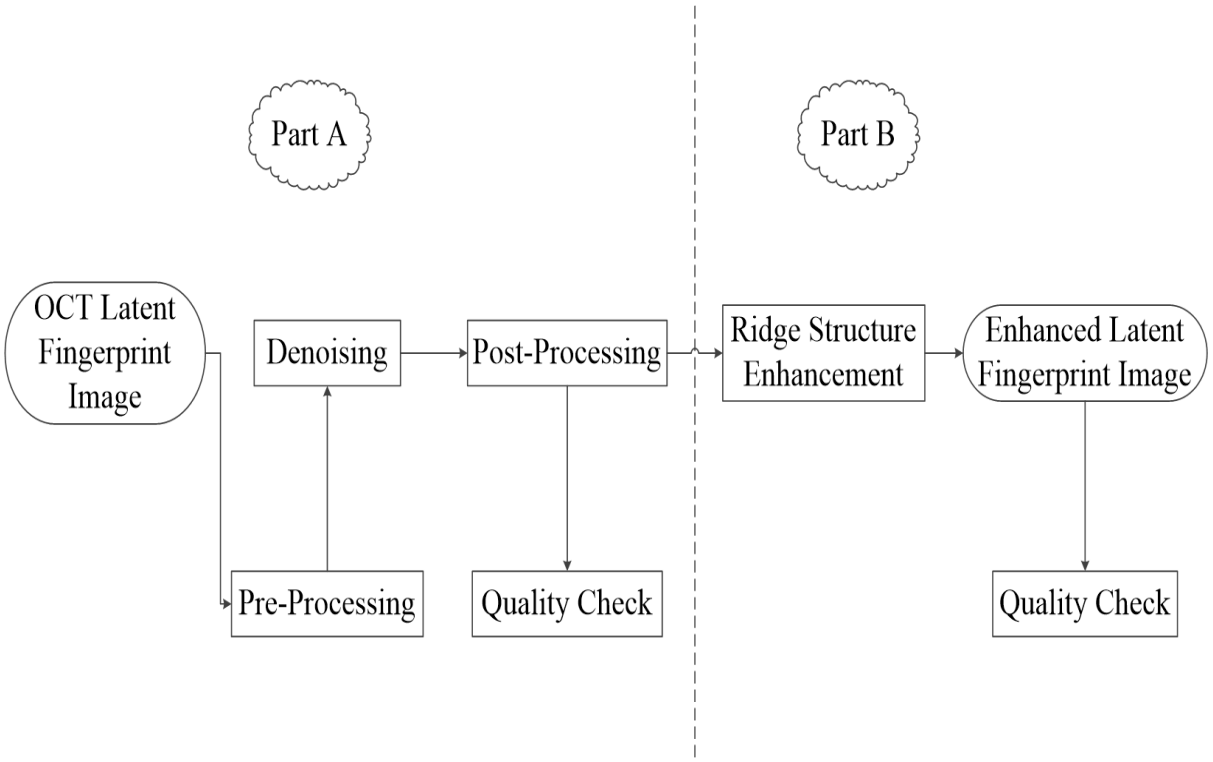

Figure 3.1: Proposed OCT latent fingerprint image enhancement

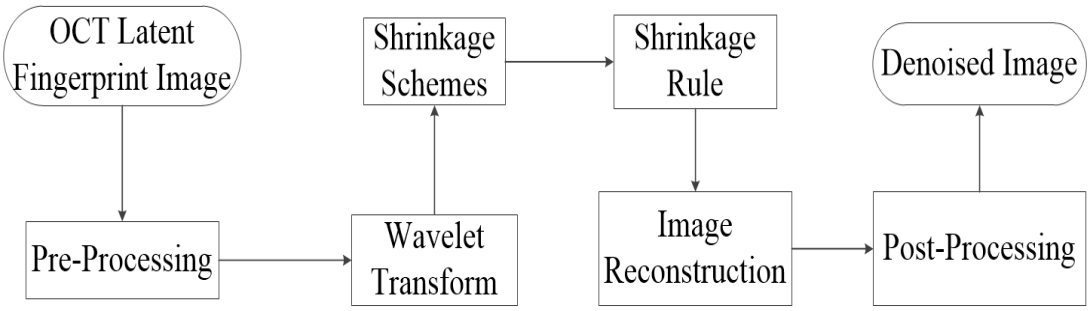

Figure 3.2: Proposed OCT latent fingerprint image denoising

3.2.1 Wavelet transform

A wavelet transform is a mathematical tool that decomposes a signal into a representation that shows signal details and trends as a function of time. There are various wavelet transforms and they include the continuous wavelet transform (CWT), the discrete wavelet transform (DWT) and the stationary wavelet transform (SWT) [98–101].

3.2.1.1 Continuous wavelet transform

The continuous wavelet transform (CWT) is a formal tool that provides an over-complete representation of a signal by letting the translation and scale parameters of the wavelets

vary continuously. Given a wavelet $\psi(t)$, the CWT of the function $f(t)$ (assuming that $f \in L^2(\mathbb{R})$) is defined as:

$$CWT(a,b) = \frac{1}{\sqrt{a}} \int_{-\infty}^{\infty} \psi\left(\frac{t-b}{a}\right) f(t)dt \tag{3.1}$$

where t is the time, a is the scale or dilation parameter which corresponds to frequency information and b is associated with the location of the wavelet function as it is shifted through the signal; therefore it corresponds with the time information in the transformation [57, 101]. The CWT is mostly used for the damping ratio of oscillating signals. The drawback of this transform is that it can not solve differential equations [101] and since a & b are continuous over L the representation of the signal is often redundant.

3.2.1.2 Discrete wavelet transform

The discrete wavelet transform (DWT) may be defined as a signal decomposition in a set of independent, spatially oriented frequency channels. The signal is convolved with low and high pass filters and produces two signals known as an approximation and details. This process is called decomposition or analysis. Decomposition is achieved by combinations of down-sampling and up-sampling as shown in Figure 3.3. In the DWT $a = 2^{-m}$ and $b = n2^{-m}$, where m and n are positive integers. The $DWT_\psi f(m,n)$ is defined as,

$$DWT_\psi f(m,n) = \int_{-\infty}^{\infty} f(t)2^{-m}\psi(2^m t - n)dt \tag{3.2}$$

where $2^{-m}\psi(2^m t - n)$ is the dilated and translated version of the mother wavelet $\psi(t)$. DWT is mostly used in image denoising, compression and classification [101]. The inverse DWT (IDWT) may be applied to assemble back the approximation and details to the original signal without any loss of information. This process is known as reconstruction or synthesis. The DWT is found almost everywhere in signal-processing applications. However, it has an inefficiency of not being translationally invariant. This problem is due to the down-sampling [100, 103] as shown in Figure 3.3.

3.2.1.3 Stationary wavelet transform

The stationary wavelet transform is the better version of the DWT. It was designed to overcome the shortfalls of DWT. The removal of down-samplers and up-samplers on DWT gave birth to SWT, which is translation invariant. The translational invariance is achieved by removing up-samplers and down-samplers in the DWT and up-sampling the

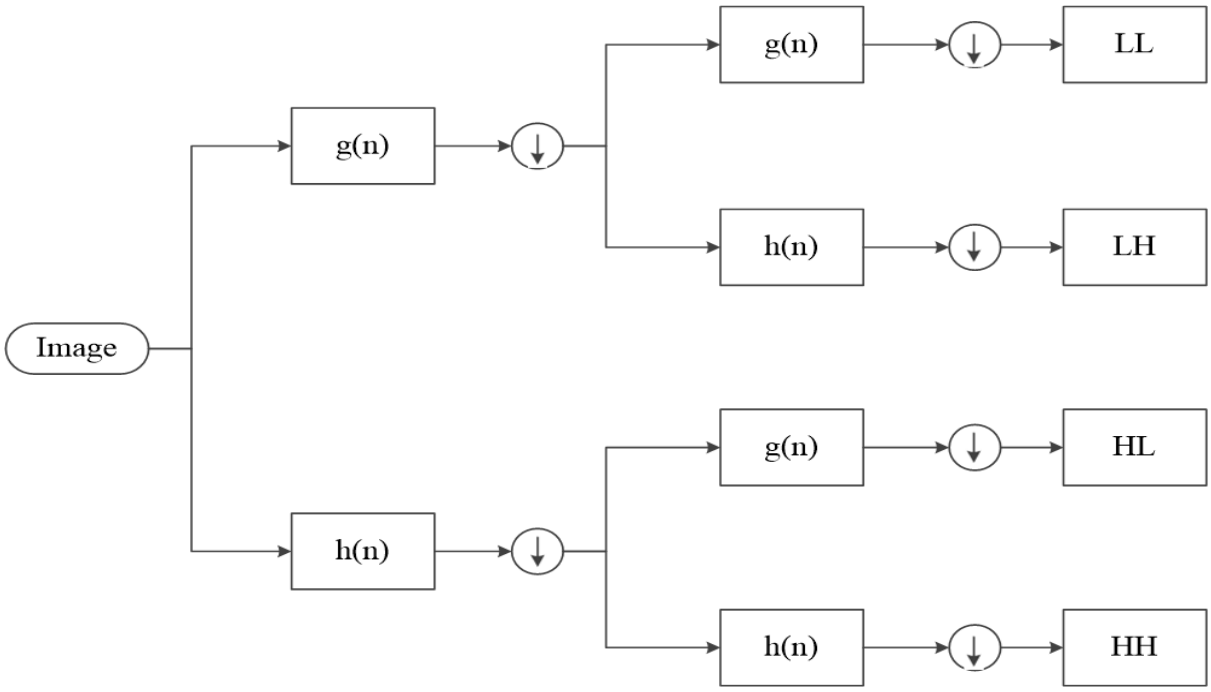

Figure 3.3: Discrete wavelet transform decomposition where $g(n)$ is the low-pass filter, $h(n)$ represents the high-pass filter. LLs represent the approximation and (LH, HL and HH) represents the detail coefficients (taken from [102]).

filter coefficients by $2^{(m-1)}$ in a^{th} level of the SWT algorithm. The algorithm is illustrated in Figure 3.4.

Different names such as redundant discrete wavelet transform, un-decimated discrete wavelet transform, over-complete wavelet transform have been given to SWT [100, 104–106]. These names come from the fact that the output of SWT contains the same number of samples as the input, therefore for a decomposition of N levels there is a redundancy of N in the wavelet coefficients.

3.2.1.4 Wavelet decomposition

If an image is convolved with a low-pass and a high-pass filter in the vertical and horizontal direction respectively, four sub-images of the original image are formed [75]. The sub-images encompass the full image, but at different resolutions and containing different components of the original image. This includes a sub-image of low frequency in both the horizontal and vertical directions (LL), sub-image with low horizontal frequency but high vertical frequency (LH), sub-image with high horizontal frequency but low vertical frequency (HL) and (HH) which has a high frequency in both the horizontal and vertical directions. Figure 3.5a shows the decomposition skeleton of the image up to level 2, where LL is the approximation image, HL, LH and HH represent image details in the horizontal, vertical and diagonal direction respectively, the subscript represents the decomposition level. The fingerprint image in Figure 3.5b taken from NIST database [79]

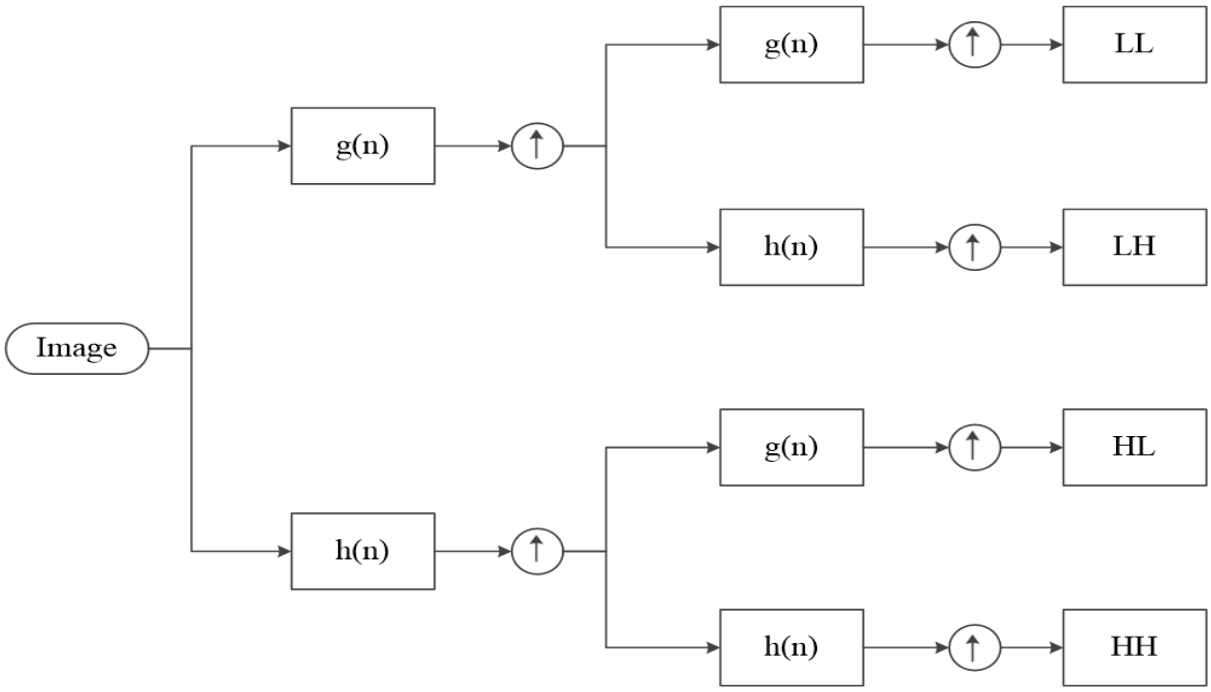

Figure 3.4: Stationary wavelet transform where $h(n)$ is the high-pass filter and $g(n)$ is the low-pass filter.

was decomposed up to level 2 by using DWT combined with *haar* wavelet. The image may be decomposed by using either the conventional DWT or the Stationary Wavelet Transform (SWT). In this work, the two well-known wavelet transforms (DWT and SWT) are used.

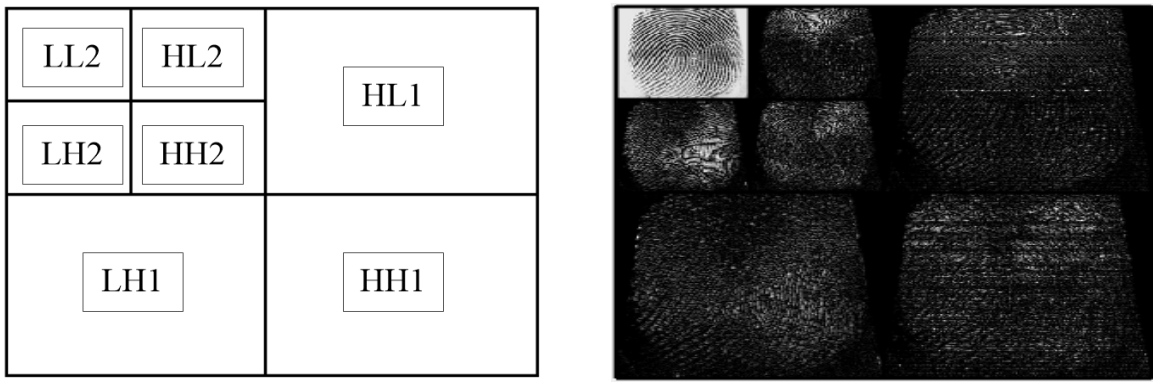

(a) (b)

Figure 3.5: (a) Image wavelet decomposition. (b) Actual fingerprint image decomposed up to level 2. The fingerprint image was obtained from the NIST online database [79].

3.2.2 Wavelets

A wavelet (or a wavelet filter) is the rapidly decaying wave-like oscillation that has zero mean and has a finite duration. Unlike Fourier transform, wavelets provide analysis of a

signal which is localized in both time and frequency. To decompose an image by using the wavelet transform, a wavelet filter is required. The signal is decomposed by using the chosen wavelet filter. This section describes some of the wavelet filters used in this work and Figure 3.6 shows their shapes.

Haar wavelet
The Haar wavelet is the oldest, simplest and the prototype of all wavelets. It is defined as the sequence of rescaled functions which together form a wavelet family. The Haar wavelet decomposes the discrete signal into two sub-signals of its half-length. The advantage of the Haar wavelet is the fact that it is memory efficient, fast and conceptually simple [98, 107, 108].

Daubechies wavelets
The Daubechies family was first described by the Belgian physicist Ingrid Daubechies. This family of wavelets is the first to have a set of scaling functions which are orthogonal. A Daubechies wavelet, ψ, has finite vanishing moments p that generate an orthonormal basis of L^2, then it has a support of a size larger than or equal to $2p-1$. The minimum size support of Daubechies is $[-p, 2p-1]$. When $p = 1$ we get the Haar wavelet. Daubechies wavelets are very useful in noise removal and compression [98, 108].

Symlets and Coiflets wavelets
The Symlets and Coiflets wavelets are nearly symmetrical wavelets which are similar to the Daubechies family. Coiflets wavelet functions have $\frac{p}{3}$ vanishing moments and scaling functions of $(\frac{p}{3} - 1)$, where p is an integer [108].

Biorthogonal wavelet
The Biorthogonal wavelet is the wavelet family where the associated wavelet transform is said to be invertible but not necessarily orthogonal. This wavelet uses one base function for decomposition and the other for reconstruction [108].

3.2.3 Shrinkage schemes

The technique of partitioning an image into the background and foreground is referred to as the image thresholding [109]. It is simple and mostly used whenever two regions need to be classified or distinguished. In wavelet transform, thresholding is done on one wavelet coefficient at a time [109]. Each coefficient is compared to the threshold value, depending on the shrinkage schemes, which are soft, hard or firm thresholding. All coefficients in hard thresholding are either zero or greater-or-equal to the threshold value, as shown in equation (3.3) [101, 110].

$$f(x)_h = \begin{cases} x, & \text{for } |x| \geq T \\ 0, & \text{for } |x| < T \end{cases}, \tag{3.3}$$

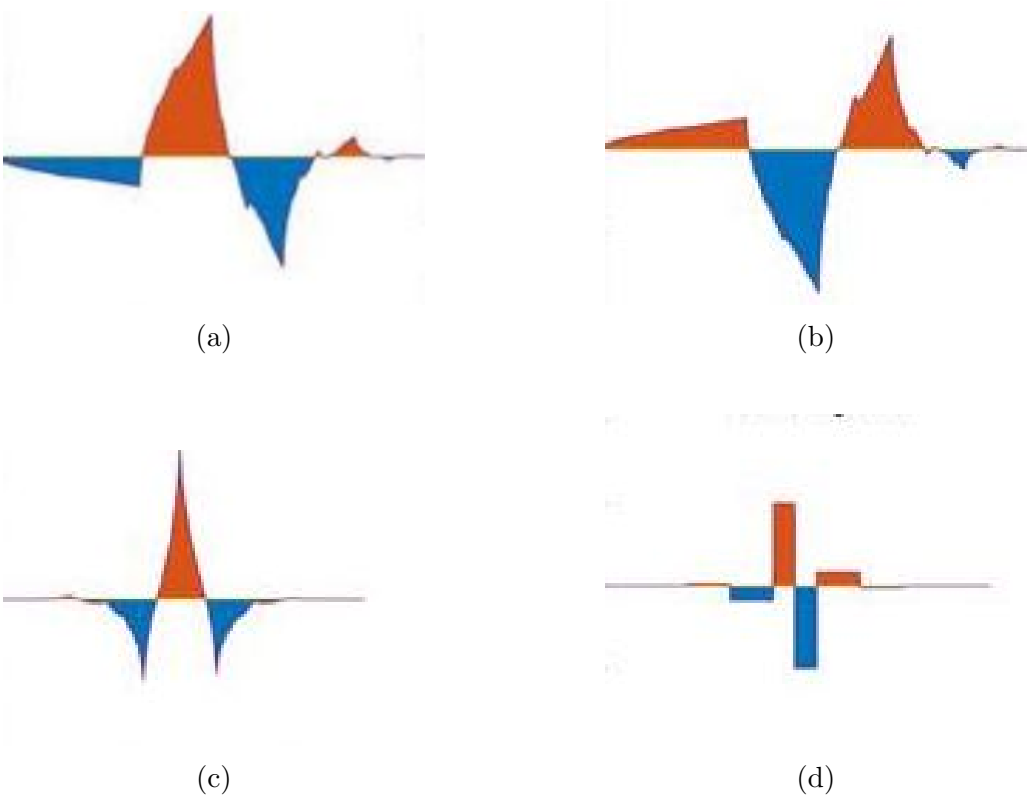

(a) (b)

(c) (d)

Figure 3.6: Different wavelets families. (a) Daubechies (b) Symlets (c) Coilets and (d) Biorthogonal.

where the threshold value is represented by, T. Wavelet coefficients are reduced to a threshold value for soft thresholding, or killed, as shown in equation (3.4) [101, 110].

$$f(x)_s = \begin{cases} sign\{x\}(|x| - T), & \text{for } |x| \geq T \\ 0, & \text{for } |x| < T \end{cases} \tag{3.4}$$

Firm thresholding requires two thresholds, a lower threshold T_1 and an upper threshold T_2 where T_2 is estimated to be twice the value of the lower threshold T_1 , *i.e* $T_2 = 2T_1$. Then firm thresholding is presented by:

$$f(x)_f = \begin{cases} 0, & \text{for } |x| \leq T_2 \\ sign\{x\}\frac{T_2(|x|-T_1)}{T_2-T_1}, & \text{for } T_1 < |x| \leq T_2 \\ x, & \text{for } |x| > T_2 \end{cases} \tag{3.5}$$

These methods are used to find the optimal threshold value, as the denoising algorithm's output is regulated by it. Different researchers have used thresholding techniques such as VisuShrink, BayesShrink, NeighShrink and NormalShrink [78, 110, 111] for image denoising.

3.2.4 Shrinkage rules

A wavelet denoising algorithm is an algorithm used to suppress noise from the image signal. This algorithm often has a unique way of computing an optimal threshold for each wavelet's detail coefficients (LH, HL and HH). That unique way of computing an optimal threshold is known as the shrinkage rule. This section presents universal shrinkage, Bayesian shrinkage, normal shrinkage, modified universal threshold and Yinping adaptive threshold shrinkage.

3.2.4.1 Universal threshold

Universal threshold, also known as VisuShrink is the thresholding technique which does not minimize the mean square error but picks an optimal threshold nearby. The universal threshold is computed from the diagonal subband HH1 as,

$$\sigma = \frac{median|HH1|}{0.6745} \tag{3.6}$$

The actual threshold value is calculated as:

$$T = \sigma\sqrt{2logM}, \tag{3.7}$$

where M is the number of pixels in an image. The universal threshold is unable to remove multiplicative noise, such as speckle noise.

3.2.4.2 Bayesian shrinkage

Bayesian shrinkage (BayesShrink) is a subband-dependent threshold. This means that at each subband and decomposition level a threshold is computed [65, 78]. The Bayesian threshold is computed as:

$$T = \frac{\sigma^2}{\sigma_s}, \tag{3.8}$$

where σ^2 is noise variance presented by equation (3.6) and σ_s is the variance of noise-free image. Since the noise and the signal are mutually independent, their variance is modelled as:

$$\sigma_s = \sigma_y - \sigma \tag{3.9}$$

where σ_y is computed as,

$$\sigma_y^2 = \frac{1}{M}\sum_{i=1}^{M}\sum_{j=1}^{M} I(i,j)^2, \tag{3.10}$$

where M is the number of pixels in image I. Then σ_s on equation (3.8) is computed as

$$\sigma_s = \sqrt{(max(\sigma_y^2 - \sigma^2), 0)} \tag{3.11}$$

3.2.4.3 Stein's unbiased risk estimator shrinkage

Stein's Unbiased Risk Estimator Shrinkage (SUREShrink) applies thresholding by applying a subband adaptive threshold. An optimal threshold is computed separately for each detail of the subband based upon Stein's Unbiased Risk Estimator (SURE) [101, 112]. The optimal threshold at level k with soft thresholding is defined as:

$$t_k^s = argmin_t SURE(t; x) \tag{3.12}$$

where t_k^s is estimated from decomposition coefficients and x is the set of noisy wavelet coefficients in a subband.

3.2.4.4 Normal shrinkage

Normal shrinkage (NormalShrink) technique is a wavelet domain denoising method based on the generalized Gaussian distribution subband coefficients modelling [65]. The threshold value of NormalShrink is defined as,

$$T = \beta\frac{\sigma^2}{\sigma_y}, \tag{3.13}$$

where σ^2 is the noise variance given by equation (3.6). The σ_y is the standard deviation of the noisy image signal, which is computed by using equation (3.10). The β constant is the scale parameter which is computed as,

$$\beta = \sqrt{log\left(\frac{L_k}{J}\right)}, \tag{3.14}$$

where L_k is the length of subband and J is the total number of decomposition levels. The NormalShrink technique outperforms both Bayesian shrinkage and universal threshold noise removal techniques, and it preserves edges efficiently [113].

3.2.4.5 Yinping adaptive threshold shrinkage

Yinping *et al.* [75] proposed an adaptive threshold method based on the wavelet transform for fingerprint denoising.

3.2.4.5.1 Threshold value computation:

Their proposed method uses the same principles of wavelet decomposition. The difference is in the way the threshold value T is computed. The threshold value, T, is critical when using wavelets. Traditionally, BayesShrink and VisuShrink are used to compute the optimal threshold. The universal threshold is given by:

$$T = \sigma\sqrt{2logN}, \tag{3.15}$$

where σ, is the noise standard deviation and N is the number of high frequency coefficients found by applying a discrete wavelet transform (DWT) to an image. The BayesShrink threshold is defined as follows:

$$T = \frac{\sigma^2_{noise}}{\sigma_{signal}}, \tag{3.16}$$

where σ^2_{noise}, is the estimate of the noise signal variance and the estimation of the standard deviation of an image is σ_{signal}.

Based on BayesShrink and VisuShrink threshold, Yinping *et al.* [75] defined an adaptive threshold shrink, which computed an adaptive threshold of different sub-images (LL) by using the different directions of coefficient details (LH, HL, HH). These were achieved as follows:

Let the original image be represented by $F(x, y)$ where $x, y = 1, 2, \ldots, M$. The image

corrupted by noise is defined as:

$$G(x, y) = F(x, y) + \Phi(x, y), \tag{3.17}$$

where $\Phi(x, y)$ is the noise function. Applying the wavelet transform, the function of the corrupted image becomes:

$$W_G = W_F + W_\Phi, \tag{3.18}$$

where W_G, W_F and W_N are the wavelet coefficients of the image containing noise, the original image and noise signal respectively. The standard deviation of the noise signal coefficients is estimated by using the median estimator with diagonal detail coefficients (HH) as follows:

$$\sigma_{W_\Phi} = \frac{median(|HH_i|)}{0.6745}, \tag{3.19}$$

where $i = 1, 2, ..., k$ k represents wavelet decomposition layers. The signal variance of the image containing noise is computed using the coefficients of each direction detail. These coefficients are as follows:

let $D = 1, 2, 3$ represent horizontal, vertical and diagonal details respectively, then, $W_G(1, i) \in LH_i$, $W_G(2, i) \in HL_i$ and $W_G(3, i) \in HH_i$. These direction details are used to estimate the noisy $(G(x, y))$ image signal noise variance by the following equation:

$$\sigma^2_{W_G}(D, i) = \frac{1}{N(i)^2} \sum_{x=1}^{N(i)} \sum_{y=1}^{N(i)} W_G(D, i), \tag{3.20}$$

Analogously, in terms of variance, the noisy image is defined as,

$$\sigma^2_{W_G} = \sigma^2_{W_F} + \sigma^2_{W_\Phi}, \tag{3.21}$$

where $\sigma^2_{W_\Phi}$ and $\sigma^2_{W_F}$ represent the variance of the noise and original signals, respectively. The variance of the original image is then defined as:

$$\sigma_{W_F}(D, i) = \sqrt{max(\sigma^2_{W_G}(D, i) - \sigma^2_{W_\Phi}(i), 0)}, \tag{3.22}$$

where $\sigma^2_{W_\Phi}(i)$ is noise in different layers. Finally, the adaptive threshold Shrink is given by:

$$T(D,i) = \begin{cases} \frac{\sigma^2_{W_\Phi}(i)}{\sigma_{W_F}(D,i)} & \text{if } \sigma_{W_F}(D,i) \neq 0 \\ max(W_G(D,i)) & \text{if } \sigma_{W_F}(D,i) = 0 \end{cases} \tag{3.23}$$

Algorithm 1: The Yinping denoising procedure.

Input: Noisy fingerprint image.
Output: Denoised image.

i. Decompose the noisy image by using forward DWT.
   a. Estimate the noise signal standard deviation (σ_{W_Φ}), by using HH_i coefficients ($i = 1, 2, \ldots, k$).
   b. Calculate the variance ($\sigma^2_{W_G}$) of the noisy image.
   c. Calculate the standard deviation (σ_{W_F}) of the original image.
ii. Threshold the wavelet coefficients in detail subband by using the Yinping adaptive threshold shrinkage (equation 3.23).
iii. Reconstruct by using IDWT to get the denoised image.
iv. Assess the performance by using image metrics quality to measure peak signal-to-noise ratio (PSNR).

3.3 Proposed Improved Denoising Technique

The adaptive threshold shrinkage method [75] is modified by using the β constant from NormalShrink, and the noise variance estimated from the diagonal subband details (HH) is computed by using (3.19). The block diagram of the proposed method is shown in Figure 3.7.

The threshold value in (3.23) is multiplied by the constant β defined in (3.14), then the threshold value is computed as:

$$T = \begin{cases} \beta_i \left(\frac{\sigma^2_{W_\Phi}(i)}{\sigma_{W_F}(D,i)} \right) & \text{if } \sigma_{W_F}(D,i) \neq 0 \\ \beta_i(max(W_{x,y}(D,i))) & \text{if } \sigma_{W_F}(D,i) = 0 \end{cases}, \tag{3.24}$$

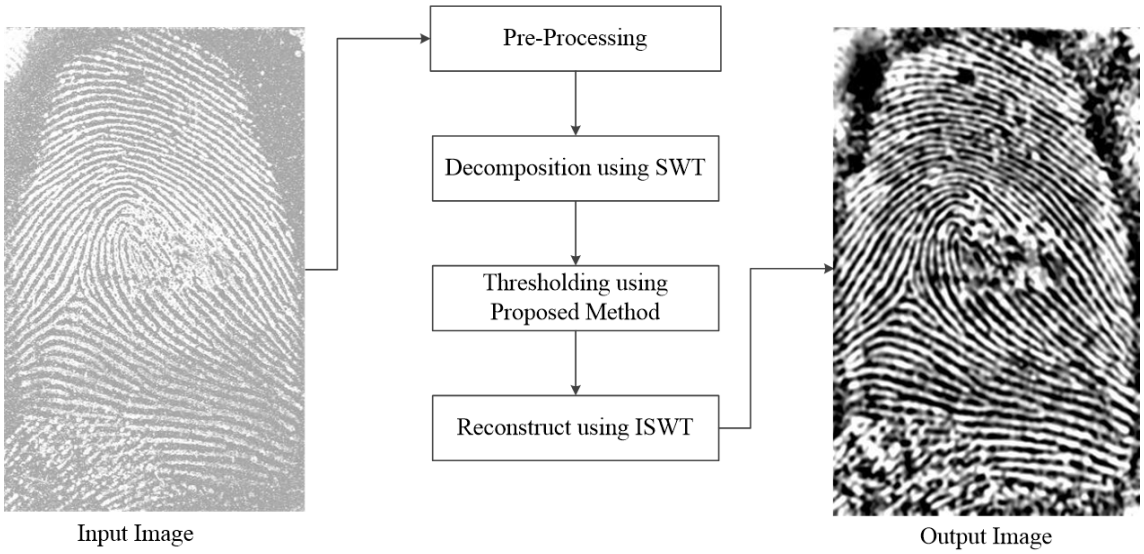

Figure 3.7: The basic structure of the proposed wavelet transform-based OCT latent fingerprint image denoising technique.

After calculating the noise variance, the new modified adaptive threshold is applied to the noisy OCT latent fingerprint image. The procedure is outlined in algorithm 2.

Algorithm 2: Image denoising.

1: **Input:** Noisy OCT latent fingerprint image; **Output:** Denoised image;
2: Decompose the noisy image by using forward SWT.

   i. Estimate the noise signal standard deviation by using (3.19).

   ii. Calculate the variance ($\sigma^2_{W_G}(D,i)$) of the noisy image.

   iii. Calculate the standard deviation ($\sigma_{W_F}(D,i)$) of the original image.

3: Threshold the wavelet coefficients in detail subband by using the proposed method (equation 3.24).
4: Reconstruct by using inverse SWT to get the denoised image.
5: Assess the performance by using image metrics quality measures (PSNR, SNR and RMSE).

3.4 Segmentation

Segmentation is the process of partitioning an image into a set of different regions. A good segmentation technique reduces processing time and removes many spurious minutia points. In this work, the morphological segmentation technique described in [114] was used.

3.4.1 Morphological operations

In image processing, morphology refers to the set of image-processing operations that process shape-based images. In a morphological operation, the value of each pixel in the output image is based on a comparison of the corresponding pixel in the input image with its neighbours. [114, 115]. Morphological operation is a non-linear shape-oriented technique that uses a 3D Structural Element (SE). A SE is a matrix used to spot the image pixel being processed and defines the neighbourhood used in the processing of each pixel in an image. The SE matrix is made up of 1's and 0's that can have any size and shape. The neighbourhood is defined by the pixels with the value of 1. In an image, isolated foregrounds may be removed by erosion while narrow regions are thickened by a dilation operation. Dilation and erosion are the two most important morphological operations. Erosion removes pixels on object boundaries while dilation adds pixels to object boundaries [115]. Dilation and erosion operations are illustrated on Figure 3.8. When performing morphological operations, the SE is positioned on the surface of the image at all possible locations and is compared with the corresponding pixels of the neighbourhoods [114].

Formally, the erosion of an image I by SE Z is denoted $I \Theta Z$. The dilation of an image I by SE Z is denoted as $I \oplus Z$.

(a) Eroded image (b) Original image (c) Dilated image

Figure 3.8: Fingerprint image before and after erosion operation (taken from [116]).

The other two important morphological operations are opening and closing. The process of erosion followed by dilation is referred to as opening, whereas the process of dilation followed by erosion is referred to as closing. Formally, the opening and closing operations of image I by a SE Z, are denoted by $I \circ Z$ and $I \bullet Z$ respectively. The results of opening are the removal of isolated foreground, while closing removes holes and changes small background regions in foreground.

3.4.2 Latent fingerprint segmentation

In this section, adapted fingerprint segmentation is explained. Figure 3.9 shows the processing procedure which is summarised as follows:

1. For a given gray scale fingerprint image, calculate the range, R, over a block of size $w \times w$ to highlight the ridges.
2. Set an appropriate threshold level for each block size (16×16), the adaptive threshold described in [117] is used.
3. Apply morphological closing operation by using a disk-shaped SE of radius r.
4. Extract the foreground, with the operation $I - I\Theta Z$, where Z is a disk-shaped SE, of radius $r = 3$. Retain only the contour with the largest perimeter. Since fingerprints are curved in nature a disk-shaped SE was chosen for the closing operation. The separation between ridges normally ranges between 3 - 18 pixels, therefore a disk with a radius of ($r = 6$), is sufficient for highlighting ridges and removing spurs.

3.4.3 Contour smoothing

To achieve better results a post-processing step is necessary. The contour filtering method in a complex Fourier transform domain proposed in [118] is used. The steps of the post-processing are as follows:

1. Find the contour of the segmented binary image.
2. Find the coordinate (i, j) of every point on the contour. Then, find the centroid of the boundary (x_c, y_c).
3. Convert the $(x - x_c, y - y_c)$ to polar coordinates (r, θ).
4. Expand r by using complex Fourier series.

3.5 Summary

In this chapter, improvements to the adaptive threshold shrinkage technique [75] were proposed. The stationary wavelet transform, combined with *boir*.2.6 [108], was used to transform an image to the wave domain. The noise coefficients were estimated using the median estimator. Finally, the adaptive threshold shrink (3.23) was multiplied by the decomposition level based, β, constant. This was a robust estimate and removal of speckle noise on latent fingerprint images acquired using OCT.

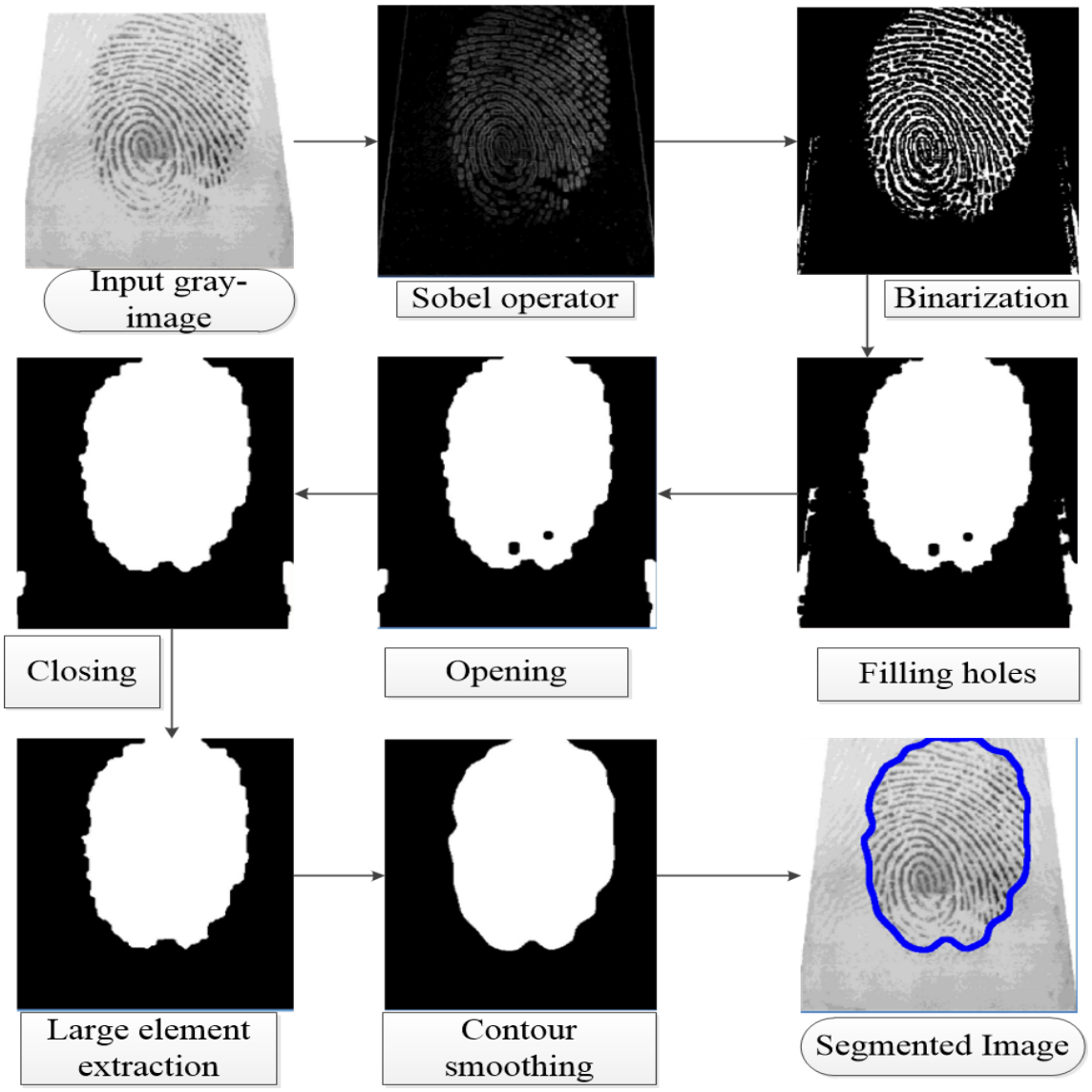

Figure 3.9: shows the fingerprint images segmentation from input to output. (taken from [114])

Chapter 4

Ridge Structure Enhancement

4.1 Introduction

This chapter discusses the Hong *et al.* [85] and Wieclaw [81] ridge structure enhancement algorithm adopted in this work. The ridge structure enhancement takes in the gray scale image from the denoising method discussed in Chapter 3. Figure 4.1 illustrates the enhancement technique.

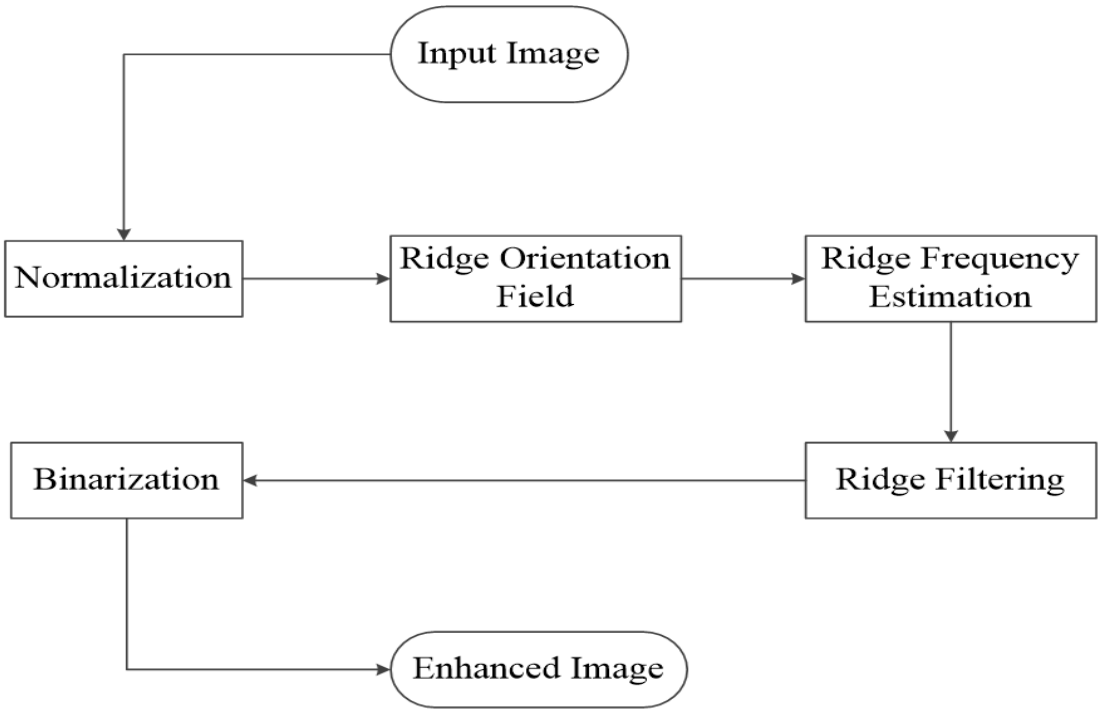

Figure 4.1: Ridge structure enhancement flow diagram.

4.2 Normalization

In image processing, normalization is the global operation that changes the pixel intensity to fit a certain desired range. The variations on an image may be caused by dust on the finger, dryness of the skin, irregular pressure on the scanner, which cause the captured images to vary. Normalization reduces the effect of the above factors, including those that occur during the image acquisition stage and also minimizes the chance of valid features being rejected. A gray scale image I, is defined as:

$$I = \{(i, j, x_{ij}) | 0 \leq i \leq N-1 \wedge 0 \leq j \leq M-1 \wedge 0 \leq x_{ij} \leq R-1\} \tag{4.1}$$

where (i, j, x_{ij}) is the pixel of the image I, with (i, j) being the position of the pixel and x_{ij} its intensity value. For simplicity, the pixel (i, j, x_{ij}) is denoted as (i, j), which is adopted in this dissertation. The normalized gray scale image G is defined as [85]:

$$G(i,j) = \begin{cases} M_0 + \sqrt{\frac{VAR_0(I(i,j)-M)^2}{VAR}}, & \text{if } I(i,j) > M \\ M_0 - \sqrt{\frac{VAR_0(I(i,j)-M)^2}{VAR}}, & \text{Otherwise} \end{cases} \tag{4.2}$$

where M and VAR represent the estimated mean and variance of image I respectively, the mean M_0 and variance VAR_0 are the desired mean and variance values of $G(i, j)$.

4.3 Ridge Orientation Field

Orientation field estimation is a technique used to enhance the global features of fingerprint images. It describes the local orientation of the ridge-valley structure at each point of a fingerprint image [22]. The orientation field of an image is constructed from directional vectors estimated from the normalized image. Figure 4.2 shows the ridge orientation at pixel (i, j). Orientation of an image can be used in singular-point detection, fingerprint image enhancement and classification [23–25].

Different techniques for estimating orientation have been developed [22, 81–83, 85]. The gradient-based technique appears to be the most common used method [81, 82, 85]. This research work adopts the same approach as [85] to calculate the gradient of the normalized image. The computed gradient is then used in the least square algorithm. In the least square-algorithm, ridge orientation estimation is based on the gradient (G_x, G_y) relationship between neighbouring pixels. Given a normalized image, $G(i, j)$, the gradient based orientation field estimation comprises the following steps [23–25, 81]:

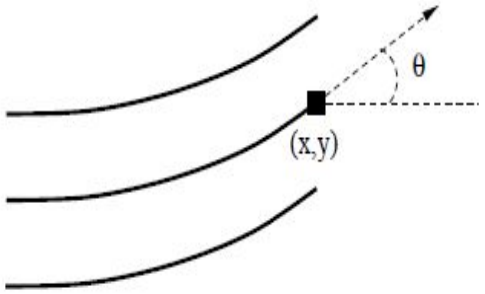

Figure 4.2: Orientation field of a ridge at pixel (i, j).

1. Divide the image G into $w \times w$ non-overlapping blocks.

2. At each pixel of the fingerprint image, $I(i, j)$, compute the gradients G_x and G_y by using the Scharr operator [119]. Each pixel of the $w \times w$ is convolved by using vertical and horizontal Scharr kernels s_y and s_x respectively in order to find the direction of the maximum intensity fluctuation.

$$S_x = \begin{bmatrix} -3 & 0 & +3 \\ -10 & 0 & +10 \\ -3 & 0 & +3 \end{bmatrix}, \; S_y = \begin{bmatrix} -3 & -10 & -3 \\ 0 & 0 & 0 \\ +3 & +10 & +3 \end{bmatrix}$$

3. If $G_x = G_y$ then add ± 1 randomly to one of the gradients *i.e* G_x or G_y. Also for $G_x = 0$ or $G_y = 0$ add ± 1 randomly to G_x or G_y .

4. Evaluate the local orientation in $w \times w$ blocks centred at pixel (x, y) by using the following equations:

$$V_y(i,j) = \sum_{u=i-\frac{w}{2}}^{i+\frac{w}{2}} \sum_{v=j-\frac{w}{2}}^{j+\frac{w}{2}} 2G_x(u,v)G_y(u,v) \tag{4.3}$$

$$V_x(i,j) = \sum_{u=i-\frac{w}{2}}^{i+\frac{w}{2}} \sum_{v=j-\frac{w}{2}}^{j+\frac{w}{2}} G_x^2(u,v) - G_y^2(u,v) \tag{4.4}$$

$$\phi_x(x,y) = \frac{1}{2} \arctan\left(\frac{V_x(i,j)}{V_y(i,j)}\right) \tag{4.5}$$

$$\theta_{gr}(i, jy) = \phi_x(i,j) + k\pi \tag{4.6}$$

where:

$$k = \begin{cases} \frac{1}{2}, & \text{if } (\phi(x,y) < 0 \wedge V_x(i,j) < 0) \vee (\phi(i,j) \geq 0 \wedge V_x(i,j) > 0 \\ 1, & \text{if } (\phi(i,j) < 0 \wedge V_x(i,j) \geq 0) \\ 0, & \text{if } \phi(i,j) \geq 0 \wedge V_x(i,j) \leq 0 \end{cases} \tag{4.7}$$

5. The estimated local ridge orientation, $\theta_{gr}(i,j)$, may not always be reliable due to noise, corrupted ridge-valley structure and minutia points on the fingerprint image. A low-pass filter is applied to reduce the effects of noise. In order to use the low-pass filter successfully, the orientation of an image must be continuous. An orientation of an image is transformed into continuous vector by using equations (4.8) and (4.9).

$$\phi_x(i,j) = \cos 2(\theta_{gr}(i,j)) \tag{4.8}$$

and

$$\phi_y(i,j) = \cos 2(\theta_{gr}(i,j)) \tag{4.9}$$

where ϕ_x and ϕ_y are the x and y components of the vector field, respectively. The computed vector field is then used for low-pass filtering as follows:

$$\phi'_x(i,j) = \sum_{u=-\frac{w_\phi}{2}}^{\frac{w_\phi}{2}} \sum_{v=-\frac{w_\phi}{2}}^{\frac{w_\phi}{2}} W(u,v)\phi_x(i-uw, j-vw) \tag{4.10}$$

and

$$\phi'_y(i,j) = \sum_{u=-\frac{w_\phi}{2}}^{\frac{w_\phi}{2}} \sum_{v=-\frac{w_\phi}{2}}^{\frac{w_\phi}{2}} W(u,v)\phi_y(i-uw, j-vw) \tag{4.11}$$

where $w_\phi \times w_\phi$ is the size of the filter and W is the low-pass filter with a unit integral.

6. The local ridge orientation of pixel (i,j) is then calculated by using

$$\Theta(i,j) = \frac{1}{2}\arctan\left(\frac{\phi'_y(i,j)}{\phi'_x(i,j)}\right) + k\pi \tag{4.12}$$

7. The reliability of the orientation $\Theta(i,j)$ of the block is estimated by using a metric referred to as coherence [120]. The coherence of the block is computed as,

$$Coh_B = \frac{|\sum_{i=1}^{w}\sum_{j=1}^{w} V_x(i,j), V_y(i,j)|}{\sum_{i=1}^{w}\sum_{j=1}^{w} |V_x(i,j), V_y(i,j)|} \tag{4.13}$$

4.4 Ridge Frequency Estimation

The distance from a given ridge to its adjacent ridges is referred to as inter-ridge distance [88]. The ridge frequency is the reciprocal of inter-ridge distance, indicating the number of ridges within a unit length of an image. The fingerprint ridge frequency describes

the local distance between ridges at each point of the fingerprint image. To estimate a frequency of an image successfully, a normalized image which is divided into $w \times w$ is required. The algorithm used in [85] for estimating frequency calculates an oriented window of size $w \times w$ for each block centred at (i, j) as follows [85]:

1. Divide image G into blocks of size $w \times w$.
2. For each block centred at (i, j) calculate an oriented window of size $I \times w$ that is defined in the ridge coordinate system [85].
3. For each block centred at (i, j), calculate the x-signature, $X[0]$, $X[1]$, ..., $X[I-1]$ of the ridges and valleys within the orientated window, where

$$X[k] = \frac{1}{w} \sum_{d=0}^{w-1} G(u, v),\ k = 0, 1, 2,\ \ldots\ , I-1 \tag{4.14}$$

$$u = i + \left(d - \frac{w}{2}\right) \cos\Theta(i, j) + \left(k - \frac{1}{2}\right) \sin\Theta(i, j) \tag{4.15}$$

$$v = i + \left(d - \frac{w}{2}\right) \sin\Theta(i, j) + \left(k - \frac{1}{2}\right) \cos\Theta(i, j) \tag{4.16}$$

4. Let $\tau(i, j)$ be the average number of pixels between two consecutive peaks in the x-signature, the the frequency, $\mu(i, j)$, is calculated as:

$$\mu(i, j) = \frac{1}{\tau(i, j)} \tag{4.17}$$

   If no consecutive peaks can be detected from the x-signature, then the frequency is assigned a value of -1 to differentiate it from the valid frequency values.

5. A fingerprint image may be affected by three factors: the area of the fingerprint that is captured, the size of the image and the resolution. These factors are related to one another as follows [121]:

$$H = 25.4 \times \frac{h}{r} \tag{4.18}$$

$$W = 25.4 \times \frac{w}{r} \tag{4.19}$$

   where h and w denote the hight and width of the image, r represents the resolution in dots per inch (dpi), and H and W denotes the hight and width of the captured area. The OCT latent fingerprint images are captured at different resolutions and have different widths and heights. Therefore, for each captured fingerprint image the value of the frequency of the ridges and valleys in a local neighbourhood lies in a different range. For example, an image of 640 by 480 pixels, 661 dpi has the range of (24.59, 18.44) millimetres. Therefore, any estimated frequency value that

is out of this range is assigned a value -1 to indicate that a frequency obtained is invalid.

6. A well defined sinusoidal-shaped wave is not formed when the blocks in which ridges and valleys occur are corrupted. Then these corrupted blocks are interpolated from the frequency of the neighbouring blocks which have well-defined frequencies. The blocks are interpolated as follows:

   (a) For each block centred at (i, j):

$$\Omega'(i,j) = \begin{cases} \Omega(i,j), & \text{if } \Omega(i,j) \neq -1 \\ \frac{\sum_{u=-\frac{w_\Omega}{2}}^{\frac{w_l}{2}} \sum_{v=-\frac{w_\Omega}{2}}^{\frac{w_l}{2}} W_g(u,v)\mu(\Omega(i-uw,j-vw))}{\sum_{u=-\frac{w_\Omega}{2}}^{\frac{w_l}{2}} \sum_{v=-\frac{w_\Omega}{2}}^{\frac{w_l}{2}} W_g(u,v)\delta(\Omega(i-uw,j-vw)+1)}, & \text{Otherwise} \end{cases} \tag{4.20}$$

   where

$$\mu(x) = \begin{cases} 0, & \text{if } x \leq 0 \\ x, & \text{Otherwise} \end{cases}$$

$$\delta(x) = \begin{cases} 0, & \text{if } x \leq 0 \\ 1, & \text{Otherwise} \end{cases}$$

   where W_g is a discrete Gaussian kernel with mean = 0 and variance = 9, and $w_\Omega = 7$ is the size of the kernel.

   (b) If there is at least one block with the frequency value of -1, then swap Ω and Ω' and go to step (a).

7. A low-pass filter is used to remove outliers in $F(i, j)$:

$$F(i,j) = \sum_{u=-\frac{w_\Omega}{2}}^{\frac{w_l}{2}} \sum_{v=-\frac{w_\Omega}{2}}^{\frac{w_l}{2}} W_l(u,v)\Omega'(i-uw, j-vw) \tag{4.21}$$

   W_l is a 2D low-pass filter with unit integral and $w_l = 7$ is the size of the filter.

4.5 Ridge Filtering

Gabor filtering [122] is a linear filter that can be used to analyse image texture. This filter is a sinusoidal plane wave which uses both frequency and orientation properties of the image. In fingerprint images, it is used to solve broken ridges and smudges. In this work, the even-symmetric Gabor filter has been used [89].

$$h(x, y : \alpha, f) = \exp\left\{ -\frac{1}{2}\left[\frac{x_\alpha^2}{\delta_x^2} + \frac{y_\alpha^2}{\delta_y^2}\right]\right\} \cos(2\pi f x_\alpha) \tag{4.22}$$

$$x_\alpha = x\cos\alpha + y\sin\alpha, \tag{4.23}$$

$$x_\alpha = y\cos\alpha - x\cos\alpha \tag{4.24}$$

where α is the orientation of the Gabor filter (obtained from section 4.3), f is the frequency of a sinusoidal plane wave (obtained from section 4.4) and δ_x and δ_y are the space constants of the Gaussian envelope along the x and y axes, respectively. In order for the Gabor filter to enhance an image, the filter has to be convolved with the pixel (i, j). The corresponding orientation value $(\Theta(i, j))$ and the frequency value $F(i, j)$ are required. This is defined mathematically as

$$E(i,j) = \sum_{u=-\frac{w_x}{2}}^{\frac{w_x}{2}} \sum_{v=-\frac{w_y}{2}}^{\frac{w_y}{2}} G(u, v; \Theta(i, j), F(i, j)N(i - u, j - v)) \tag{4.25}$$

where $N(i - u, j - v)$ is the normalized fingerprint image, $F(i, j)$ is the ridge frequency image, $\Theta(i, j)$ is the orientation image and w_x & w_y are the width and height of the Gabor filter mask, respectively. The problem with the original Hong *et al.* [85] enhancement technique is the fact that the values of the standard deviation δ_x and δ_y are fixed to the value 4. Using the fixed values forces the bandwidth of the filter to be constant; this means that the variations that occur in the value of the ridge frequency are not taken into account. Therefore, for fingerprint images that exhibit significant variation in the frequency value, enhancement artefacts will occur. Therefore, in this work, we adopt the solution proposed in [89]. Instead of using fixed values Thai *et al.* [89] used the standard deviation values δ_x and δ_y as the function of ridge frequency, defined as [89, 123]:

$$\delta_x = k_x F(i, j), \tag{4.26}$$

$$\delta_y = k_y F(i, j), \tag{4.27}$$

where k_x is a constant variable for δ_x, k_y is a constant variable for δ_y and F is the ridge frequency image. Furthermore Thai *et al.* set the filter size to depend on standard deviation parameters to accommodate Gabor waveforms of different bandwidth sizes.

$$w_x = 6\delta_x \tag{4.28}$$

$$w_y = 6\delta_y \tag{4.29}$$

where δ_x and δ_y are the standard deviation of the Gaussian envelope along the x and y axes, the width and height of the Gabor filter mask are represented by w_x and w_y, respectively.

4.6 Binarization

The method of converting image pixel values to binary values is referred to as the binarization. A threshold pixel value is used to binarize the image into light and dark pixels of 1's and 0's (0 and 255 for display) respectively. Images can be binarized locally or globally. In global binarization, single threshold value is used to binarize the image whilst in local binarization, the threshold value is calculated locally, region by region. An example of global thresholding method is the fixed thresholding method. In the fixed thresholding method the threshold value, T, is used to assign 0's and 1's for all pixels in a given image [93]. The binarized value of a pixel (i, j), $G(i, j)$ is given by:

$$G(i,j) = \begin{cases} 1, & \text{if f(x,y)} \geq T \\ 0, & \text{Otherwise} \end{cases}, \tag{4.30}$$

where, $f(x, y)$ is the value of a pixel in gray scale image and $G(x, y)$ is its corresponding pixel in the binarized image.

4.7 Summary

This chapter has presented normalization, ridge orientation, ridge frequency, ridge filtering, binarization [85] and the Wieclaw [22] technique of computing the gradient. The results of this section combined with different wavelet denoising techniques are presented and discussed in Chapter 6.

Chapter 5

Quality Estimation

5.1 Introduction

Fingerprint image quality can be defined based on the number of features contributing to matching or the degree of clarity between the ridges and valleys, as well as the visibility of matching features [26]. Examining the quality of the fingerprint image before taking it to the recognition system (RS) improves the performance of RS significantly [28]. Fingerprint image quality may be influenced by two factors: acquisition devices and individual artefacts [27]. It is known that for each fingerprint-capturing device, quality assessment is different [27, 28]. Individual artefacts include skin characteristics such as oiliness, moisture, creases, elasticity, temperature and scars. Fingerprint quality estimation methods are divided into three classes that include methods based on classifiers and those that are based on local and global features. In this work the quality estimation methods used are peak to-signal-noise-ratio (PSNR), signal-noise-ratio (SNR), root mean square error (RMSE), structural similarity index measure (SSIM) and orientation certainty level (OCL). The PSNR, SNR, RMSE, SSIM are used since they are the standard image quality measures while OCL is used because it analyses the consistency of the dominant orientation of ridges. If the orientation of ridges is not consistent, the OCL is able to mark that block as unreliable. In layman terms, it measures how "parallel" the ridges are to one another. A good-quality image has a near parallel ridge flow [28].

5.2 Orientation Certainty Level

OCL measures the energy concentration along the dominant direction of the ridges. It is defined as the ratio between two eigenvalues of the covariance matrix of the gradient vector [27]. The fingerprint image is split-up into 32×32 non-overlapping pixel blocks to

estimate OCL for local quality analysis, as shown in Figure 5.1, using a Hessian matrix to estimate certainty. Let H be the Hessian matrix constructed from the gradient vector of N point image block, then H is defined as:

$$H = \frac{1}{N}\sum \begin{pmatrix} dx \\ dy \end{pmatrix} \begin{bmatrix} dx & dy \end{bmatrix} = \begin{bmatrix} c_{xx} & c_{xy} \\ c_{yx} & c_{yy} \end{bmatrix} \tag{5.1}$$

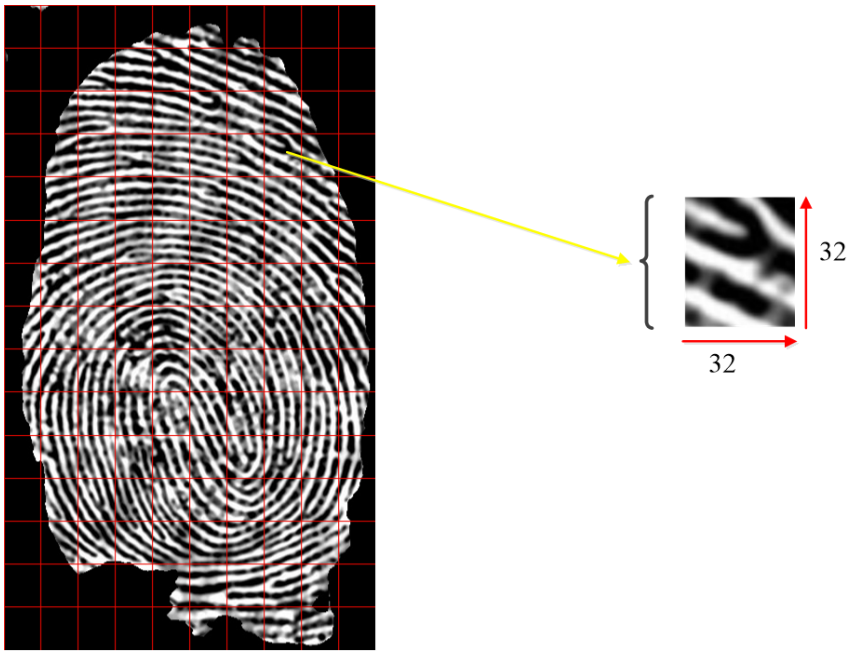

Figure 5.1: Non-overlapping 32×32 pixels blocks that.

where dx and dy are intensity gradients computed by using the Sobel operator. The eigenvectors of H indicate the principal and pure curvature directions. These curvature directions are denoted by λ_a and λ_b, given in equations 5.2 and 5.3 respectively.

$$\lambda_a = \frac{c_{xx} + c_{yy} + \sqrt{(c_{xx} - c_{yy})^2 + (4c_{xy})^2}}{2} \tag{5.2}$$

$$\lambda_b = \frac{c_{xx} - c_{yy} + \sqrt{(c_{xx} - c_{yy})^2 + (4c_{xy})^2}}{2} \tag{5.3}$$

The greatest curvature direction is represented by λ_a while the least curvature direction is represented by λ_b. Orientation certainty is defined as:

$$orientation\_certainty = 1 - \frac{\lambda_b}{\lambda_a} \tag{5.4}$$

Equation 5.4 shows that orientation certainty ranges between 0 and 1. The value 0 means that the ridges and valleys are not consistent. This could represent a background with no ridges and valleys. The value 1 means that valleys and ridges in the block are consistent in the same direction. The classification of the blocks is given in Table 5.1 and visually shown in Figure 5.2

Table 5.1: Classification levels of the orientation certainty value [28].

OCL Range	**Classification Level**
$0.8 \leq \text{OCL} \leq 1$	Good block
$0.04 \leq \text{OCL} \leq 0.8$	Normal block
$0.01 \leq \text{OCL} \leq 0.4$	Bad block
$0 \leq \text{OCL} \leq 0.01$	Very bad block or background

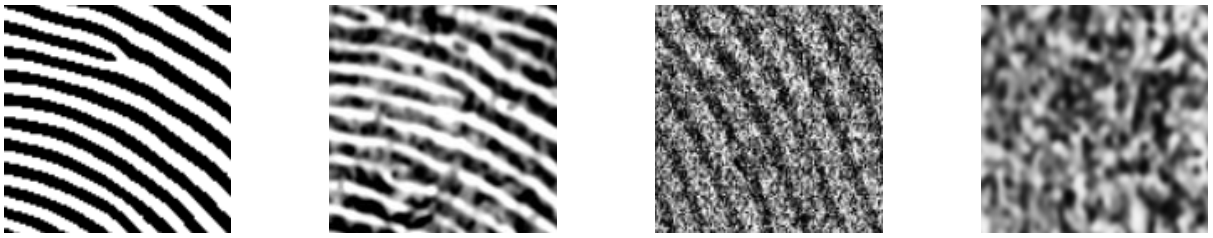

(a) Good (b) Normal (c) Bad (d) Very bad

Figure 5.2: Fingerprint blocks.

5.3 Quality Assessment Metrics

Measuring the quality of an image is not an easy task. The signal-to-noise ratio (SNR), peak signal-to-noise ratio ($PSNR$) the mean square error (MSE), root mean square error ($RMSE$) and structural similarity index ($SSIM$) are widely used to assess the quality of images. These are defined [20] as:

$$SNR = \frac{\sigma(s)}{\sigma(n)} \tag{5.5}$$

where $\sigma(s)$ is the standard deviation of the signal and $\sigma(n)$ is the standard deviation of the noise.

$$MSE(r,d) = \frac{1}{N}\sum_{i=1}^{N}(r_i - d_i)^2 \tag{5.6}$$

$$RMSE(r,d) = \sqrt{MSE(r,d)} \tag{5.7}$$

where r and d are the reference and resultant clean images respectively, N is the total number of pixels and, i denotes the pixel being compared.

$$PSNR = 10log_{10}\left(\frac{MAX_I^2}{MSE}\right) \tag{5.8}$$

where MAX_I is the maximum intensity of the image. When an image is represented by using 8 bits per sample, MAX_I is equal to 255.

$$SSIM(w_1, w_2) = \frac{(2\mu_{w_1}\mu_{w_2} + C_1)(2\sigma_{w_1 w_2} + C_2)}{(\mu_{w_1}^2 + \mu_{w_2}^2 + C_1)(\sigma_{w_1}^2 + \sigma_{w_2}^2 + C_2)} \tag{5.9}$$

where $SSIM$ is calculated between multiple windows across images (w_1 and w_2 define a window). μ_{w_1} is the mean of w_1, μ_{w_2} is the mean of w_2, $\sigma_{w_1}^2$ is the variance of w_2 and $\sigma_{w_2}^2$ is the variance of w_2, and $\sigma_{w_1 w_2}$ is the covariance of w_1 and w_2. C_1 and C_2 are stabilization variables.

Darlowa *et al.* [20] used these three metrics, SNR, MSE, and SSIM to assess quantitatively the algorithms used to reduce speckle noise in OCT fingertip images.

5.4 Summary

Quality estimation techniques used to estimate latent fingerprint images' quality have been discussed. They will be used in the next chapter to evaluate the proposed techniques.

Chapter 6

Experimental Results and Discussion

The five wavelet transform based techniques and the ridge structure enhancement discussed in the previous chapters have been implemented and tested on a self-acquired OCT latent fingerprint database. This chapter presents the results obtained from the experiments, discusses what those results entail.

6.1 Data Acquisition

This section describes the device used to acquire latent fingerprints image and also explains how the fingerprint images are acquired.

6.1.1 Optical coherence tomography

In this work, a custom-made spectral domain OCT (SD-OCT) system according to the specifications shown in Table 6.1 was used. In an OCT system, the central wavelength is responsible for penetration depth into the sample under examination [124]. The average power is the power of the broadband light source. In our OCT machine, the broadband light source is the superluminescent diode. The axil scan rate is the speed at which the sample is scanned. Effective focal length is the optimal distance where a sample or surface should be placed.

The schematic diagram of the SD-OCT is shown in Figure 6.1. Diffraction grating is an optical component with a periodic structure that splits and diffracts light into several beams travelling in different directions. A beam splitter is an optical device that splits a beam of light in two. The DSP is the digital signal processor.

Table 6.1: Specifications of the customized latent fingerprint OCT acquisition device.

Base Unite	**GAN610**
Central wavelength	930 nm
Average power	10 mW
Axil scan rate	100 kHz
Imaging depth	2.9 mm
Scanning Lens	**Key Specifications**
Effective focal length	110 mm
Maximum scannable area	28.9×28.9 mm^2

6.1.2 Acquisition process

- Latent fingerprints were acquired from brass (door handle), stainless steel (knife), mirror, bullet cartridge, plastic and glass at a 100 axil scan rate.
- Each participant placed a finger on each substrate to leave a fingerprint. The OCT system would start acquiring a print impression left on the substrates as shown in Figure 6.1. The self-acquired database consisted of 270 latent fingerprint images. The database was constructed from 5 participants and 6 substrates, from each participant, 3 fingers were considered (*i.e.* index finger, middle finger thumb). Each finger impression was acquired 3 times, hence,
  $5 \times 6 \times 3 \times 3 = 270$ fingerprint images.
- The OCT machine produces a 3D-volume data per fingerprint. The 3D-data must then be projected into a 2D-fingerprint image. The 2D-fingerprint image is obtained by applying the maximum intensity projection technique as shown in Figure 6.2.
- To acquire a good fingerprint successfully from glass, mirror and plastic substrates, the scanner should be perpendicular to the substrate (right angle). For brass and stainless still, the substrate (or the scanner) should be at an angle of between 3^o and 10^o. This is done to reduce the reflection that causes immense speckle noise.

Maximum Intensity Projection (MIP)

MIP is the method for 3D-data that projects maximum intensity in the visualization plane. It enhances the ridges and valleys of the latent fingerprint image by making them stand out from the substrate. The latent fingerprint images in Figure 6.3 were taken by an OCT device from different substrates.

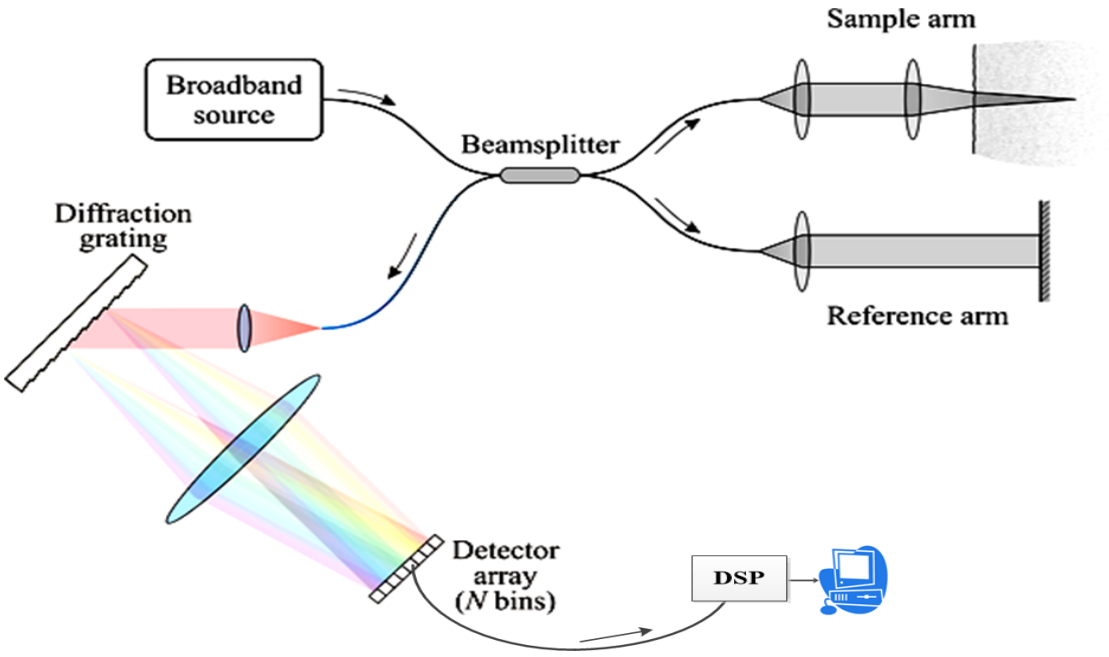

Figure 6.1: Schematic diagram of the SD-OCT (adapted from [125]).

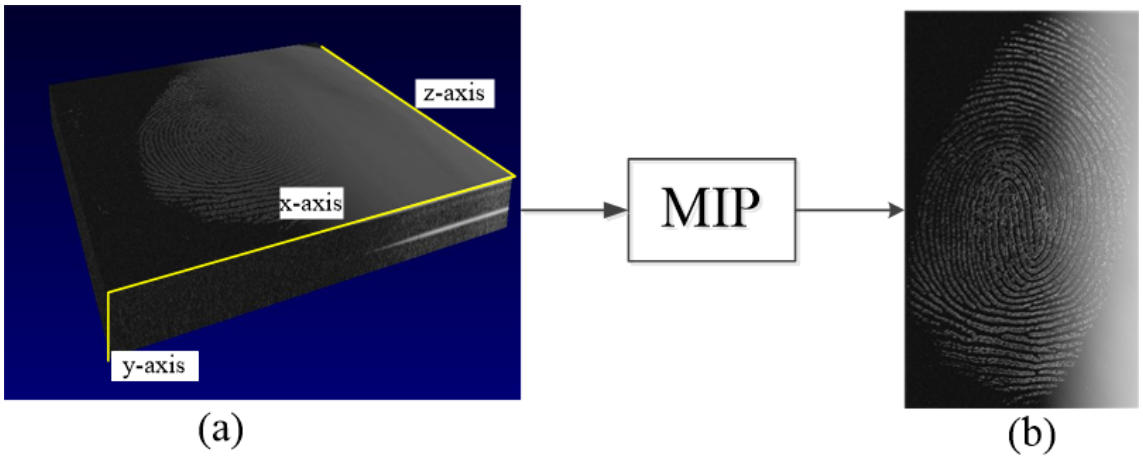

Figure 6.2: Conversion of 3D to 2D latent fingerprint images, (a) 3D-image and (b) 2D-image with z the vertical axis and x the horizontal axis

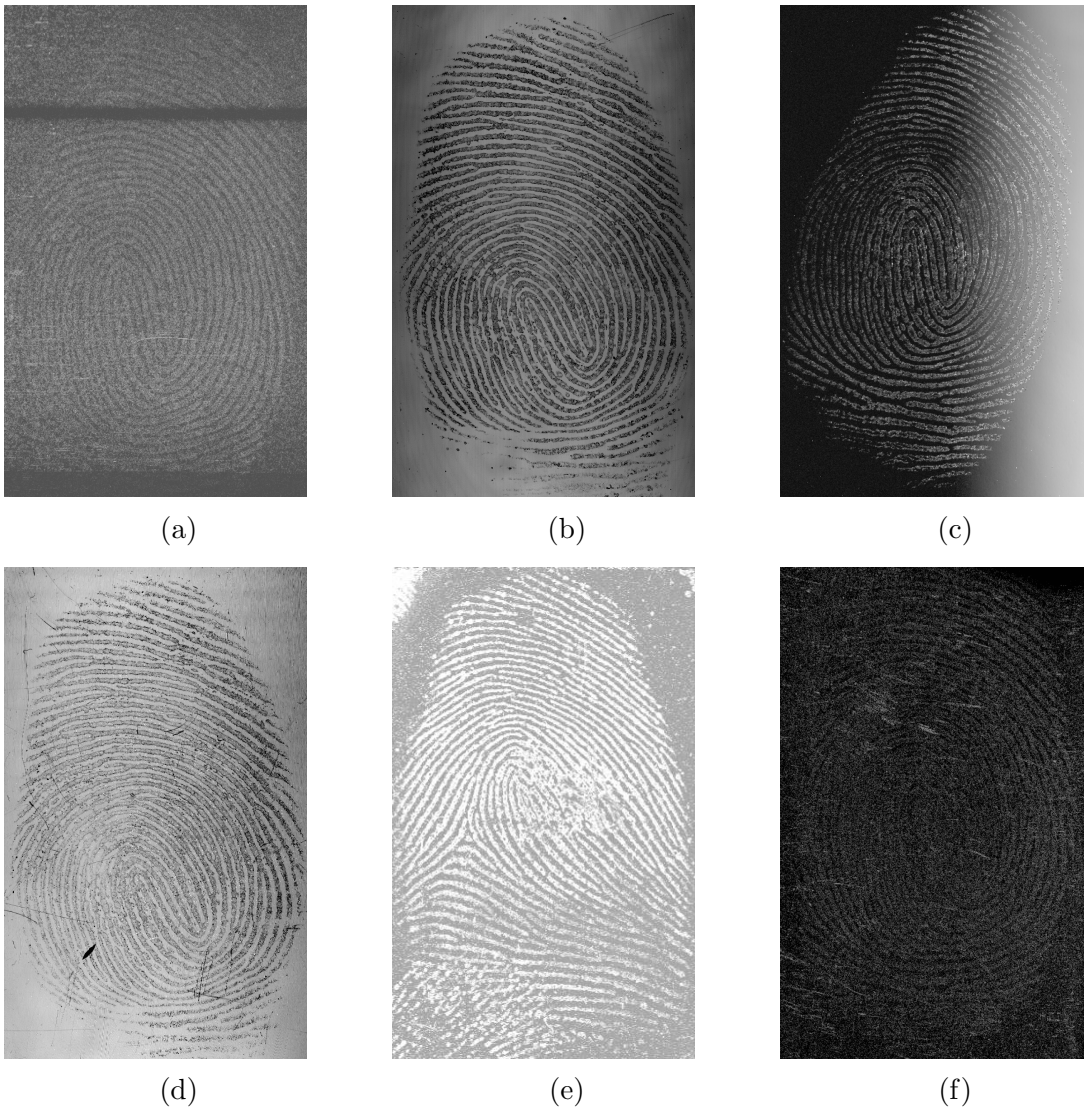

Figure 6.3: Latent fingerprint images captured by OCT, (a) Brass, (b) Glass, (c) Mirror, (d) Plastic (e) Stainless steel (f) Bullet cartridge.

6.2 OCT Compared to Traditional Fingerprints

In this section, unprocessed OCT latent fingerprint images are compared to fingerprints lifted by using traditional techniques.

6.2.1 Robon powder blue

Badiye *et al.* [3] developed and lifted latent fingerprint images on 20 different surfaces. Among the 20 surfaces 5 (glass, mirror, plastic, brass and doorknob) are common in our

study. The results in [3] are displayed in Figures 6.4 to 6.8 for comparison.

1. The subjects were asked to wash and dry their hands to prevent any contamination by any substance.
2. The subjects were asked to close their palm for about 2 minutes to create sweat.
3. The participants were then asked to touch the surfaces of the given objects as they would normally do in daily routine, thus leaving fingerprints on them.
4. The fingerprints were then left in the lab for 24 hours. The Robin powder blue manufactured by Reckitt Benckiser (India) Limited was used to develop latent fingerprints on 20 different surfaces.
5. The powder formed clumps when kept in an open space, therefore the powder was kept in a sterile, airtight glass jar and sealed.
6. The powder blue was sprinkled over the surface carrying the latent fingerprints, and a powdering method using a soft feather brush was used to remove excess powder by tapping and slowly using the brush in order to get clear prints.
7. The developed fingerprints were then photographed by using a DSLR camera. The photographs captured were transferred on to a laptop and were cropped and resized in Microsoft Office Picture Manager software.

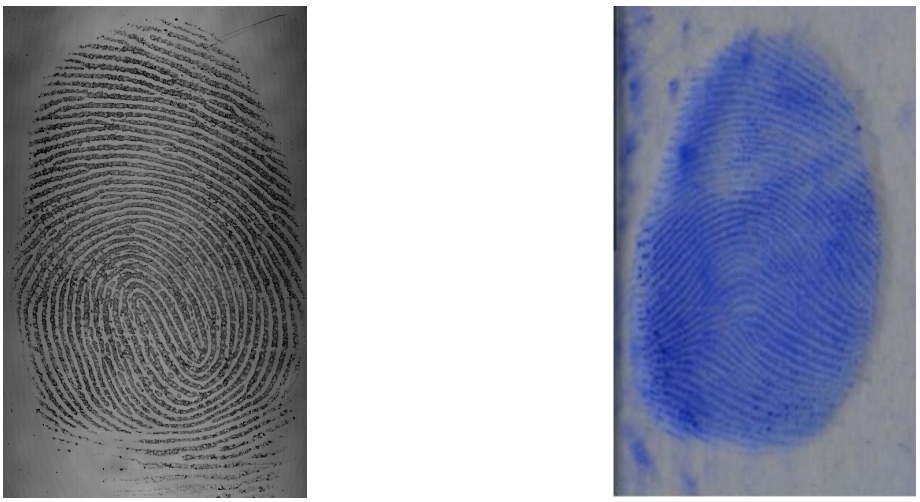

(a) (b)

Figure 6.4: Latent fingerprint image taken from glass.

The fingerprint image in Figure 6.4a was taken by OCT while the one in Figure 6.4b was developed by Robin powder blue. The image captured by OCT from the glass is more precise than the image developed by using Robin powder blue.

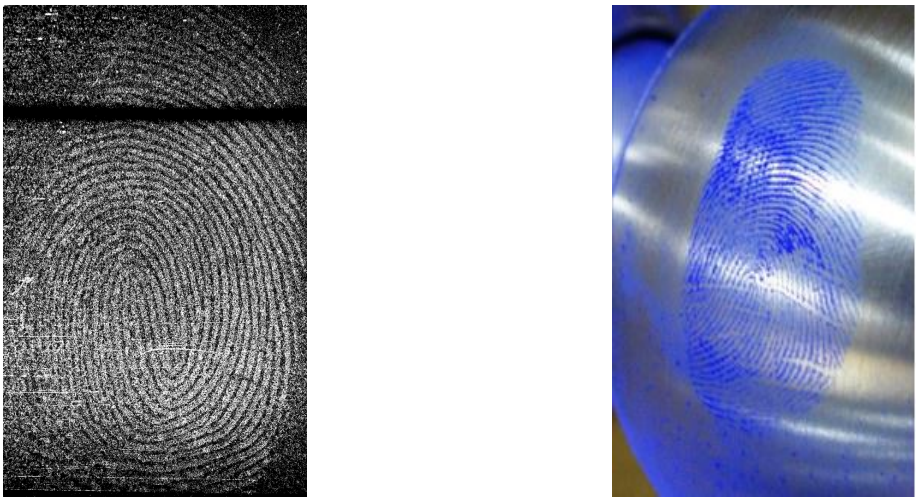

(a) (b)

Figure 6.5: latent fingerprint image taken from door knob

The fingerprint images in Figure 6.5 were both taken from the doorknob. Fingerprint images in Figure 6.5a and 6.5b were obtained by using OCT and Robin powder blue respectively. Considering the fact that no technique can develop or capture fingerprint images on all surfaces, both the OCT and Robin powder blue performed relatively well.

(a) (b)

Figure 6.6: Latent fingerprint image taken from plastic.

The fingerprint image in Figure 6.6a was obtained by OCT, while the one in Figure 6.6b was developed by Robin powder blue. The image captured by OCT from the plastic is clearer than the image developed by using Robin powder blue.

(a) (b)

Figure 6.7: Latent fingerprint from a mirror.

The fingerprint images in Figures 6.7a and 6.7b were taken from glass mirror and smartphone screen respectively. A mirror is a glass coated with a metal amalgam while a smartphone screen is made up of glass and plastic film covered with a grid of electrical conductors. Therefore, it is logical to compare a smartphone screen to a mirror. Good-quality images were observed for both techniques.

(a) (b)

Figure 6.8: Latent fingerprint obtained from stainless steel.

The fingerprint image in Figure 6.8a was obtain by using OCT while the one in Figure 6.8b was developed by Robin powder blue. In Figure 6.8, the fingerprint image taken by the OCT is very noisy, while the print developed by Robin powder blue is smudged at the centre. This does not imply that Robin powder blue failed to develop the fingerprint on stainless steel. With an appropriate enhancement technique, the fingerprint taken by the OCT may be improved.

6.2.2 Unfired Bullet Cartridge

Sullivan *et al.* [126] used a (Cyanoacrylate, gun blue, BY40) to develop latent fingerprints on unfired and fired brass bullet cartridge. In our work, we are only interested in the unfired part of their work. The following is the summary of steps they have taken to perform their experiments:

1. The casings were submerged in methanol to and wiped with the paper towel to remove any previous fingerprints.
2. The nose, chin, and eyebrow regions of the face were rubbed with the finger used to make the fingerprint, and the finger was rolled onto the casing to produce a latent fingerprint.
3. The fingerprints were obtained from two participants. The cartridges were placed on a test tube support rack and set in a Cyanosafe Ductless Cyanoacrylate Fuming Chamber by Sirchie Fingerprint Laboratories.
4. Once cyanoacrylate fuming was complete, the casing was submerged in a blue gun solution of 30 *ml* and water 30 *ml* Birchwood Casey Perma Blue Liquid Gun Blue for 30 seconds.
5. The cartridges were then again submerged in water. Once dry, the cartridges were rinsed with BY40, then water, and placed on a test tube support rack to dry.
6. Lastly, the casing was observed under an alternative light source of 450nm with orange goggles.

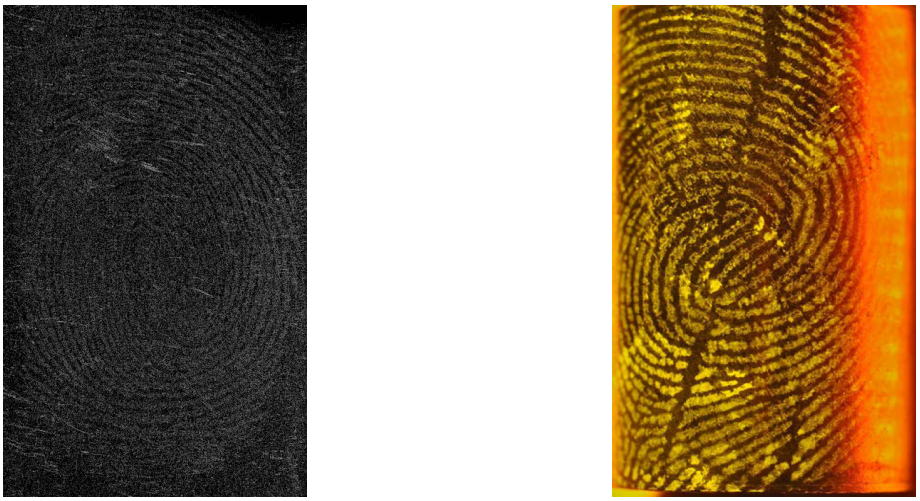

(a) (b)

Figure 6.9: Latent fingerprint from a bullet case.

The fingerprint images in Figures 6.9a and 6.9b were taken from a brass bullet cartridge. The fingerprint image taken by the OCT is smudged, meaning that the ridges and valleys

are not clear. Despite the bad fingerprint imprinted on the bullet cartridge, OCT managed to acquire a print. The fingerprint image developed by using (Cyanoacrylate, gun blue, BY40) [126] is clear. However, the technique requires much time to perform, and if the fingerprint is damaged, it will be hard to tell if the print was already damaged or not.

6.2.3 Section summary

In this section, OCT fingerprint images were compared to the state-of-the-art [3, 126] techniques for fingerprint development. We observed that OCT was a good candidate for the contactless technique that could replace these techniques.

6.3 Denoising Results

This section presents the denoising results of VisuShrink, BayesShrink, SUREShrink, NormalShrink, adaptive threshold and the proposed method. The values for PSNR, SNR and RMSE are measured in decibels and the values highlighted in bold are optimal at each level for the specified wavelet filter. The Figures 6.10, 6.11, 6.12, 6.13, 6.14 and 6.15 shows the visual results of the denoising techniques.

Table 6.2: PSNR, SNR and RMSE and SSIM values for each technique with *haar* as a wavelet filter at decomposition levels 1 to 4.

	PSNR ↑	**SNR ↑**	**RMSE ↓**	**SSIM ↑**
Level 1				
VisuShrink	**8.5786**	**2.4910**	**1.1032**	6.3922 %
BayesShrink	8.5771	2.4895	**1.1032**	6.3928 %
SUREShrink	8.5692	2.4817	1.1044	6.3898 %
NormalShrink	8.4428	2.3552	1.2636	5.2160 %
Adapt. Threshold	8.4354	2.3478	1.2646	5.2164 %
Proposed Method	8.4915	2.4039	1.1531	**6.3934** %
Level 2				
VisuShrink	8.5408	2.4532	1.1345	5.7381 %
BayesShrink	**8.5582**	**2.4706**	1.0981	6.3073 %
SUREShrink	8.5539	2.4663	**1.0915**	6.3408 %
NormalShrink	8.4433	2.3557	1.2653	5.2169 %
Adapt. Threshold	8.4354	2.3478	1.2646	5.2164 %
Proposed Method	8.4956	2.4079	1.1531	**6.3934** %
Level 3				
VisuShrink	8.5521	2.3933	1.3231	5.0965 %
BayesShrink	**8.5533**	**2.4657**	1.1092	6.3025 %
SUREShrink	8.5512	2.4636	**1.0970**	6.3461 %
NormalShrink	8.4427	2.3551	1.2650	5.2170 %
Adapt. Threshold	8.4354	2.3478	1.2646	5.2164 %
Proposed Method	8.4984	2.4108	1.1531	**6.3934** %
Level 4				
VisuShrink	8.4734	2.3858	1.2439	5.2085 %
BayesShrink	**8.5592**	**2.4717**	1.1075	6.3297 %
SUREShrink	8.5524	2.4648	**1.0894**	6.3790 %
NormalShrink	8.4416	2.3540	1.2633	5.2167 %
Adapt. Threshold	8.4354	2.3478	1.2646	5.2164 %
Proposed Method	8.5053	2.4177	1.1531	**6.3934** %

Table 6.2 VisuShrink outperforms the other techniques at level 1 in terms of PSNR, SNR and RMSE. The proposed technique is better than other techniques in terms of SSIM at all levels of decomposition, while BayesShrink is better in terms of PSNR and SNR from levels 2 to 4. The SUREShrink has better RMSE from levels 2 to 4. BayesShrink and VisuShrink performed very well with a *haar* wavelet filter.

Table 6.3: PSNR, SNR and RMSE and SSIM values for each technique with *db2* as a wavelet filter at decomposition levels 1 to 4.

	PSNR ↑	**SNR ↑**	**RMSE ↓**	**SSIM ↑**
Level 1				
VisuShrink	**8.5627**	**2.4751**	**1.1201**	6.3452 %
BayesShrink	8.5625	2.4749	1.1202	6.3452 %
SUREShrink	8.5616	2.4741	1.1220	6.3432 %
NormalShrink	8.4498	2.3622	1.2616	5.2183 %
Adapt. Threshold	8.4473	2.3597	1.2621	5.2197 %
Proposed Method	8.5055	2.4180	1.1257	**6.4022** %
Level 2				
VisuShrink	8.5226	2.4350	1.2152	6.0041 %
BayesShrink	8.5492	2.4616	1.1322	6.3113 %
SUREShrink	8.5567	2.4691	1.1246	6.3368 %
NormalShrink	8.4498	2.3622	1.2616	5.2183 %
Adapt. Threshold	8.4473	2.3597	1.2621	5.2197 %
Proposed Method	**8.5580**	**2.4704**	**1.0844**	**6.5027**%
Level 3				
VisuShrink	8.4631	2.3755	1.2687	5.8966 %
BayesShrink	8.5458	2.4583	1.1365	6.3021 %
SUREShrink	**8.5541**	**2.4665**	1.1261	6.3342 %
NormalShrink	8.4498	2.3622	1.2616	5.2183 %
Adapt. Threshold	8.4473	2.3597	1.2621	5.2197 %
Proposed Method	8.5488	2.4612	**1.0934**	**6.4813** %
Level 4				
VisuShrink	8.4487	2.3612	1.2472	6.0285 %
BayesShrink	8.5458	2.4583	1.1326	6.3141 %
SUREShrink	**8.5573**	**2.4697**	1.1180	6.3586 %
NormalShrink	8.4498	2.3622	1.2616	5.2183 %
Adapt. Threshold	8.4473	2.3597	1.2621	5.2197 %
Proposed Method	8.5377	2.4501	**1.1080**	**6.4409** %

In Table 6.3, *db*2 is used as the wavelet filter. VisuShrink Technique performs better at level 1 while the proposed method is effective at level 2 and has a better SSIM value at all levels of decomposition. SUREShrink is effective at levels 3 and 4. The results in Table 6.3 show that *db*2 is a better version of the *haar* wavelet filter since it achieves overall improvement of results.

Table 6.4: PSNR, SNR and RMSE value for each technique with *sym4* as a wavelet filter at decomposition levels 1 to 4.

	PSNR ↑	**SNR ↑**	**RMSE ↓**	**SSIM ↑**
Level 1				
VisuShrink	8.5502	2.4626	**1.0901**	6.3490
BayesShrink	8.5499	2.4623	1.0903	6.3523
SUREShrink	8.5517	2.4641	1.0903	6.3547
NormalShrink	8.4509	2.3633	1.2620	5.2206
Adapt. Threshold	8.4514	2.3638	1.2621	5.2210
Proposed Method	**8.5715**	**2.4839**	1.1068	**6.5392**
Level 2				
VisuShrink	8.5157	2.4281	1.1461	6.2689 %
BayesShrink	8.5490	2.4614	1.1213	6.3438 %
SUREShrink	8.5518	2.4643	1.1226	6.3445 %
NormalShrink	8.4509	2.3633	1.2620	5.2206 %
Adapt. Threshold	8.4514	2.3638	1.2621	5.2210 %
Proposed Method	**8.5701**	**2.4825**	**1.1056**	**6.5307** %
Level 3				
VisuShrink	8.4834	2.3958	1.1374	6.2827 %
BayesShrink	8.5480	2.4604	1.1223	6.3467 %
SUREShrink	8.5532	2.4656	1.1234	6.3435 %
NormalShrink	8.4509	2.3633	1.2620	5.2206 %
Adapt. Threshold	8.4514	2.3638	1.2621	5.2210 %
Proposed Method	**8.5690**	**2.4815**	**1.1097**	**6.5199** %
Level 4				
VisuShrink	8.4929	2.4053	1.1358	6.3201 %
BayesShrink	8.5488	2.4612	1.1227	6.3451 %
SUREShrink	8.5545	2.4669	1.1225	6.3493 %
NormalShrink	8.4509	2.3633	1.2620	5.2206 %
Adapt. Threshold	8.4514	2.3638	1.2621	5.2210 %
Proposed Method	**8.5587**	**2.4711**	**1.1110**	**6.5123** %

In Tables 6.4 and 6.5 the proposed technique dominates the optimal results. This is due to the fact that *sym*4 and *bior*2.6 wavelet filters are steeper and they have many overlapping windows that enhance the technique's adaptability.

Table 6.5: PSNR, SNR and RMSE value for each technique with *haar* as a wavelet filter at decomposition levels 1 to 4.

	PSNR ↑	**SNR ↑**	**RMSE ↓**	**SSIM ↑**
Level 1				
VisuShrink	8.5668	2.4792	1.1144	6.3573 %
BayesShrink	8.5664	2.4788	1.1142	6.3573 %
SUREShrink	8.5619	2.4743	1.1156	6.3555 %
NormalShrink	8.4500	2.3624	1.2629	5.2189 %
Adapt. Threshold	8.4477	2.3601	1.2626	5.2207 %
Proposed Method	**8.6003**	**2.5127**	**1.1083**	**6.5410** %
Level 2				
VisuShrink	8.5237	2.4361	1.1642	6.1838 %
BayesShrink	8.5595	2.4719	1.1196	6.3436 %
SUREShrink	8.5570	2.4694	1.1187	6.3473 %
NormalShrink	8.4500	2.3624	1.2629	5.2189 %
Adapt. Threshold	8.4477	2.3601	1.2626	5.2207 %
Proposed Method	**8.6062**	**2.5186**	**1.1103**	**6.5315** %
Level 3				
VisuShrink	8.4414	2.3538	1.2534	5.2066 %
BayesShrink	8.5590	2.4714	1.1207	6.3420 %
SUREShrink	8.5575	2.4699	1.1192	6.3468 %
NormalShrink	8.4500	2.3624	1.2629	5.2189 %
Adapt. Threshold	8.4477	2.3601	1.2626	5.2207 %
Proposed Method	**8.6018**	**2.5142**	**1.1106**	**6.5233** %
Level 4				
VisuShrink	8.5002	2.4126	1.1943	6.2233 %
BayesShrink	8.5591	2.4715	1.1198	6.3455 %
SUREShrink	8.5569	2.4693	1.1187	6.3501 %
NormalShrink	8.4500	2.3624	1.2629	5.2189 %
Adapt. Threshold	8.4477	2.3601	1.2626	5.2207 %
Proposed Method	**8.5905**	**2.5029**	**1.1115**	**6.5158** %

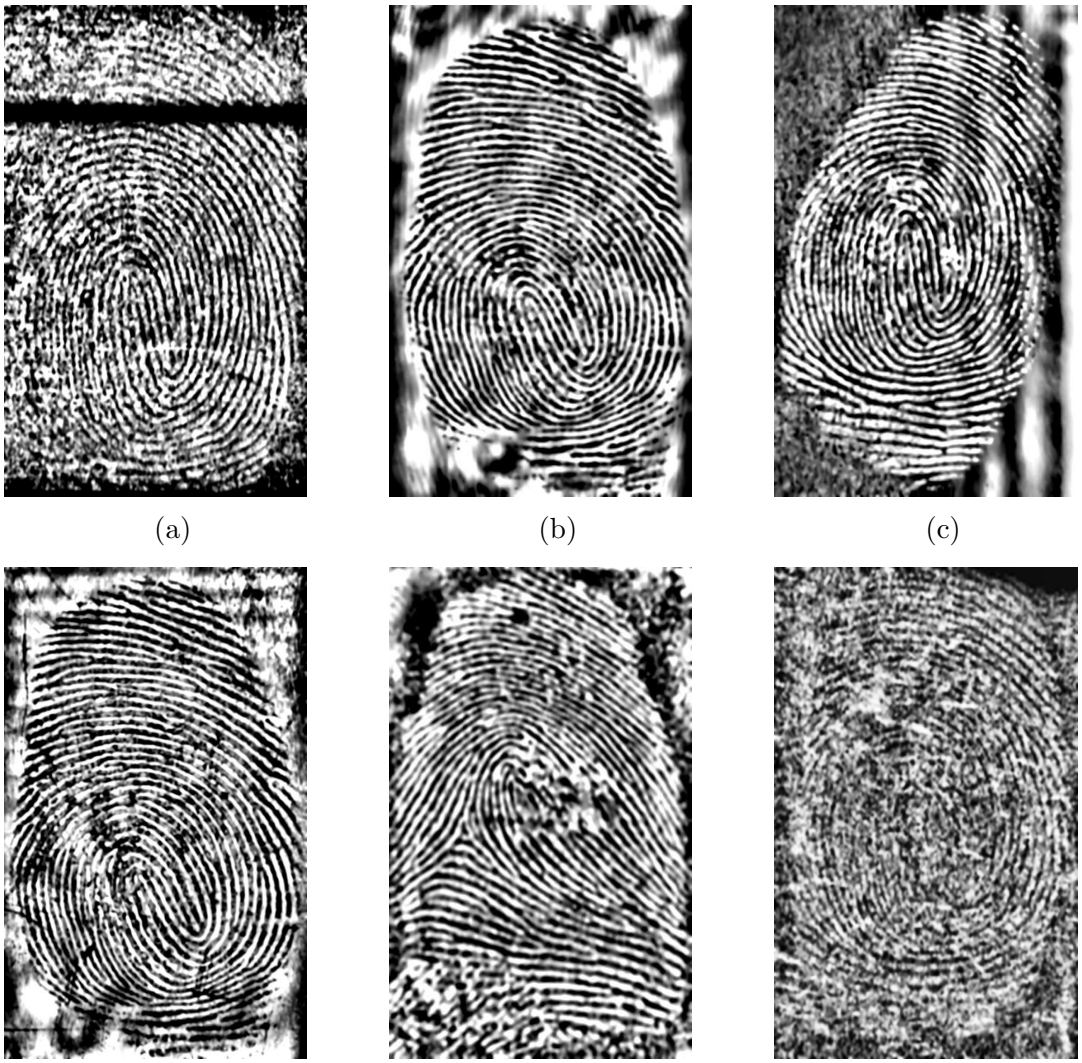

(a) (b) (c)

(d) (e) (f)

Figure 6.10: Some latent fingerprint images denoised by VisuShrink, (a) Brass, (b) Glass, (c) Mirror, (d) Plastic (e) Stainless steel (f) Bullet cartridge.

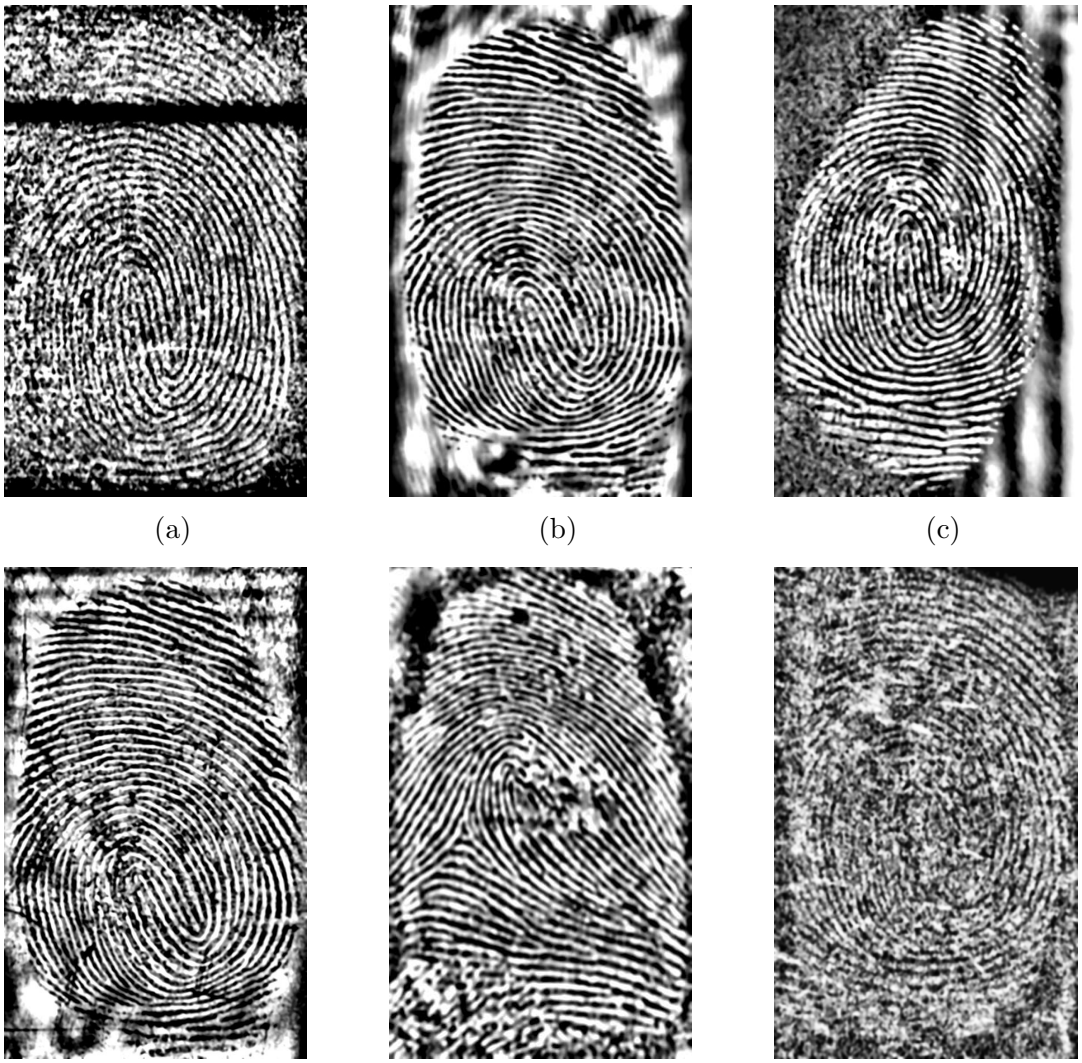

(a) (b) (c)

(d) (e) (f)

Figure 6.11: Some latent fingerprint images denoised by BayesShrink, (a) Brass, (b) Glass, (c) Mirror, (d) Plastic (e) Stainless steel (f) Bullet cartridge.

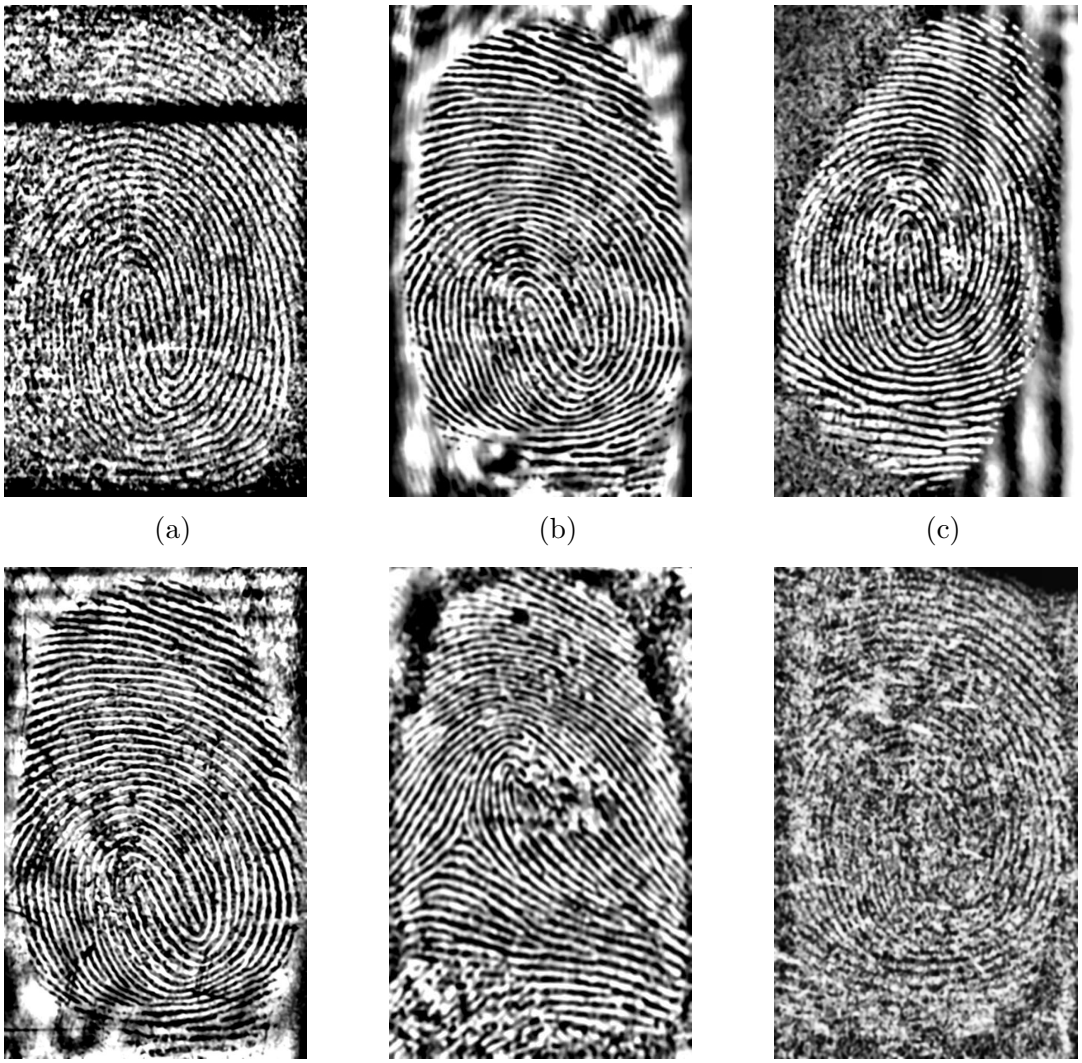

(a) (b) (c)

(d) (e) (f)

Figure 6.12: Latent fingerprint images denoised by SUREShrink, (a) Brass, (b) Glass, (c) Mirror, (d) Plastic (e) Stainless steel (f) Bullet cartridge.

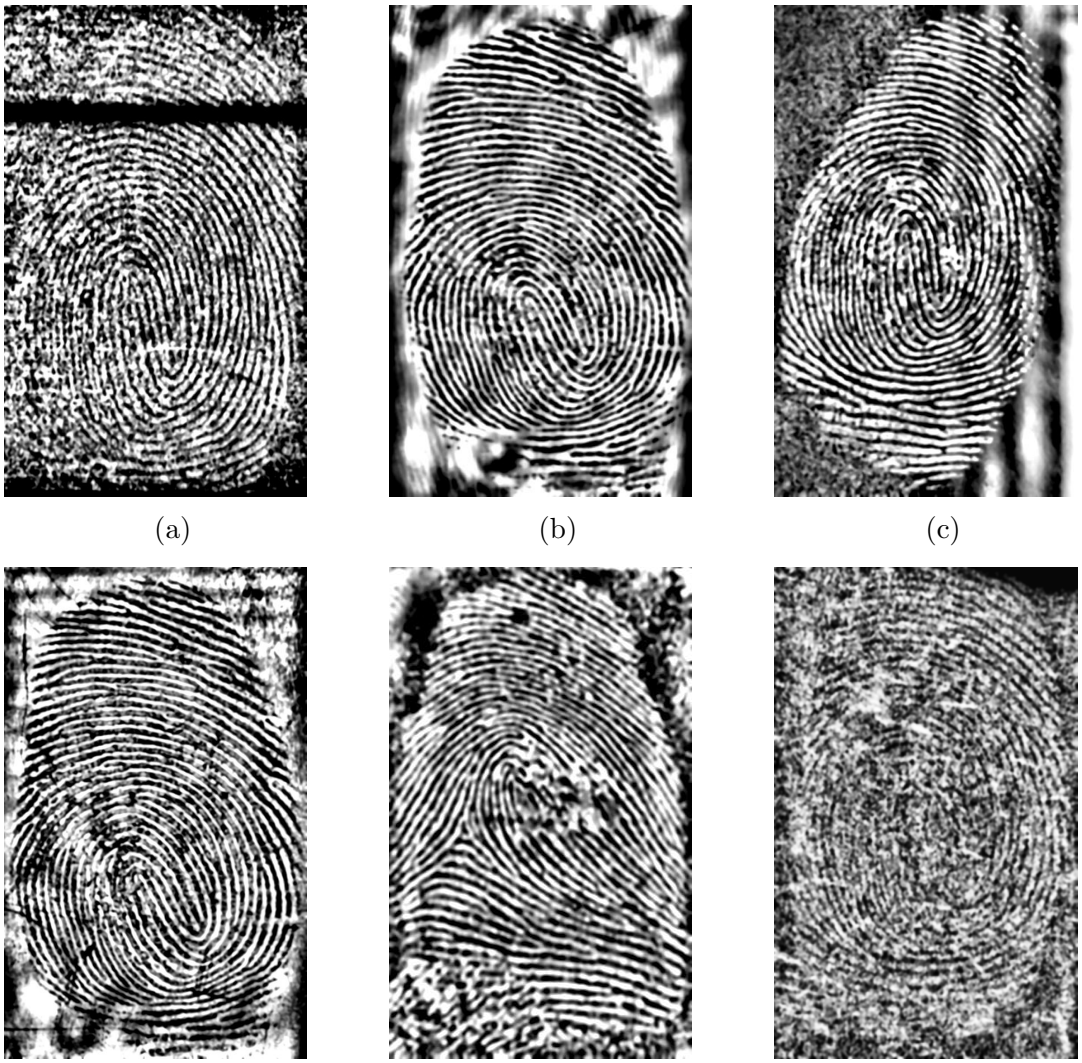

Figure 6.13: Latent fingerprint images denoised by NormalShrink, (a) Brass, (b) Glass, (c) Mirror, (d) Plastic (e) Stainless steel (f) Bullet cartridge.

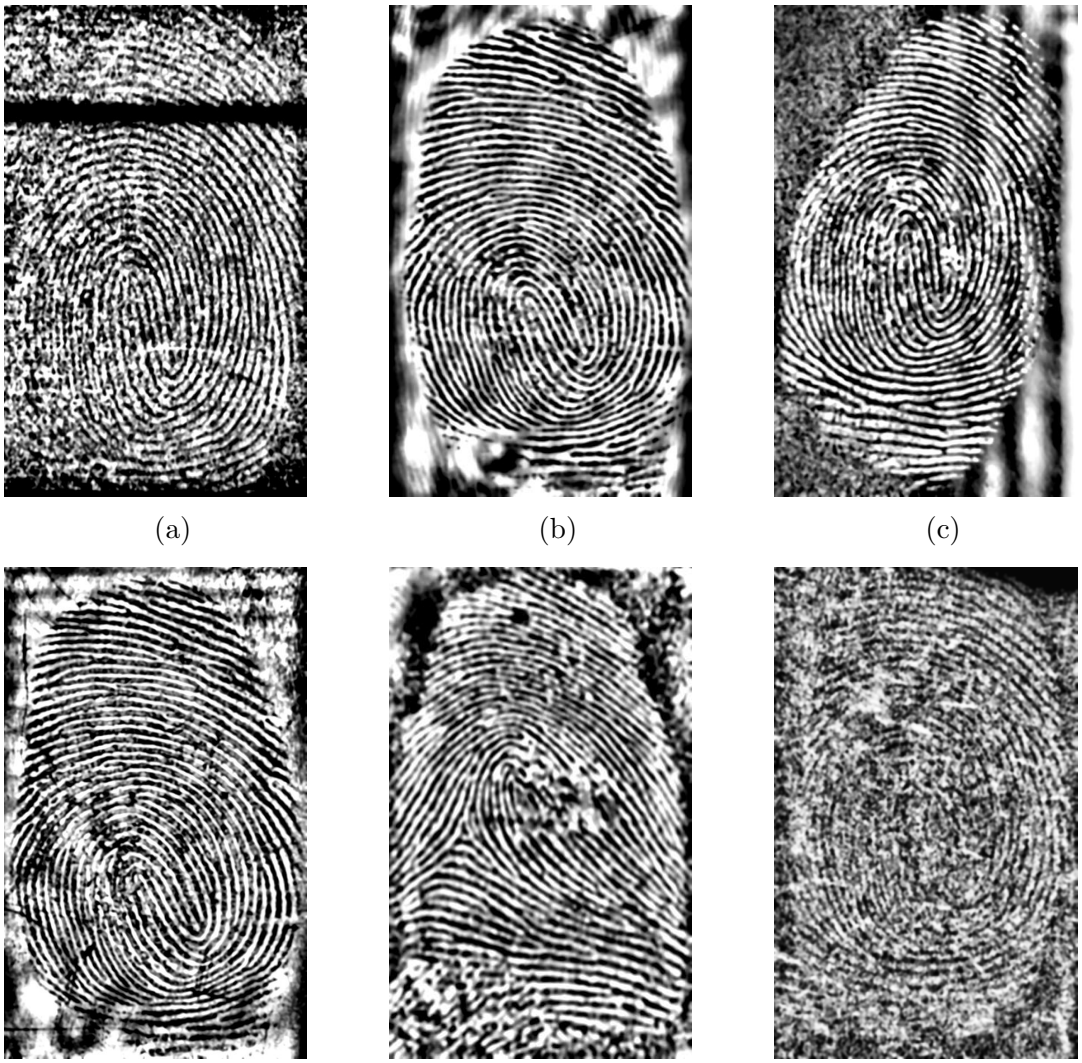

Figure 6.14: Latent fingerprint images denoised by adapt. threshold, (a) Brass, (b) Glass, (c) Mirror, (d) Plastic (e) Stainless steel (f) Bullet cartridge.

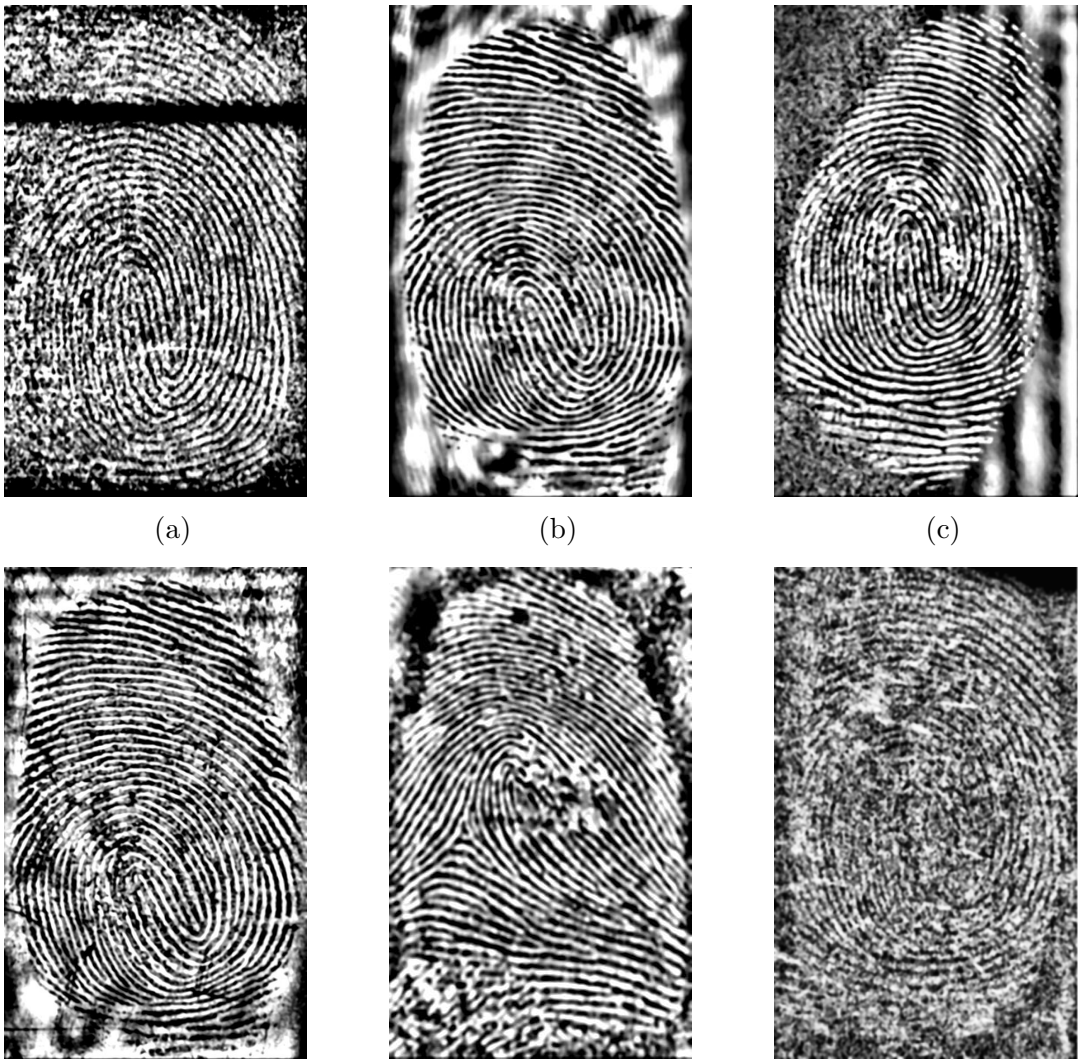

(a) (b) (c)

(d) (e) (f)

Figure 6.15: Latent fingerprint images denoised by the proposed method, (a) Brass, (b) Glass, (c) Mirror, (d) Plastic (e) Stainless steel (f) Bullet cartridge.

Table 6.6: OCL measure of each fingerprint image denoised by different denoising techniques with different filters at different levels of decomposition.

Levels	Visu-Shrink	Bayes-Shrink	SURE-Shrink	Normal-Shrink	Adapt. Threshold	Proposed Method
haar						
1	70.6104	72.2662	**72.2516**	72.2347	72.2401	72.2448
2	70.5241	72.2450	72.2808	72.2329	**72.2401**	72.2312
3	68.3122	**72.2450**	72.2808	72.2296	72.2401	72.2286
4	68.9367	**72.3362**	72.3020	72.2282	72.2401	72.2317
db2						
1	72.1198	72.1054	72.1029	72.2315	72.2336	**72.2422**
2	72.0506	72.2341	72.1921	72.2315	72.2336	**72.2370**
3	71.7564	72.2945	72.2071	72.2315	**72.2336**	72.2324
4	**72.2739**	72.3119	72.2717	72.2315	72.2336	72.2345
sym4						
1	72.2235	72.2150	72.2198	72.2224	72.2256	**72.2331**
2	**72.4911**	72.281	72.237	72.2224	72.2256	72.2195
3	**72.9184**	72.2959	72.3188	72.2224	72.2256	72.2247
4	**73.0229**	72.2911	72.3172	72.2224	72.2256	72.2247
bior2.6						
1	72.1467	72.1506	72.1459	72.2232	72.2257	**72.2257**
2	**72.2389**	72.2050	72.1771	72.2232	72.2257	72.2238
3	**72.5688**	72.2238	72.2010	72.2232	72.2257	72.2295
4	**72.7013**	72.2248	72.1998	72.2232	72.2257	72.2300

6.3.1 Wavelet filter based analysis

In Table 6.6, the *haar* wavelet filter row shows that OCL values of VisuShrink, BayesShrink, NormalShrink and the proposed technique decrease with an increase in decomposition levels. SUREShrink OCL values increase with an increase in decomposition levels while adaptive threshold OCL values are the same at all levels of decomposition.

The *db2* wavelet filter row shows that OCL values for BayesShrink and SUREShrink increase with decomposition levels while NormalShrink and adaptive threshold remain constant at all decomposition levels. The proposed technique's OCL values decrease with an increase in decomposition levels.

The *sym4* wavelet filter row shows that the OCL values of VisuShrink, BayesShrink and SUREShrink increase with an increase in decomposition levels while NormalShrink and adaptive threshold have constant OCL values. The OCL values of the proposed method decrease with an increase in decomposition levels.

The *bior2.6* wavelet filter row shows that the OCL values of the proposed technique, VisuShrink, SUREShrink and BayesShrink improve with an increase in decomposition

levels while NormalShrink and adaptive threshold remain constant throughout the decomposition levels.

6.3.2 Technique-based analysis

The OCL values of the adaptive threshold depend on the wavelet filter used. The *haar* wavelet filter has the lowest OCL value while *bior2.6* has the highest, because *haar* is computationally efficient, compared to other wavelet filters [127].

The optimal OCL value for NormalShrink is achieved at level 1, *haar* wavelet filter. The other filters (*i.e db*2, *sym4* and *boir*2.6) OCL values remain constant at all decomposition levels. The best value for adaptive threshold is achieved on a *bior2.6* wavelet filter. At level 1, *haar* filter, the optimal OCL value for the proposed technique is achieved.

The VisuShrink technique has the highest OCL value at level 4 *sym4* wavelet filter, however, higher levels of wavelet decomposition distort the image [103], hence the high OCL value at levels 2 and 3 are not recommended in this study.

6.3.3 OCL values after segmentation

i. In Table 6.7, at *haar* level 1, BayesShrink has the better OCL value while at level 2, SUREShrink is desirable at *haar* levels 2 and 4. The proposed technique is effective at *haar* level 4 of decomposition.

ii. On the *db2* wavelet filter row, the proposed technique at levels 1 and 3 has the better OCL values while BayesShrink is effective at levels 2 and 4.

iii. On *sym4* wavelet filter row, the proposed technique is superior at level 1, VisuShrink is effective at levels 2 and 4 and BayesShrink is better at level 4.

iv. On the *bior2.6* wavelet filter, at level 1, the proposed technique is effective, at level 2, the adaptive threshold is better, while BayesShrink and VisuShrink are desirable at levels 3 and 4 respectively.

v. Figures 6.16 & 6.17 were constructed using the OCL results on Table 6.7 after segmentation. Comparing Table 6.6 and Table 6.7 we observe that the results has improved by 3%.

vi. In Figure 6.16a, all the methods perform better at level 1 with BayesShrink the best. At level 2 the proposed technique is efficient with the better OCL value.

vii. In Figure 6.16b, level 4 is the most effective level of decomposition with the highest OCL value of 75.278% by BayesShrink, followed by SUREShrink with an OCL value of 75.2628 %.

Table 6.7: OCL values of fingerprint images after successful denoising and segmentation of the fingerprint images.

Levels	**Visu-Shrink**	**Bayes-Shrink**	**SURE-Shrink**	**Normal-Shrink**	**Adapt. Threshold**	**Proposed Method**
haar						
1	73.4913	75.2938	75.1104	75.0315	74.9645	75.0539
2	72.7586	74.9417	75.0513	74.9741	74.9645	75.0309
3	69.8371	74.9356	75.1798	75.0086	74.9645	75.0512
4	70.1719	75.0633	75.0683	75.0420	74.9645	75.1936
db2						
1	75.0077	75.1570	74.9181	75.1321	75.0246	75.1624
2	74.4223	75.1482	74.9974	75.1321	75.0246	75.1362
3	73.5959	75.1116	75.1627	75.1321	75.0246	75.1894
4	73.8668	75.2780	75.2628	75.1321	75.0246	75.0084
sym4						
1	75.0458	75.1395	75.0658	75.1793	75.1811	75.1870
2	75.2423	75.1133	75.0541	75.1793	75.1811	75.0849
3	75.3578	75.3060	75.1541	75.1793	75.1811	75.0672
4	75.6958	75.1745	75.1515	75.1793	75.1811	75.0717
bior2.6						
1	75.0344	75.0076	75.0452	75.0979	75.1213	75.1581
2	74.9379	75.0989	74.9991	75.0979	75.1213	75.0487
3	75.0839	75.1442	75.0413	75.0979	75.1213	75.0300
4	75.2695	75.1503	75.0629	75.0979	75.1213	75.0022

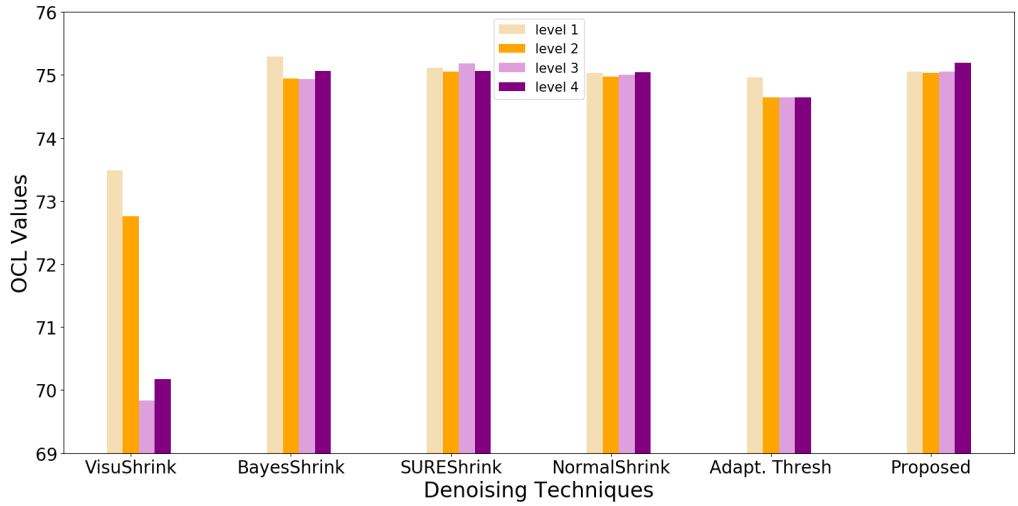

(a)

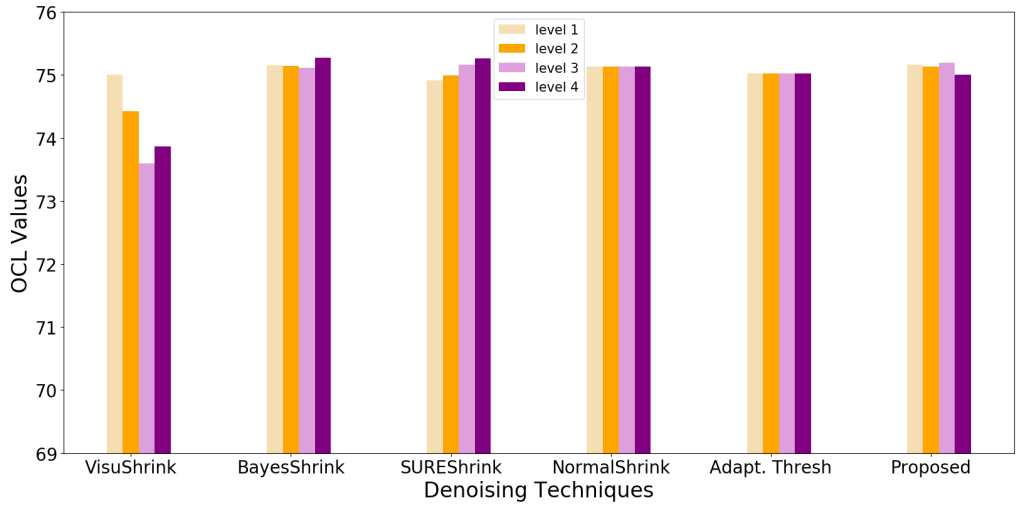

(b)

Figure 6.16: OCL values of *haar* and *db2* wavelet filters after successfully denoising, segmenting and applying ridge structure enhancement: (a) *haar* wavelet filter, (b) *db2* wavelet filter.

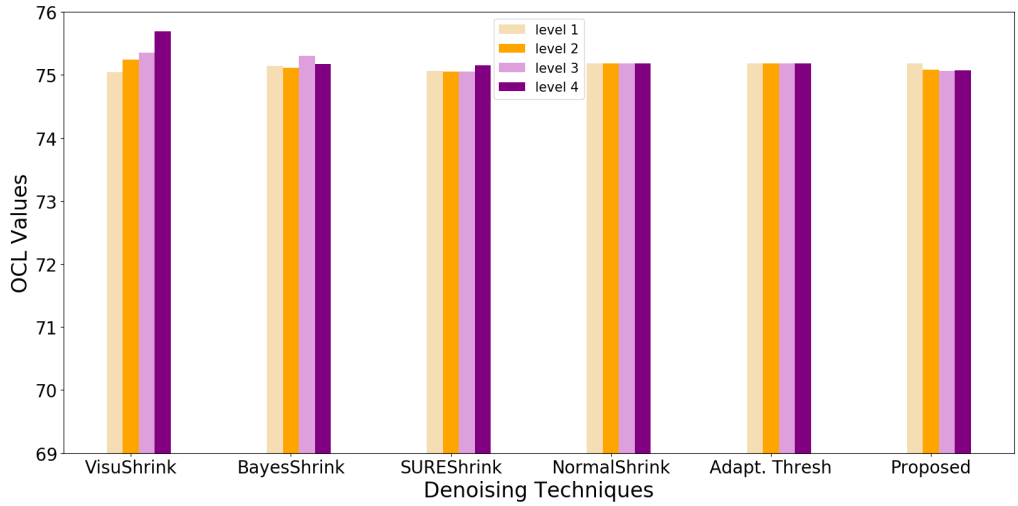

(a)

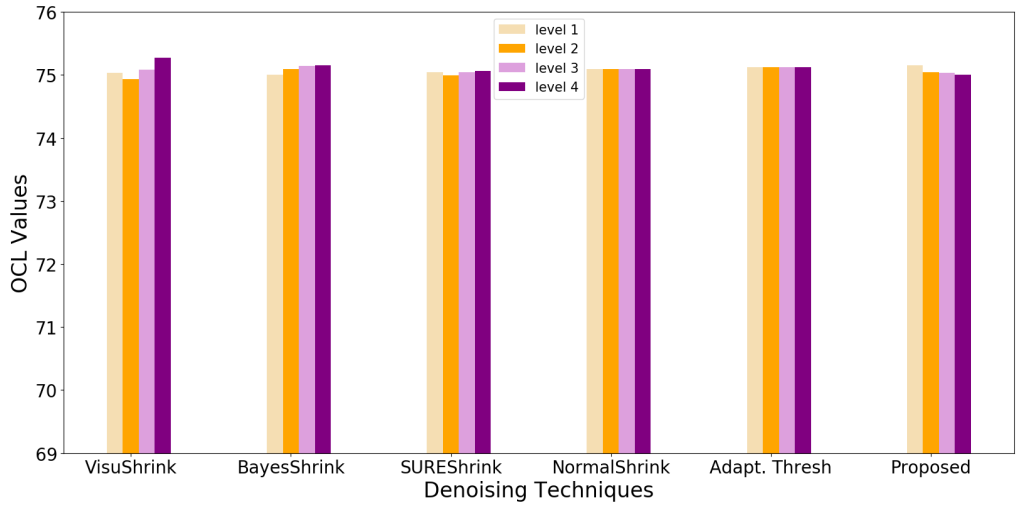

(b)

Figure 6.17: OCL values of *sym4* and *bior2.6* wavelet filters after successfully denoising, segmenting and applying ridge structure enhancement: (a) *sym4* wavelet filter, (b) *bior2.6* wavelet filter.

6.3.4 Section summary

In this section, we confirmed that as the wavelet filtering graduality increases, the wavelet denoising techniques perform better. It is observed that the proposed technique preserve the structure of the original image better. Moreover, we have found that as the decomposition level increases, the image is distorted, therefore levels 1 and 2 are recommended for better results.

6.4 Ridge Structure Enhancement

This section presents results of the ridge structure enhancement combined with different denoising techniques (*i.e.* VisuShrink, BayesShrink, SUREShrink, NormalShrink, adaptive threshold and the proposed method). The OCL is measured for each combination and the best combination is revealed.

Figure 6.18: Latent fingerprint images denoised by the proposed technique, (a) Brass, (b) Glass, (c) Mirror, (d) Plastic (e) Stainless steel (f) Bullet cartridge.

Table 6.8: OCL values of fingerprint images after successfully applying denoising, segmentation and ridge structure enhancement.

Levels	**Visu-Shrink**	**Bayes-Shrink**	**SURE-Shrink**	**Normal-Shrink**	**Adapt. Threshold**	**Proposed Method**
haar						
1	85.9284	85.8228	85.9740	86.23010	86.2561	86.1300
2	85.2992	86.0114	85.937	86.1626	86.2561	86.2016
3	82.7818	86.0542	85.7905	86.1392	86.2561	86.1967
4	82.3376	86.0163	86.0528	86.2194	86.2561	86.1816
db2						
1	85.7582	86.0378	85.9096	86.1842	86.2185	86.1569
2	85.7700	86.1001	86.0552	86.1842	86.2185	86.2189
3	85.1936	86.1662	86.0053	86.1842	86.2185	86.2259
4	85.0817	86.1105	86.3231	86.1842	86.2185	86.2523
sym4						
1	86.0914	86.1865	86.1234	86.1376	86.1678	86.1577
2	86.3219	86.2412	86.1324	86.1376	86.1678	86.2507
3	85.8599	85.953	86.1389	86.1376	86.1678	86.1361
4	86.2983	86.2473	85.9545	86.1376	86.1678	86.1539
bior2.6						
1	86.1539	86.0663	86.0349	86.2052	86.3245	86.3884
2	86.1750	86.1655	86.0903	86.2052	86.3245	86.2733
3	86.0774	86.0493	86.0612	86.2052	86.3245	86.2697
4	86.2230	85.9631	86.1262	86.2052	86.3245	86.2565

6.4.1 Orientation estimation results

i. Figures 6.19 and 6.20 were constructed using the OCL data on Table 6.8. Comparing Table 6.7 and Table 6.8 we observed that the OCL values had improved by 11 % because after ridge structure enhancement had been applied, fingerprint ridges and valleys were more clear and dominant. This is also shown in Figures 6.19 and 6.20.

ii. In Figure 6.19b we observe that SUREShrink is effective with an OCL value of 86.3231 at level 4 wavelet decomposition. VisuShrink is better at level 2 as shown in Figure 6.20a while adaptive threshold dominates level 1 decomposition in Figure 6.19a.

iii. Figure 6.20b, shows that the proposed method is optimal at level 1 with an OCL value of 86.3884. Throughout this research, the proposed method has displayed better results with a *bior*2.6 wavelet filter.

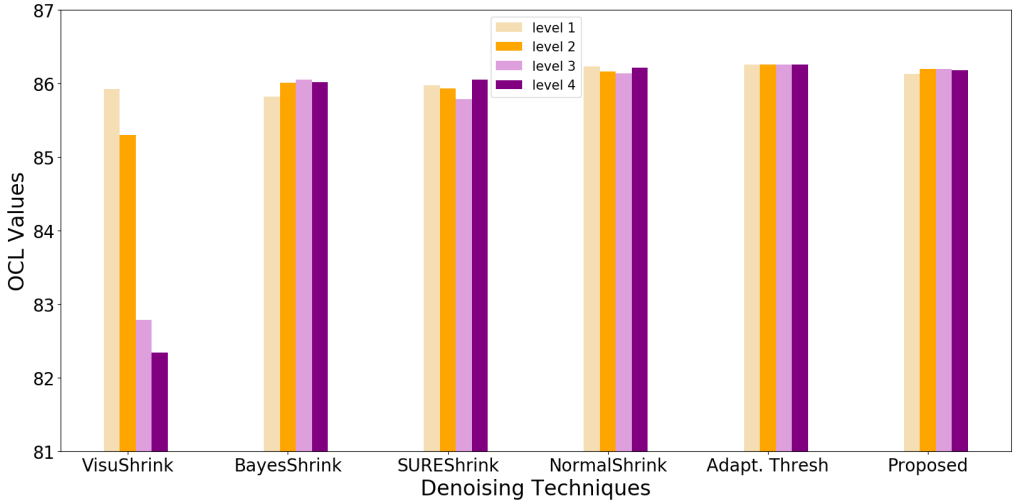

(a)

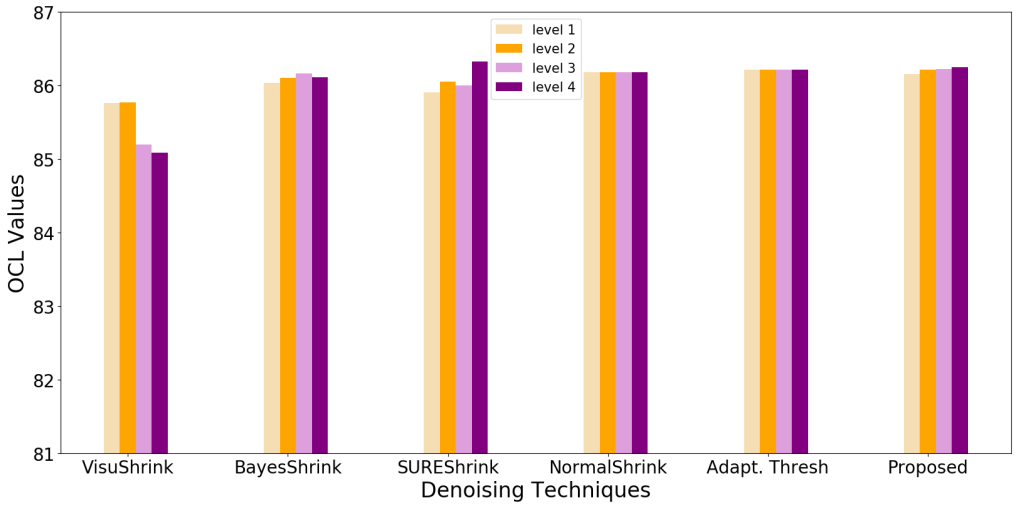

(b)

Figure 6.19: OCL values of *haar* and *db2* wavelet filter after successfully denoising, segmenting and applied ridge structure enhancement: (a) *haar* wavelet filter, (b) *db2* wavelet filter.

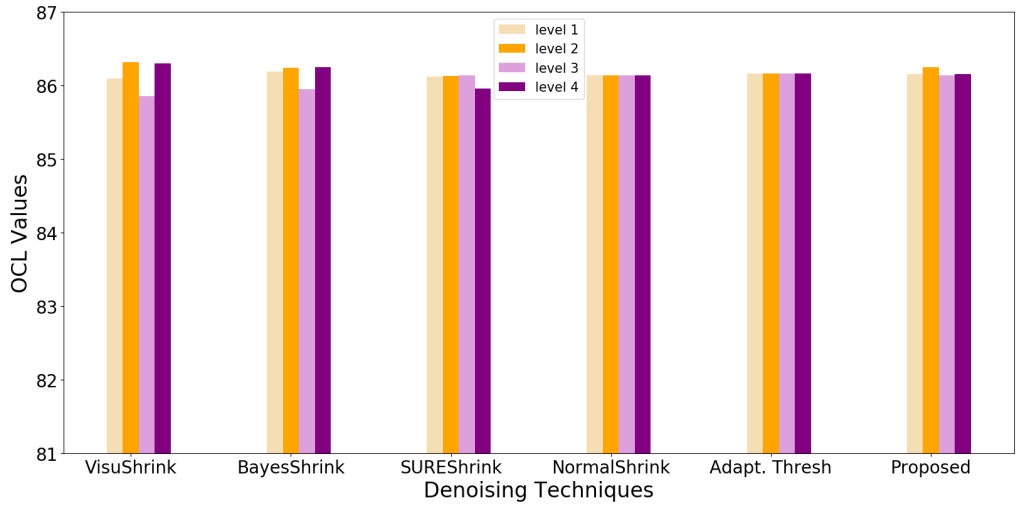

(a)

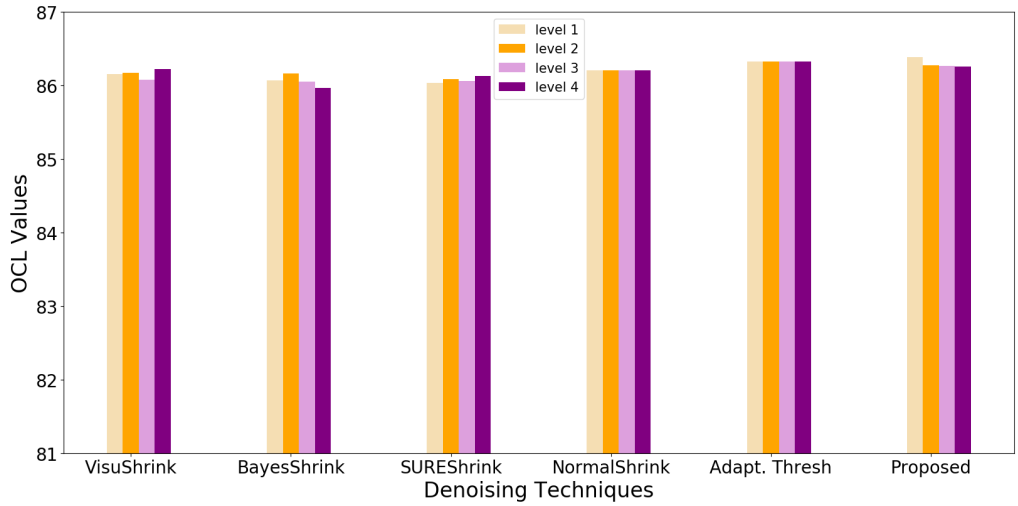

(b)

Figure 6.20: OCL values of *sym4* and *bior2.6* wavelet filter after successfully denoising, segmenting and applied ridge structure enhancement: (a) *sym4* wavelet filter, (b) *bior2.6* wavelet filter

6.5 Recommended Enhancement

The proposed method with *sym*4 or *bior*2.6 at level 1 or 2 is recommended for OCT denoising of latent fingerprint images. After denoising, segmentation is required to improve the quality of the fingerprint by removing the background. Segmentation is regarded as the preprocessing technique of ridge structure enhancement. Enhancing the ridge structure includes normalization, ridge orientation field, ridge frequency estimation, ridge filtering and binarization. The combination of the proposed wavelet denoising technique and ridge structure enhancement is the proposed enhancement technique. Figure 6.21 shows the recommended enhancement technique for OCT images of latent fingerprints.

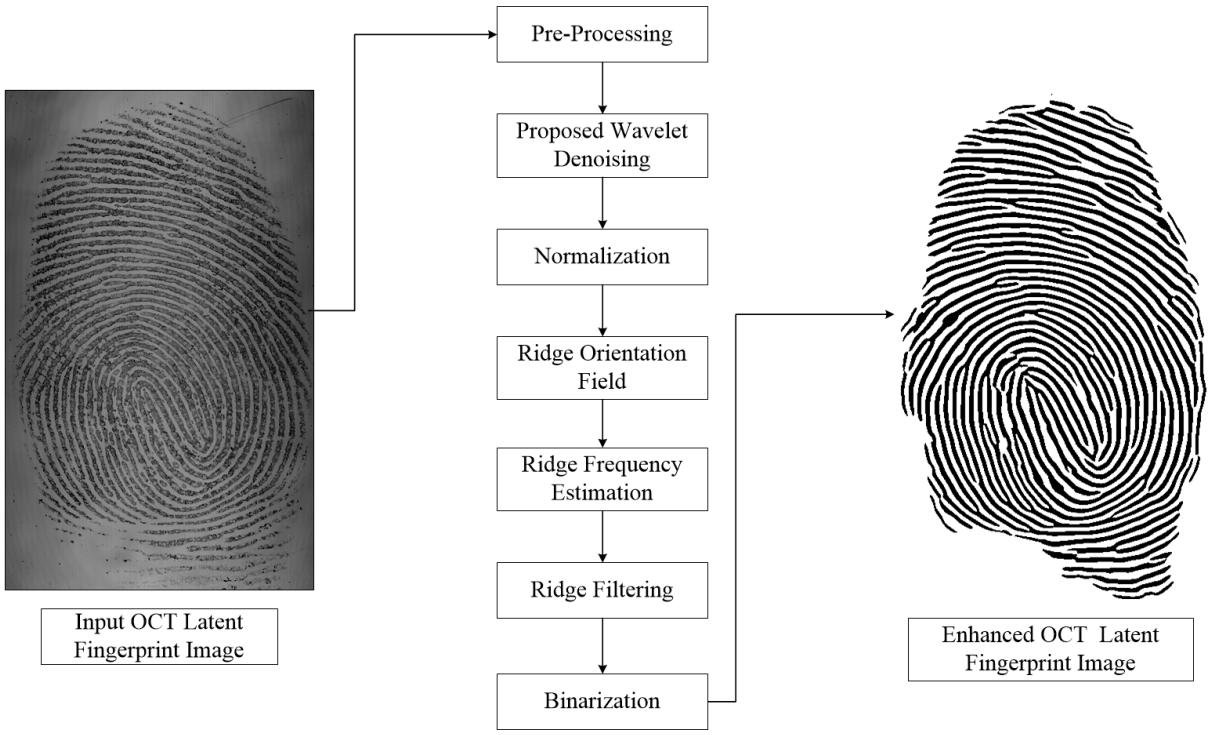

Figure 6.21: Recommended OCT enhancement procedure.

6.6 Summary

This chapter presented quality check techniques which can be used to assess the fingerprint images before and after enhancement. In this work, we only used PSNR, SNR, RMSE and OCL to assess the performance of our enhancement techniques. Levels 1 and 2 are recommended for denoising, since a higher level distort the image.

Chapter 7

Conclusions and Future Work

7.1 Conclusions

This research has focused on latent fingerprint acquisition, denoising, ridge structure enhancement and quality estimation. The current latent fingerprint acquisition techniques are destructive, harmful to users and time-consuming. The OCT device addresses these limitations, since it is contactless and penetrates the surface few millimetres. Latent fingerprints have been acquired successfully from glass, plastic, brass, stainless steel, mirror and bullet cartridge.

Different methods have been investigated and implemented in an effort to remove speckle noise effect. These techniques include VisuShrink, BayesShrink, SUREShrink, NormalShrink, adaptive Threshold. The NormalShrink and adaptive threshold have been modified to form a new technique for speckle noise removal. The proposed denoising technique removes speckle noise effectively. This robustness of the proposed technique is demonstrated by its better PSNR, SNR, RMSE and SSIM values.

The combination of the proposed wavelet denoising technique and the ridge structure enhancement technique has successfully helped to improve the quality of latent fingerprint images. This is evident from the results of the OCL.

The quality estimation methods *i.e.* PSNR, SNR, RMSE, SSIM and OCL were investigated and implemented in this work. The highest value of PSNR was found to be 8.6062, SNR was 2.5186, SSIM was 6.5410%, OCL was 86.3884% and the minimum RMSE was 1.0844.

7.2 Application

The OCT device may be used by forensic scientists to acquire latent fingerprints from various surfaces. The proposed wavelet-based denoising technique may be used to denoise medical images taken by OCT or ultrasound, in addition to latent fingerprints.

7.3 Future Work

Some future research that can be carried out from this work are:

1. Expanding the OCT latent fingerprint database.
2. Further assessing the quality of OCT latent fingerprint images by using other existing techniques.
3. Designing and implementing fingerprint recognition based on OCT latent fingerprint images.

Bibliography

[1] Rohan Nimkar and Agya Mishra. Fingerprint segmentation algorithms: A literature review. *International Journal of Computer Applications*, 95(5), 2014.

[2] Jiangyang Zhang, Rongjie Lai, and C-C Jay Kuo. Latent fingerprint detection and segmentation with a directional total variation model. In *Image Processing (ICIP), 2012 19th IEEE International Conference on*, pages 1145–1148. IEEE, 2012.

[3] Ashish Badiye and Neeti Kapoor. Efficacy of robin® powder blue for latent fingerprint development on various surfaces. *Egyptian Journal of Forensic Sciences*, 5(4):166–173, 2015.

[4] Satish Kumar Dubey, Dalip Singh Mehta, Arun Anand, and Chandra Shakher. Simultaneous topography and tomography of latent fingerprints using full-field swept-source optical coherence tomography. *Journal of Optics A: Pure and Applied Optics*, 10(1):015307, 2008.

[5] Marcus Leich, Stefan Kiltz, Jana Dittmann, and Claus Vielhauer. Non-destructive forensic latent fingerprint acquisition with chromatic white light sensors. In *Media Watermarking, Security, and Forensics III*, volume 7880, page 78800S. International Society for Optics and Photonics, 2011.

[6] Richa Rohatgi and AK Kapoor. Development of latent fingerprints on wet non-porous surfaces with spr based on basic fuchsin dye. *Egyptian Journal of Forensic Sciences*, 6(2):179–184, 2016.

[7] Dusting for fingerprints - elizabeth reninger. `https://elizabeth-reninger.com/dusting-for-fingerprints/`. (Accessed on 02/08/2019).

[8] Peter Kiran A Dakshinamurthy S. Study on efficiency of alternate light source for detection of latent fingerprints. volume 9, page 555774, 2018.

[9] Apollo Chun-Yen Lin, Hsing-Mei Hsieh, Li-Chin Tsai, Adrian Linacre, and James Chun-I Lee. Forensic applications of infrared imaging for the detection and recording of latent evidence. *Journal of forensic sciences*, 52(5):1148–1150, 2007.

[10] Nicole J Crane, Edward G Bartick, Rebecca Schwartz Perlman, and Scott Huffman. Infrared spectroscopic imaging for noninvasive detection of latent fingerprints. *Journal of forensic sciences*, 52(1):48–53, 2007.

[11] Naoki Saitoh and Norimitsu Akiba. Ultraviolet fluorescence imaging of fingerprints. *The Scientific World Journal*, 6:691–699, 2006.

[12] Touch dna - an overview sciencedirect topics. `https://www.sciencedirect.com/topics/neuroscience/touch-dna`. (Accessed on 11/07/2019).

[13] What is touch dna? - scientific american. `https://www.scientificamerican.com/article/experts-touch-dna-jonbenet-ramsey/`. (Accessed on 11/07/2019).

[14] How to swab for touch dna evidence. `https://blog.puritanmedproducts.com/how-to-swab-for-touch-dna-evidence`, . (Accessed on 11/07/2019).

[15] Your fingerprints are about to reveal a lot more about you. `https://www.popularmechanics.com/technology/security/a17172/your-fingerprints-are-about-to-reveal-a-lot-more-about-you/`. (Accessed on 11/07/2019).

[16] The hidden data in your fingerprints. `http://theconversation.com/the-hidden-data-in-your-fingerprints-95491`. (Accessed on 11/07/2019).

[17] Alenrex Maity, Anshuman Pattanaik, Santwana Sagnika, and Santosh Pani. A comparative study on approaches to speckle noise reduction in images. In *Computational Intelligence and Networks (CINE), 2015 International Conference on*, pages 148–155. IEEE, 2015.

[18] Sukhjinder Kaur. Noise types and various removal techniques. *International Journal of Advanced Research in Electronics and Communication Engineering (IJARECE)*, 4(2):226–230, 2015.

[19] Ma Yinping and Huang Yongxing. Adaptive threshold based on wavelet transform fingerprint image denoising. In *Proceedings of the 2012 International Conference on Computer Science and Electronics Engineering - Volume 03*, ICCSEE '12, pages 494–497. IEEE Computer Society, 2012. ISBN 978-0-7695-4647-6. doi: 10.1109/ICCSEE.2012.139.

[20] Luke Nicholas Darlow, Sharat Saurabh Akhoury, and James Connan. A review of state-of-the-art speckle reduction techniques for optical coherence tomography fingertip scans. In *Seventh International Conference on Machine Vision (ICMV 2014)*, volume 9445, page 944523. International Society for Optics and Photonics, 2015.

[21] Sisanda Makinana, Portia N Khanyile, and Rethabile Khutlang. Latent fingerprint wavelet transform image enhancement technique for optical coherence tomography. In *Artificial Intelligence and Pattern Recognition (AIPR), International Conference on*, pages 1–5. IEEE, 2016.

[22] L. Wieclaw. Gradient based fingerprint orientation field estimation. *Journal of Medical Informatics & Technologies*, Vol. 22:203–207, 2013.

[23] Sarat C Dass and Anil K Jain. Fingerprint classification using orientation field flow curves. In *ICVGIP*, pages 650–655, 2004.

[24] Ravinder Kumar, Pravin Chandra, and M Hanmandlu. Fingerprint singular point detection using orientation field reliability. In *Advanced Materials Research*, volume 403, pages 4499–4506. Trans Tech Publ, 2012.

[25] M James Stephen, Prasad Reddy, et al. Enhancing fingerprint image through ridge orientation with neural network approach and ternarization for effective minutiae extraction. *International Journal of Machine Learning and Computing*, 2(4):397, 2012.

[26] Anush Sankaran, Mayank Vatsa, and Richa Singh. Automated clarity and quality assessment for latent fingerprints. In *Biometrics: Theory, Applications and Systems (BTAS), 2013 IEEE Sixth International Conference on*, pages 1–6. IEEE, 2013.

[27] Shan Juan Xie, JuCheng Yang, Dong Sun Park, Sook Yoon, and Jinwook Shin. Fingerprint quality analysis and estimation approach for fingerprint matching. In *State of the art in Biometrics*. InTech, 2011.

[28] Shan Juan Xie, Sook Yoon, Jinwook Shin, and Dong Sun Park. Effective fingerprint quality estimation for diverse capture sensors. *Sensors*, 10(9):7896–7912, 2010.

[29] E. Lim, K. . Toh, P. N. Suganthan, X. Jiang, and W. . Yau. Fingerprint image quality analysis. In *2004 International Conference on Image Processing, 2004. ICIP '04.*, volume 2, pages 1241–1244 Vol.2, Oct 2004. doi: 10.1109/ICIP.2004.1419530.

[30] Jianjiang Feng, Soweon Yoon, and Anil K. Jain. Latent fingerprint matching: Fusion of rolled and plain fingerprints. In Massimo Tistarelli and Mark S. Nixon, editors, *Advances in Biometrics*, pages 695–704, Berlin, Heidelberg, 2009. Springer Berlin Heidelberg. ISBN 978-3-642-01793-3.

[31] Soweon Yoon, Eryun Liu, and Anil K Jain. On latent fingerprint image quality. In *Computational Forensics*, pages 67–82. Springer, 2015.

[32] 02_latent_print.pdf. http://d1zh4ok0q8k7dm.cloudfront.net. (Accessed on 09/19/2018).

[33] Ning Zhang, Chengming Wang, Zhenwen Sun, Zhigang Li, Lanchi Xie, Yuwen Yan, Lei Xu, Jingjing Guo, Wei Huang, Zhihui Li, et al. Detection of latent fingerprint hidden beneath adhesive tape by optical coherence tomography. *Forensic science international*, 287:81–87, 2018.

[34] Sarah Fieldhouse, Robin Parsons, Stephen Bleay, and Laura Walton-Williams. The effect of dna recovery on the subsequent quality of latent fingermarks: A pseudo-operational trial. *Forensic Science International*, 307:110076, 2020.

[35] Sangeeta Aditya, AK Sharma, CN Bhattacharyya, and Keya Chaudhuri. Generating str profile from "touch dna". *Journal of forensic and legal medicine*, 18 (7):295–298, 2011.

[36] Sarah Fieldhouse, Eliska Oravcova, and Laura Walton-Williams. The effect of dna recovery on the subsequent quality of latent fingermarks. *Forensic science international*, 267:78–88, 2016.

[37] Melanie J Bailey, Robert Bradshaw, Simona Francese, Tara L Salter, Catia Costa, Mahado Ismail, Roger P Webb, Ingrid Bosman, Kim Wolff, and Marcel de Puit. Rapid detection of cocaine, benzoylecgonine and methylecgonine in fingerprints using surface mass spectrometry. *Analyst*, 140(18):6254–6259, 2015.

[38] How does fingerprint drug testing work? `https://www.news-medical.net/life-sciences/How-Does-Fingerprint-Drug-Testing-Work.aspx`, . (Accessed on 12/04/2019).

[39] T Spear, J Clark, M Giusto, N Khoshkebari, M Murphy, and J Rush. Fingerprints & cartridge cases: how often are fingerprints found on handled cartridge cases and can these fingerprints be successfully typed for dna? california dept. of justice, bureau of forensic services. *California Criminalistics Institute*, 2005.

[40] KM Sharavana Raju, Mohammad Shahnawaz Nasir, and T Meera Devi. Filtering techniques to reduce speckle noise and image quality enhancement methods on satellite images. *IOSR Journal of Computer Engineering (IOSR-JCE)*, 15(4):10–15, 2013.

[41] Cedric Neumann. Fingerprints at the crime-scene: Statistically certain, or probable? *Significance*, 9(1):21–25, 2012.

[42] Gurvinder Singh Bumbrah, Rakesh Mohan Sharma, and Om Prakash Jasuja. Emerging latent fingerprint technologies: a review. *Research and Reports in Forensic Medical Science*, 6:39–50, 2016.

[43] Ronny Merkel. *New Solutions for an Old Challenge: Chances and Limitations of Optical, Non-Invasive Acquisition and Digital Processing Techniques for the Age Estimation of Latent Fingerprints*. Logos Verlag Berlin GmbH, 2014.

[44] Dan P Popescu, Costel Flueraru, Youxin Mao, Shoude Chang, John Disano, Sherif Sherif, Michael G Sowa, et al. Optical coherence tomography: fundamental principles, instrumental designs and biomedical applications. *Biophysical reviews*, 3(3):155, 2011.

[45] Yongzhao Du, Gangjun Liu, Guoying Feng, and Zhongping Chen. Speckle reduction in optical coherence tomography images based on wave atoms. *Journal of biomedical optics*, 19(5):056009, 2014.

[46] Guohua Liu, Ziyu Wang, Guoying Mu, and Peijin Li. Efficient oct image enhancement based on collaborative shock filtering. *Journal of healthcare engineering*, 2018:1–7, 2018.

[47] Desmond C Adler, Tony H Ko, and James G Fujimoto. Speckle reduction in optical coherence tomography images by use of a spatially adaptive wavelet filter. *Optics letters*, 29(24):2878–2880, 2004.

[48] Pamela D. Williams. Dusting for fingerprints. https://2encourage.blogspot.com/2017/10/dusting-for-fingerprints.html, October 2017. (Accessed on 05/29/2020).

[49] Evident. https://www.shopevident.com/category/latent-fingerprints-2/rough-surface-fingerprint-tape. (Accessed on 05/29/2020).

[50] Scenescope ruvis latent fingerprint detection - horiba. https://www.horiba.com/us/en/scientific/products/forensics/ruvis-applications/details/scenescope-ruvis-reflected-ultra-violet-imaging-system-158/. (Accessed on 04/30/2020).

[51] Latent fingerprint detection - applications - spex forensics. https://spexforensics.com/applications/latent-fingerprint-detection. (Accessed on 05/28/2020).

[52] Peter Kiran A Dakshinamurthy S. Study on efficiency of alternate light source for detection of latent fingerprints. *J Forensic Sci & Criminal Inves*, 9(5):555774, 2018.

[53] Contactless latent fingerprint detection (eviscan). https://www.eviscan.com/en/. (Accessed on 02/01/2019).

[54] Ankita Katiyar and V Santhi. Region based speckle noise reduction approach using fuzzy techniques. In *Intelligent Computing, Instrumentation and Control Technologies (ICICICT), 2017 International Conference on*, pages 673–676. IEEE, 2017.

[55] P.S. Hiremath, Prema T. Akkasaligar, and Sharan Badiger. Speckle noise reduction in medical ultrasound images. In Gunti Gunarathne, editor, *Advancements and Breakthroughs in Ultrasound Imaging*, chapter 8. IntechOpen, Rijeka, 2013. doi: 10.5772/56519. URL https://doi.org/10.5772/56519.

[56] Liton Devnath and Rafiqul Islam. *Fingerprint Image De-noising by Various Filters for Different Noise using Wavelet Transform.* PhD thesis, 02 2016.

[57] Ajay Kumar Boyat and Brijendra Kumar Joshi. A review paper: noise models in digital image processing. *arXiv preprint arXiv:1505.03489*, 2015.

[58] Samuel W. Hasinoff. *Photon, Poisson Noise*, pages 608–610. Springer US, Boston, MA, 2014.

[59] Photonnoise — scientific volume imaging. "https://svi.nl/PhotonNoise". (Accessed on 02/28/2019).

[60] Pawan Patidar, Manoj Gupta, Sumit Srivastava, and Ashok Kumar Nagawat. Image de-noising by various filters for different noise. *International journal of computer applications*, 9(4):45–50, 2010.

[61] Manohar Annappa Koli. Review of impulse noise reduction techniques. *International Journal on Computer Science and Engineering*, 4(2):184, 2012.

[62] C Anjanappa and Sheshadri HS. Development of mathematical morphology filter for medical image impulse noise removal. In *2015 International Conference on Emerging Research in Electronics, Computer Science and Technology (ICERECT)*, pages 311–318. IEEE, 2015.

[63] Lufeng Bai. A new nonconvex approach for image restoration with gamma noise. *Computers & Mathematics with Applications*, 77(10):2627–2639, 2019.

[64] Rafael C Gonzalez and Paul Wintz. Digital image processing(book). *Reading, Mass., Addison-Wesley Publishing Co., Inc.(Applied Mathematics and Computation*, (13):451, 1977.

[65] E Jebamalar Leavline, S Sutha, and D Asir Antony Gnana Singh. Wavelet domain shrinkage methods for noise removal in images: A compendium. *International Journal of Computer Applications*, 33(10):28–32, 2011.

[66] What are the mean and median filters? `https://www.markschulze.net/java/meanmed.html`. (Accessed on 02/01/2019).

[67] Annatoma Arif, Tuo Li, and Chi-Hao Cheng. Blurred fingerprint image enhancement: algorithm analysis and performance evaluation. *Signal, Image and Video Processing*, 12(4):1–8, 2018.

[68] Anil K Jain. *Fundamentals of digital image processing*. Englewood Cliffs, NJ: Prentice Hall,, 1989.

[69] Nivedita Soni and Ayasha Siddiqua. Filtering techniques used for blurred images in fingerprint recognition. *International Journal of Scientific and Research Publications*, 3(5), 2013.

[70] Devi Radhakrishnan and P. Sujatha. Enhancement of fingerprint image using wiener filter. *International Journal of Engineering & Technology*, 7:206, 12 2017.

[71] Nina Nuria Br Karo, Asti Yulia Sari, Nur Aziza, Hadrians Kesuma Putra, et al. The enhancement of fingerprint images using gabor filter. In *Journal of Physics: Conference Series*, volume 1196, page 012045. IOP Publishing, 2019.

[72] Smrity Prasad and N Ganesan. An image sharpening method by suppressing the noise. *International Journal of Computer Applications*, 51(16).

[73] Zhi-guo Qu, Ping Wang, Ying-hui Gao, Peng Wang, and Zhen-Kang Shen. Frequency domain filtering of gradient image for contour detection. *Optik*, 124 (13):1398–1401, 2013.

[74] S Neethu, S Sreelakshmi, and Deepa Sankar. Enhancement of fingerprint using fft× fft filter. *Procedia Computer Science*, 46:1561–1568, 2015.

[75] Ma Yinping and Huang Yongxing. Adaptive threshold based on wavelet transform fingerprint image denoising. In *2012 International Conference on Computer Science and Electronics Engineering*, pages 494–497. IEEE, 2012.

[76] K Sasirekha and K Thangavel. A novel wavelet based thresholding for denoising fingerprint image. In *2014 International Conference on Electronics, Communication and Computational Engineering (ICECCE)*, pages 119–124. IEEE, 2014.

[77] Dario Maio, Davide Maltoni, Raffaele Cappelli, James L. Wayman, and Anil K. Jain. Fvc2000: Fingerprint verification competition. *IEEE transactions on pattern analysis and machine intelligence*, 24(3):402–412, 2002.

[78] Nasar Iqbal. Reduction of Noise from Fingerprint Images using Stationary Wavelet Trasnform. *International Journal of Engineering Works (ISSN: 2409-277)*, 4(12): 104–108, December 2017. doi: 10.5281/zenodo.1133286.

[79] Gregory Fiumara, Patricia Flanagan, John Grantham, Kenneth Ko, Karen Marshall, Matthew Schwarz, Elham Tabassi, Brian Woodgate, and Christopher Boehnen. National Institute of Standards and Technology Special Database 302: Nail to Nail Fingerprint Challenge. Technical Note 2007, National Institute of Standards and Technology, August 2018.

[80] Farzana Zaki, Yahui Wang, Hao Su, Xin Yuan, and Xuan Liu. Noise adaptive wavelet thresholding for speckle noise removal in optical coherence tomography. *Biomed. Opt. Express*, 8(5):2720–2731, May 2017. doi: 10.1364/BOE.8.002720.

[81] Lukasz Wieclaw. Fingerprint orientation field enhancement. In *Computer Recognition Systems 4*, pages 33–40. Springer, 2011.

[82] Shoba Dyre and CP Sumathi. Reliable orientation field estimation of fingerprint based on adaptive neighborhood analysis. *ICTACT Journal on Image & Video Processing*, 7(3):1456–1462, 2017.

[83] M Kocevar, S Klampfer, A Chowdhury, and Z Kacic. Low-quality fingerprint image enhancement on the basis of oriented diffusion and ridge compensation. *Elektronika ir Elektrotechnika*, 20(8):49–55, 2014.

[84] http://bias.csr.unibo.it/fvc2004/download.asp. (Accessed on 12/19/2019).

[85] Lin Hong, Yifei Wan, and Anil Jain. Fingerprint image enhancement: Algorithm and performance evaluation. *IEEE transactions on pattern analysis and machine intelligence*, 20(8):777–789, 1998.

[86] Nalini K. Ratha, Shaoyun Chen, and Anil K. Jain. Adaptive flow orientation-based feature extraction in fingerprint images. *Pattern Recognition*, 28:1657–1672, 1995.

[87] A Ravishankar Rao and Brian G Schunck. Computing oriented texture fields. *CVGIP: Graphical Models and Image Processing*, 53(2):157–185, 1991.

[88] Iwasokun Gabriel Babatunde, Akinyokun Oluwole Charles, and Olabode Olatunbosun. Uniformity level approach to fingerprint ridge frequency estimation. *International Journal of Computer Applications*, 62(22):8887, 2013.

[89] Thai Raymond. Fingerprint image enhancement and minutiae extraction. *Report in the School of Computer Science and Software Engineering*, 2003.

[90] Sujata Saini and Komal Arora. A study analysis on the different image segmentation techniques. *International Journal of Information & Computation Technology*, 4(14): 1445–1452, 2014.

[91] Song Yuheng and Yan Hao. Image segmentation algorithms overview. *arXiv preprint arXiv:1707.02051*, 2017.

[92] K Krishna Prasad and PS Aithal. Fingerprint image segmentation: A review of state of the art techniques. *International Journal of Management, Technology, and Social Sciences (IJMTS)*, 2(2):28–39, 2017.

[93] Naresh Garg and N Garg. Binarization techniques used for grey scale images. *International Journal of Computer Applications*, 71(1):8–11, 2013.

[94] Jamileh Yousefi. Image binarization using otsu thresholding algorithm. *University of Guelph, Ontario, Canada*, 2011.

[95] M Arif Wani and Bruce G. Batchelor. Edge-region-based segmentation of range images. *IEEE Transactions on Pattern Analysis and Machine Intelligence*, 16(3): 314–319, 1994.

[96] Elham Tabassi and Patrick Grother. *Fingerprint Image Quality*, pages 482–490. Springer US, Boston, MA, 2009. ISBN 978-0-387-73003-5. doi: 10.1007/978-0-387-73003-5_52. URL https://doi.org/10.1007/978-0-387-73003-5_52.

[97] MM Hadhoud, WS ElKilani, and MI Samaan. An adaptive algorithm for fingerprints image enhancement using gabor filters. In *Computer Engineering & Systems, 2007. ICCES'07. International Conference on*, pages 227–236. IEEE, 2007.

[98] Ajay Boyat and Brijendra Kumar Joshi. Image denoising using wavelet transform and median filtering. In *2013 Nirma University International Conference on Engineering (NUiCONE)*, pages 1–6. IEEE, 2013.

[99] Guy P Nason and Bernard W Silverman. The stationary wavelet transform and some statistical applications. In *Wavelets and statistics*, pages 281–299. Springer, 1995.

[100] James E Fowler. The redundant discrete wavelet transform and additive noise. *IEEE Signal Processing Letters*, 12(9):629–632, 2005.

[101] Hesham Nasif. Wavelet applicability in the area of signal processing. 2015. doi: 10.13140/RG.2.1.1074.9844.

[102] Ana SOVIĆ-Damir SERŠIĆ. Signal decomposition methods for reducing drawbacks of the dwt. *Engineering Review*, 32(2):70–77, 2012.

[103] S. S. Mgaga, N. P. Khanyile, and J. Tapamo. A review of wavelet transform based techniques for denoising latent fingerprint images. In *2019 Open Innovations (OI)*, pages 57–62, Oct 2019. doi: 10.1109/OI.2019.8908252.

[104] Matthias Holschneider, Richard Kronland-Martinet, Jean Morlet, and Ph Tchamitchian. A real-time algorithm for signal analysis with the help of the wavelet transform. In *Wavelets*, pages 286–297. Springer, 1990.

[105] Markus Lang, Haitao Guo, Jan E Odegard, C Sidney Burrus, and Raymond O Wells. Noise reduction using an undecimated discrete wavelet transform. *IEEE Signal Processing Letters*, 3(1):10–12, 1996.

[106] Radu Zaciu, Claudiu Lamba, Constantin Burlacu, and Gabriel Nicula. Image compression using an overcomplete discrete wavelet transform. *IEEE Transactions on Consumer Electronics*, 42(3):800–807, 1996.

[107] T Grover. Denoising of medical images using wavelet transform. *Imp J Interdiscip Res*, 2:541–8, 2016.

[108] Vaishali S Jabade and Sachin R Gengaje. Literature review of wavelet based digital image watermarking techniques. *International Journal of Computer Applications*, 31(1):28–35, 2011.

[109] Pankaj Hedaoo and Swati S Godbole. Wavelet thresholding approach for image denoising. *International Journal of Network Security & Its Applications (IJNSA)*, 3(4):16–21, 2011.

[110] Abdullah Al Jumah. Denoising of an image using discrete stationary wavelet transform and various thresholding techniques. *Journal of Signal and Information Processing*, 4(01):33, 2013.

[111] Payal Gupta and Amit Garg. Image denoising using bayes shrink method based on wavelet transform. *International Journal of Electronic and Electrical Engineering*, 8(1):33–40, 2015.

[112] Fei Xiao and Yungang Zhang. A comparative study on thresholding methods in wavelet-based image denoising. *Procedia Engineering*, 15:3998–4003, 2011.

[113] Lakhwinder Kaur, Savita Gupta, and RC Chauhan. Image denoising using wavelet thresholding. In *ICVGIP*, volume 2, pages 16–18, 2002.

[114] Mamdouh F Fahmy and MA Thabet. A fingerprint segmentation technique based on morphological processing. In *IEEE International Symposium on Signal Processing and Information Technology*, pages 000215–000220. IEEE, 2013.

[115] Dilation and erosion :: Morphological operations (image processing toolbox user's guide). `http://matlab.izmiran.ru/help/toolbox/images/morph2.html`. (Accessed on 05/12/2020).

[116] Raffaele Cappelli. *Fingerprint Sample Synthesis*, pages 513–523. Springer US, Boston, MA, 2009. ISBN 978-0-387-73003-5. doi: 10.1007/978-0-387-73003-5_3. URL `https://doi.org/10.1007/978-0-387-73003-5_3`.

[117] Point operations - adaptive thresholding. `https://homepages.inf.ed.ac.uk/rbf/HIPR2/adpthrsh.htm`. (Accessed on 01/20/2020).

[118] Rafael C Gonzalez, Richard Eugene Woods, and Steven L Eddins. *Digital image processing using MATLAB*. Pearson Education India, 2004.

[119] Ross Philip Holder and Jules-Raymond Tapamo. Using facial expression recognition for crowd monitoring. In *Pacific-Rim Symposium on Image and Video Technology*, pages 463–476. Springer, 2017.

[120] Michael Kass and Andrew Witkin. Analyzing oriented patterns. *Computer vision, graphics, and image processing*, 37(3):362–385, 1987.

[121] David Zhang, Feng Liu, Qijun Zhao, Guangming Lu, and Nan Luo. Selecting a reference high resolution for fingerprint recognition using minutiae and pores. *IEEE Transactions on Instrumentation and Measurement*, 60(3):863–871, 2010.

[122] John Daugman and Cathryn Downing. Gabor wavelets for statistical pattern recognition. In *The handbook of brain theory and neural networks*, pages 414–420. 1998.

[123] Nontokozo Portia Khanyile. Fingerprint identification using distributed computing. *University of KwaZulu-Natal ResearchSpace*, 2012.

[124] Silke Aumann, Sabine Donner, Jörg Fischer, and Frank Müller. *Optical Coherence Tomography (OCT): Principle and Technical Realization*, pages 59–85. Springer International Publishing, Cham, 2019. ISBN 978-3-030-16638-0. doi: 10.1007/978-3-030-16638-0_3. URL `https://doi.org/10.1007/978-3-030-16638-0_3`.

[125] JC Clements, AV Zvyagin, KKMBD Silva, T Wanner, DD Sampson, and WA Cowling. Optical coherence tomography as a novel tool for non-destructive measurement of the hull thickness of lupin seeds. *Plant Breeding*, 123(3):266–270, 2004.

[126] KATIE JO SULLIVAN. Optimized development of latent fingerprints on unfired and fired brass cartridge casings. *Forensic Science Internship, Marshall University, West Virginia, USA*.

[127] Piotr Porwik and Agnieszka Lisowska. The haar-wavelet transform in digital image processing: its status and achievements. *Machine graphics and vision*, 13(1/2): 79–98, 2004.